7-18-2016

Ion-Containing Diels-Alder Poly(phenylene)s: Chemistry, Physical and Transport Properties, and Vanadium Redox Flow Battery Performance

Timothy D. Largier
University of Connecticut - Storrs, tim.largier@gmail.com

Ion-Containing Diels-Alder Poly(phenylene)s: Chemistry, Physical and Transport Properties, and Vanadium Redox Flow Battery Performance

Timothy D. Largier, PhD

University of Connecticut, 2016

ABSTRACT

In this study the physical, electrochemical, and transport properties, as well as performance in a working vanadium redox flow battery, was reported for a series of anionic and cationic Diels-Alder poly(phenylene)s. Parent methylated and non-methylated Diels-Alder poly(phenylene) homopolymers, and random and block copolymers, were synthesized. The parent materials displayed good solubility in various organic solvents, high glass transition temperatures (365-390 °C) and good thermal stabilities (>552 °C). Correlations were found between *–mer* length and inter-chain spacing, glass transition temperature, and occupied volume. Sulfonated materials were synthesized that displayed good mechanical and thermal properties. A sulfonated poly(phenylene) with an IEC of 2.0 meq/g had a conductivity of 88.4 mS/cm and water uptake of 61.1%. The material had comparable ion conductivity and free water content, however significantly lower methanol permeability, when compared to the commercial standard Nafion 117, suggesting smaller and less interconnected ionic regions. A series of quaternary ammonium homopolymers and random copolymers were synthesized that displayed moderate mechanical strength and thermal stability (>190 °C). An aminated homopolymer had an IEC of 2.2 meq/g, and possessed an ion conductivity of 26.9 mS/cm and a water content of 73.1%. The quaternary ammonium random copolymers displayed lower water content, as well as superior mechanical properties and alcohol rejection, suggesting larger and well-defined hydrophobic regions. A state of water

analysis revealed decreased available free water, which resulted in lowered ion conductivities. Homogeneous amination preparation of the random and block copolymers resulted in adverse effects on mechanical, electrochemical, and transport properties, indicating a dilution effect.

The sulfonated poly(phenylene)s displayed high coulombic and moderate voltage efficiencies. The materials were optimized through control of ion content (IEC) and membrane thickness, resulting in superior performance over Nafion 117 at current densities of 10-50 mA/cm^2. The quaternary ammonium materials displayed poor performance, predominantly due to electrochemical limitations resulting in poor voltage efficiency. Random copolymerization improved the coulombic efficiency at the cost of increased ohmic resistance. Membranes displayed no failure after 40 charge-discharge cycles. Rigorous *ex-situ* stability testing revealed discoloration and loss of flexibility in all materials. The effect appeared to be reduced in quaternary ammonium materials, suggesting electrostatic effects.

Ion-Containing Diels-Alder Poly(phenylene)s: Chemistry, Physical and Transport Properties, and Vanadium Redox Flow Battery Performance

Timothy D. Largier

B.S., University of Connecticut, 2011

A Dissertation

Submitted in Partial Fulfillment of the

Requirements for the Degree of

Doctor of Philosophy

at the

University of Connecticut

2016

APPROVAL PAGE

Doctor of Philosophy Dissertation

Ion-Containing Diels-Alder Poly(phenylene)s: Chemistry, Physical and Transport Properties, and Vanadium Redox Flow Battery Performance

Presented by

Timothy D. Largier, B.S.

Major Advisor _____
Christopher Cornelius

Associate Advisor _____
Yongku Cho

Associate Advisor _____
Radenka Maric

Associate Advisor _____
Mu-Ping Nieh

Associate Advisor _____
Steven Suib

University of Connecticut

2016

Acknowledgements

First and foremost, I would like to thank my mentor and major advisor, Dr. Chris Cornelius. It has been a privilege working under his guidance. His passion and dedication to the sciences is unparalleled, and has allowed for my graduate experience to be one of great learning and personal growth. I would also like to thank those within the research group that have contributed to this dissertation through ideas and discussion: Dr, Donghui Wang, Dr. Fei Huang, Wenjian Zheng, Wayz Khan, Behrooz Motealleh, and Wheaton Schroeder.

I would like to recognize my committee members, Dr. Yongku Cho, Dr. Radenka Maric, Dr. Mu-Ping Nieh, and Dr. Steven Suib for their time, interest, and insightful questions. It was an honor to present my work to this distinguished committee. Dr. Yu Lei was not available to sit on the final committee, however, I would like to extend thanks for his continued time and support leading up to the oral defense.

My parents, Damian and Beverley Largier, have been an incredible support system over the course of my life and education. Through their example, I have learnt the value of hard work and commitment. Finally, I owe a great deal to my wife-to-be, Joanna. Her unwavering love and support has kept me focused and determined through my most challenging endeavors.

Table of Contents

Table of Figures

List of Tables

Chapter 1 Introduction

The United States Energy Information Administration has predicted that energy consumption will increase by 56% by 2040.[1] To meet this growing demand, renewable energy solutions have received growing attention. Traditional solutions, such as lithium ion systems, are costly, have limited energy availability, degrade in capacity, and are typically highly flammable. Alternative energy storage solutions are required to ensure the energy needs of the future are met. Redox flow batteries (RFB) offer several advantages over current energy storage technologies. They are an economical, low vulnerability way to store large amounts of energy, and are incredibly versatile due to a modular power and capacity (**Figure 1- 1**). That is, the power is set by the cell stack size, and the capacity by the volume of electrolyte. Traditional RFB's had issues regarding opposing electrolyte solutions that were highly incompatible. Ion crossover had the potential to drastically lower efficiencies as electrolytes were irreversibly consumed, calling for expensive electrolyte recoveries.[2–4]

The all-vanadium redox battery (VRB), patented in 1986 by the University of South Wales,[5] presented a solution to this issue. Ion crossover in this system may lower efficiencies, but irreversible electrolyte consumption is unlikely and electrolyte recovery can be accomplished through simple electrochemical oxidation. Significant attention has therefore gone into the development and optimization of VRB systems. The ion exchange membranes in these systems are needed to maintain the ion balance between the two electrolytes in a redox flow battery. Obtaining an ideal ionomer for this application has proven challenging, as the ideal membrane requires high proton conductivity, high chemical stability, a low vanadium ion permeability, and low electric area resistivity.[6]

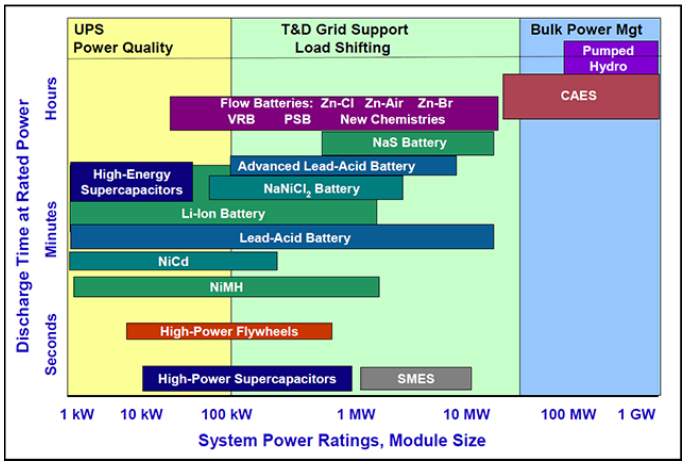

Figure 1- 1. Comparison of existing energy storage technologies.[7]

Phenylated materials have long been considered for applications that take advantage of their physical and chemical stabilities. In recent years, a series of poly(phenylene) ionomers have developed that show great promise in ion exchange applications.[8–11] Such work has confirmed the importance of ionomers of this nature, yet work is needed to fully understand their potential. The work in this study focuses on the chemical, physical and transport properties, of a series of highly phenylated Diels-Alder ion exchange membranes, as well as analysis in a working vanadium redox flow battery. The objective is to obtain a thorough understanding of how ionomer chemistry, morphology, and electro-transport properties affect VRB performance. In addition, permeability studies give insight into observed inefficiencies, and degradation studies will be used to predict long term battery performance.

In this dissertation, the first chapters provide a brief literature review of the synthesis and characterization of ionomers relevant to this research, an introduction to vanadium redox flow batteries, as well as a list of chemical reagents and description of material characterization techniques. Chapter 4 describes the synthesis, as well as a chemical, physical, and morphological

characterization of the parent Diels-Alder homopolymer and multi-block poly(phenylene)s. Chapter 5 discusses the effect of chemistry and morphology on electrochemical and transport properties, and the state of water, for a series of sulfonated Diels-Alder poly(phenylene)s. Chapter 6 provides a similar analysis for quaternary ammonium Diels-Alder poly(phenylene)s, as well as the effect of random and block copolymerization. Chapter 7 and 8 provide an analysis of the functionalized materials in a working vanadium redox flow battery, as well as *in-situ* and *ex-situ* studies pertaining to membrane stability. Conclusions and recommendations for this work are addressed in Chapter 9.

1.2 References

[1] Conti, J.; Holtberg, P.; Napolitano, S. *International Energy Outlook 2014*; U.S. Energy Information Administration, **2014**.

[2] Bartolozzi, M. *J. Power Sources* **1989**, *27*, 219–234.

[3] Li, B.; Li, L.; Wang, W.; Nie, Z.; Chen, B.; Wei, X.; Luo, Q.; Yang, Z.; Sprenkle, V. *J. Power Sources* **2013**, *229*, 1–5.

[4] Ang, P.; Remick, R. *US Pat. 4,485,154* **1984**.

[5] Skyllas-Kazacos, M.; Grossmith, F. *J. Electrochem. Soc.* **1987**, 2950–2953.

[6] Li, X.; Zhang, H.; Mai, Z.; Zhang, H.; Vankelecom, I. *Energy Environ. Sci.* **2011**, *4*, 1147.

[7] Environmental and Energy Study Institute, *Energy Storage*, August **2013**.

[8] Fujimoto, C. H.; Hickner, M. A.; Cornelius, C. J.; Loy, D. A. *Macromolecules* **2005**, 5010–5016.

[9] Hibbs, M.; Fujimoto, C.; Cornelius, C. *Macromolecules* **2009**, *42*, 8316–8321.

[10] He, L.; Fujimoto, C. H.; Cornelius, C. J.; Perahia, D. *Macromolecules* **2009**, 7084–7090.

[11] Fujimoto, Cy, et al. *Journal of membrane science* **2012**, *423*, 438-449.

Chapter 2 Literature Review

2.1 Branched Diels-Alder Poly(phenylene)s

2.1.1 Synthesis, Physical and Chemical Properties

Diels-Alder reactions are useful chemical reactions for the [4 + 2] cycloaddition between a conjugated diene and substituted alkene. The reaction was first described in 1928,[1] earning its discoverers the Nobel Prize in Chemistry. The driving force behind the reaction is the formation of σ-bonds, which have greater stability than π-bonds. It was considered particularly useful for the formation of unsaturated six membered systems, with good control over regio- and stereo-chemical properties. Despite an early discovery, there were few reports of synthesis that employed a Diels-Alder step-growth polymerization. The highest success was obtained through polymerizations that utilized the dienes cyclopentadienone,[2] 2-pyrone,[3] or thiophene dioxide.[4]

Mukamal *et al.* published a detailed synthesis of branched diels-alder poly(phenylenes) through the reaction of diethynylbenzenes and biscyclopentadienones.[5] Of particular interest was a polyphenylene that showed considerably high molecular weights, solubility in common organic solvents, and a thermal stability of up to 550 °C. In a following publication, the effect of alkylene chains in the repeat unit was investigated.[6] All polymers were colorless, soluble in organic solvents, and showed good thermal stability that decreased with increasing alkylene chain length. The polymerization followed a second-order rate law, with Arrhenius activation parameters consistent with Diels-Alder reactions, a low ΔH and a large negative ΔS. An investigation into the regioselectivity and kinetics of diels-alder polymerizations was performed.[7] It was found that both types of catenation were possible, with a ratio of para to meta varying with reaction temperature, from 0.55 at 100 °C to 1.0 at 255 °C. However, a later study concluded that 83% of isolated

polymer was of the m,m-isomer.[8] Therefore the high degree of solubility has been attributed to meta-catenation, as well as significant twisted conformations that limit or block conjugation.[9] Meta linkages, reducing polymer symmetry and increasing entropy, have also been shown to decrease the glass transition temperature, a phenomenon has been widely documented in other polymer systems.[10,11]

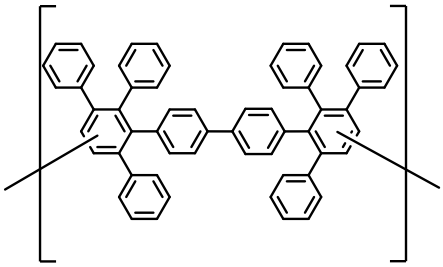

Figure 2 - 1. Structure of a phenylated poly(phenylene), as reported by Mukamal *et al*.[5]

Kumar and Neenan synthesized a series of branched poly(phenylene)s via a reaction between various diacetylenes and bis(cyclopentadienones) (**Figure 2 - 2**).[12] The materials had glass transition temperatures from 245 to 270 °C, and onsets of decomposition of 310-480°C. Molecular weight was heavily dependent on reactant concentration. All products were soluble in a wide range of organic solvents.

Shifrina *et al.* studied the synthesis and chemistry of Diels-Alder poly(phenylene)'s.[8] By varying reaction times from 18 to 72 hours at 240 °C, molecular weights were obtained from 1.2E04 - 1.2E05 g/mol. It was determined via a model compound that the *m,m*-isomer was the main product, up to 83% of the yield. The poly(phenylene) was subject to intramolecular oxidative cyclodehydrogenation with copper (II) trifluoromethanesulfonate and aluminum chloride. The

crosslinked material was insoluble, but extended π-conjugation and ordering of the crosslinked products were demonstrated by Raman spectroscopy. In a following publication, a detailed analysis of the thermodynamics of phenylated polyphenylene was studied.[13] The thermodynamic characteristics of the synthesis reaction were estimated from 0-600 K. The temperature, enthalpy and entropy, the parameters of glass transition state were estimated.

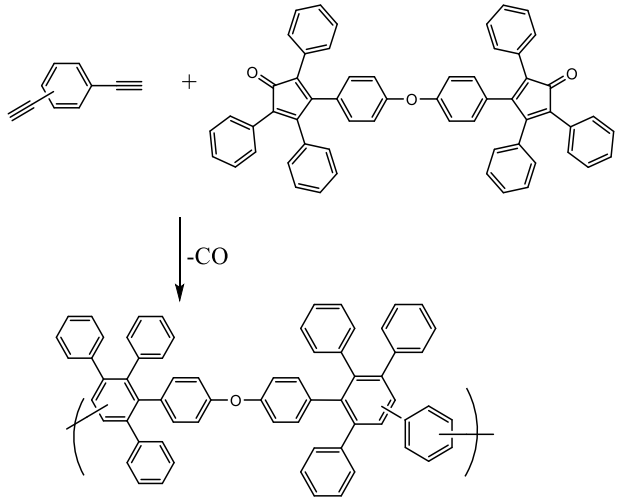

Figure 2 - 2. The scheme for a series of synthesized Diels-Alder poly(phenylene)s by Kumar *et al.*[12]

2.1.2 Summary

Branched Diels-Alder poly(phenylene)s have received much attention due to their high glass transition temperatures and thermal stabilities. The synthesis of the materials has been shown to be sensitive to time, temperature, and reactant concentration. Due to a high degree of meta-catenation, conjugation is disrupted and the materials are soluble in a wide range of organic solvents. Thermodynamic studies have shown that Diels-Alder polymerizations follow a second-

order rate law, with Arrhenius activation parameters consistent with Diels-Alder reactions, a low enthalpy and a large negative entropy.

2.2 Anionomers

2.2.1 Synthesis of Sulfonate Anionomers

The three most commonly studied classes of random anionomers are carboxylate, sulfonate, and phosphonate ionomers. Each fixed ion carrier has a different ionic interaction strength, which will affect anionomer properties, and require specific conditions during synthesis. Sulfonated ionomers are some of the most commonly used of all commercially available ionic polymers, and have been subject to several in depth reviews covering their preparation and properties.[14,15] These materials can be synthesized by either copolymerization of ionic monomers, or via post polymerization functionalization. A brief review of the two synthetic methods will be presented here.

The homogeneous sulfonation of high molecular weight polyaromatics had posed a great challenge to researchers due to uncontrolled crosslinking during the sulfonation reaction. In 1962, Turbak was able to obtain reproducible high molecular weight water soluble non-cross-linked polystyrenes and poly(vinyl toluenes).[16] This was accomplished using sulfur trioxide with alkyl phosphate as a complexing agent in dichloroethane. It was discovered that the complex readily reacts with hydrogen compounds but does not attack aromatic rings, even at elevated temperatures. In a 1972 patent, N. H. Canter applied a similar method to the sulfonation of a common rubber ethylene-propylene-diene terpolymer (EPDM).[17] Low sulfonated butyl rubber showed an overall increase in viscosity, tensile strength, modulus, and elongation. Higher sulfonated materials had

lower elongations to break, but all properties declined at 1.74 sulfonate mole percent. It was concluded that rheological properties were dependent on the radius of the neutralizing ion. A synthetic method using sulfur trioxide with alkyl phosphate was attempted in non-chlorinated hydrocarbon solvents,[18] but was proven less effective due to the insolubility of the sulfonating agent. This was overcome using long chained hydrocarbon-soluble acyl sulfates, allowing effective polystyrene sulfonation in cyclohexane at 50 °C. Additional studies on sulfonated EPDM found that through careful selection of the EPDM backbone, the molecular weight and sulfonated content could be controlled in order to obtain materials with excellent mechanical properties and low melt viscosities.[19] In order to better under polymer sulfonation chemistry in EPDM rubbers, W. A. Thaler performed an investigation into the sulfonation of the bicyclic olefins ethylidene norbornane (ENBH) and dihydrodicyclopentadiene (DCPDH).[20] Sulfonation of ENBH formed a sultone with a rearranged carbon skeleton by a substitution mechanism, and sulfonation of DCPDH formed a regiospecific sulfonic acid by retro-Wagner Meerwein elimination. Thaler and Dubreuil continued this investigation by studying type I and II monocyclic olefins and type I and type II cyclic olefins.[21]

A slightly different synthetic method for the sulfonation of polyphenylene oxide (PPO) was performed by Chludzinski *et al*. (**Figure 2 - 3**).[22] The reaction was performed using chlorosulfonic acid at ambient conditions in chloroform. The ion exchange capacity could be easily controlled by changing the molar ratio of chlorosulfonic acid to polymer repeat unit. The membrane morphological properties and performance as a reverse osmosis membrane were investigated. The material in both the proton and sodium forms displayed excellent chemical and physical stabilities, as well as good flux and ion rejection characteristics. These properties could optimized by changing the materials IEC. In 1975, H.S. Makowski performed a reaction using

acetic acid and sulfuric acid ("acetyl sulfate") in dichloromethane at 10 °C to produce lightly sulfonated polystyrene.[23] Bishop *et al*. observed the properties of dilute solution of poly(oxy-1,4-phenyleneoxy-1,4-phenylenecarbonyl-1,4-phenylene) (PEEK) in sulfuric acid and chlorosulfonic acid.[24] It was reasoned that PEEK was expanded by relatively short range steric and electrostatic interactions, with some non-ideality caused by long-range electrostatic forces and the Donnan effect. The molecular weight, the hydrodynamic radius, and the radius of gyration significantly increased after exposure to chlorosulfonic acid or 100% sulfuric acid. This was attributed to aggregation due to the formation and linkage of sulfone groups on aromatic rings.

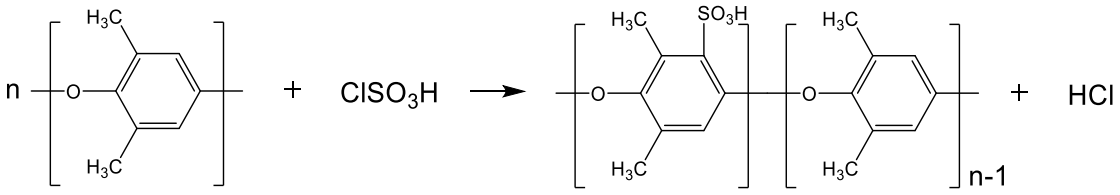

Figure 2 - 3. The sulfonation of polyphenylene oxide using chlorosulfonic acid.

Although this review is primarily focused on the synthesis of sulfonated ionomer via post-polymerization functionalization, efforts to better control ionomer chemistry through ionic copolymerization reactions has led to an increased understanding of material properties. Therefore noteworthy contributions will be briefly discussed.

Significant work has been performed regarding sulfonation by direct emulsion copolymerization between a styrene sulfonic acid or salt, and a diene monomer. In 1980, Weiss *et al.* studied the copolymerization of butadiene with sodium styrene sulfonate.[25] The report discussed emulsifier type and concentration, monomer feed ratio, chain transfer agent

concentration, and reaction conversion. Higher conversions were observed for non-ionic emulsifiers, however polymer molecular weight seemed unaffected. As expected, higher concentrations of chain transfer agent (dodecanethiol) lowered molecular weight and reduced crosslinking. One challenge associated with emulsion copolymerization is that there is little control over the distribution of sulfonated groups without decreasing the extent of reaction or changing the monomer charge.[26] Siadat *et al* reported that better control could be achieved by using olefinic sulfonic acid esters instead of styrene sulfonates, as esters have better monomer compatibility with diene monomers.[27] Using a similar method to the ones discussed, Siadat *et al*. also reported the copolymerization of butadiene and isoprene with several different sulfonic acid salt group monomers, including sodium styrene sulfonate.[28]

Weiss *et al.* went on to synthesize sulfonated polystyrene by emulsion copolymerization of styrene and sodium styrene sulfonate (NaSS).[29] Up to 40 mole percent NaSS was used in the feed, and up to 30 mole percent NaSS detected in the polymer. The kinetics of this reaction was discussed in a paper by Turner *et al*.[30] It was found that the copolymerization rate of styrene and NaSS drastically differed to the homopolymerization rate of styrene. One cause, confirmed by electron microscopy, was attributed to an increase in the number of polymerizing particles. It was also proposed that there was some "gel effect" that occurs due to the intermolecular association of incorporated metal sulfonate units in the growing polymer particles. Ponrathnam *et al* provided evidence that counterion affinity for a polyelectrolyte is dependent on the both the counterion selectivity and the solvent dielectric constant.[31] This confirmed the hypothesis that copolymerization kinetics were impacted by electrostatic repulsion of ionic charges between comonomer, polyelectrolyte, and solvent.

Weiss *et al.* performed a comparison of styrene monomers prepare by sulfonating polystyrene, and copolymerizing styrene with styrene sulfonate.[32] Significant differences were observed in solubility behavior, the effect sulfonation concentration has on Tg, and the hydration and adsorption kinetics. It was proposed that these differences were attributed to differences in sulfonate distribution. It was also noted that data suggested greater phase separation of ion rich and ion poor clusters in the copolymers.

2.2.2 Summary

Sulfonated ionomers are some of the most commonly used of all commercially available ionic polymers, and can be synthesized by either copolymerization of ionic monomers, or via post polymerization functionalization. Two leading methods have allowed for successful homogeneous post polymerization sulfonation. The first typically involves the sulfonation of a polyaromatic using a sulfonating and complexing agent in a chlorinated solvent. It has also been shown that sulfonation is possible in non-chlorinated solvents through the use of a long chained hydrocarbon-soluble sulfonating agents. The second method involves exposure to high concentrations of sulfuric or chlorosulfonic acid, at both ambient and sub-ambient temperatures. This method allows for easily controlled ion exchange capacities, by altering the molar ratio of the sulfonating agent.

Sulfonate copolymerization of ionic monomers has been performed by direct emulsion copolymerization, typically between a styrene sulfonic acid, salt or acid esters, and a diene monomer. Important factors include emulsifier type and concentration, monomer feed ratio, and chain transfer agent concentration. Higher conversions were observed for non-ionic emulsifiers, however polymer molecular weight seemed unaffected. Higher concentrations of chain transfer

agent lowered molecular weight and reduced crosslinking. Sulfonate ionomers synthesized by ionic monomer copolymerization, when compared to those synthesized by post polymerization sulfonation, showed significant differences in solubility behavior. Other differences include a variation in sulfonation concentration, Tg, and the hydration and adsorption kinetics. This has been attributed to differences in sulfonate distribution, causing greater phase separation of ion rich and ion poor clusters in the copolymers.

2.3 Cationomers

2.3.1 Synthesis of Nitrogen-containing Phenylated Cationomers

Nitrogen-containing polyelectrolytes are quaternary ammonium polymers which may carry protonated or alkylated amine groups. An in depth review of the preparation of these materials has been reported.[14,33] Synthesis typically involve the polymerization of monomers already in the cationic form, or chemical modification of a polymer. The latter method will be the focus of this review. In addition, the review will place particular emphasis on aromatic and aromatic ether based ionomers, due to the relevance these ionomers have with the materials discussed in this work.

Aromatic ethers have received much attention for their strong thermochemical stability and high glass transition temperatures. Zschocke *et al.* first produced quaternary ammonia polyether sulfone (QA-PSU) by post-polymerization chloromethylation, followed by quaternary amination.[34] Materials were produced with an ion exchange capacity (IEC) from 0.5 to 1.8 meq/g and excellent alkaline stability. Pan *et al.* described a novel detailed route to obtain QA-PSU.[35] PSU was initially chloromethylated using chloromethymethylether, zinc and trifluoroacetic acid. The resulting polymer was purified, dissolved into dimethylformamaide, and then bubbled with

trimethylamine gas. The ionomer was soluble in organic solvents, showed good chemical and thermal stability, as well as adequate mechanical strength. IEC's were obtained from 1.03 to 1.17 meq/g, giving conductivities between 10 and 22 mS/cm.

Quaternary ammonium polysulfone based materials synthesized in a similar fashion has shown great promise in alkaline polymer fuel cells.[35–40] Wang *et al.* performed a thorough investigation of reaction time and temperature in relation to polymer gelation during the synthesis of chloromethylated PSU.[41] In the same study, the effect of tertiary amine type on conductivity was observed. Trimethylamine had the greatest conductivity, concluding that steric hindrance played a major role in ion transport. Some work has been done to observe the performance of diamines on ionomer performance. Park *et al.* studied both diamine alkyl length and monoamine/diamine ratios optimize ion transport and stability of QA-PSU's.[42,43] It was observed that for the case of diamines only, conductivity increases with increasing alkyl length. Mono-/diamine (3:1) mixtures displayed superior conductivities and higher water uptakes than pure mono- or diamine ionomers. Wang *et al.* investigated poly(arylene ether sulfone)s with quaternary guanidinium groups as hydroxide exchange membranes.[44] Materials were synthesized up to an IEC of 1.85 mequiv/g, with conductivities up to 67 mS/cm. Although good thermal and dimensional stability was reported, chemical stability testing was limited. Another method has been reported to prepare aminated monomers via a Mannich reaction.[45] The synthetic method allowed for complete control over the amount of ammonium groups and their location along the polymer backbone. The procedure did not use chloromethyl methyl ether, and so is potentially less environmentally hazardous. The partially fluorinated ionomer exhibited good dimensional stability at high IEC's, and conductivities up to 84 mS/cm at room temperature.

Another ionomer which has received significant attention is quaternary ammonium poly(phenylene oxide) (PPO). Xu *et al.* reported facile preparation of quaternary ammonium PPO through bromination, and not chloromethylation.[46] It was shown that at low temperatures bromine substitution was more favorable on the aryl ring, while benzene substitution more favorable approaching 130 °C. Additional following publications describe the preparation of quaternary ammonium PPO with trimethylamine and type II anion exchange membranes.[47,48] A series of papers investigated bromomethylation and quaternization of PPO with 4-vinylpyridine and pyridine.[49,50] The position of the bromine, the amination procedure, the extent of amination, and the permeaselectivity of various monovalent anions were investigated. Lin *et al.* presented the synthesis of guanidinium-based PPO ionomers.[51] Due to the high alkalinity of guanidinium hydroxide, materials exhibited high water uptakes and ion conductivities. Materials were thermally stable, but chemical stability was only tested in 1 mol/dm^3 solutions. Lin *et al.* also synthesized a benzimidazolium-based PPO ionomer.[52] The material revealed good conductivity, proper water uptake and good thermal stability. Significant losses, however, were observed in IEC, water uptake and conductivity after treatment in a 2 M KOH solution for seven days.

Fang *et al.* prepared a novel quaternized poly(phthalazinon ether sulfone ketone) (PPES) via chloromethylation for anion exchange membrane fuel cells.[53] The material had a conductivity of 5 mS/cm at 100% humidity, increasing to 140 mS/cm in a 2 M KOH. The material exhibited loss of functionality at higher KOH concentrations. Xing *et al.* studied the effect of amination time, temperature, and amination species as a function of IEC, water content and area resistance.[54] It was found that both IEC and water content significantly increase with increasing amination time, temperature and concentration, while area resistance decreases. An in depth look at the properties

of chloromethylated PPES has been performed,[55] as well a synthetic method using chloromethyl octyl ethers, a lower toxicity chloromethylation agent.[56]

2.3.2 Synthesis of Nitrogen-containing Phenylated Alternating and Block Cationomers

Anion exchange membranes, although effective ion carriers, suffer from large water uptake, loss of mechanical properties once hydrated, and high solvent permeability. Various techniques have been employed to improve these properties, most notably the use of physical or ionic crosslinking,[57–59] or cationomer-polymer blends.[60,61] A third method involves alternating or block copolymers, a technique widely used in the study of cation exchange membranes to improve ion exchange properties while reducing solvent permeability and swelling.

The study of alternating and block copolymers by polymer chemical modification has only recently gained attention. Hwang *et al.* synthesized block poly(ethersulfone)s via chloromethylation and subsequent amination using trimethylamine.[62] In a second publication, Hwang *et al.* studied the effect amination procedure had on the morphology and ion content of the ionomer.[63] In the first method, chloromethylated PSU was cast from DMF, and then soaked in a QA-PSU/methanol solution, at 60 °C for 16 hours. The solution was prepared by dissolving 0.002 g of TMA to 1 g of chloromethylated polymer, and adding methanol (4:1). In the second method, chloromethylated PSU was dissolved in a 3:1 volume ratio of DMF and *tert*-amylalchohol. 0.002 g of trimethylamine against 1 g of chloromethylated polymer was then added. The solution was heated to 120 °C with stirring, to allow macroreticular structure formation and amination of the

polymer. Once complete the ionomer was cast on a glass plate. Hwang observed that the second method gave significantly higher ion exchange capacities, and lower area resistivity's.

Yan *et al.* revisited the synthesis of alternating QA-PSU copolymers, but via bromination followed by subsequent amination.[64] It was shown that bromination allowed for quantitative control over the ion content within the polymer, and relatively short reaction times. In this study two amination techniques were employed. The first, termed "heterogeneous amination", involved casting of brominated PSU polymer in chloroform, followed by submersion in 45% (w/w) trimethylamine solution for 48 hours. In the second method, termed "homogeneous amination", 300% molar excess of 45% (w/w) aqueous trimethylamine solution was added to a solution of 8% brominated PSU in DMAc, sealed in a container for 48 hours. The aminated polymer was then filtered onto a glass plate and cast. Copolymers were found to have lower water uptakes and conductivities than homopolymers. In addition when plotted against water uptake, no difference between homogeneous and heterogeneous samples were observed for methanol permeability or conductivity. It was noted that large water uptakes caused hydrated conductivity to decrease with increasing IEC.

Tanaka *et al.* synthesized poly(arylene ether) multiblock copolymers containing quaternized ammonio-substituted fluorine groups.[65] Scanning transmission electron microscopy confirmed well developed hydrophilic/hydrophobic phase separation, and interconnected ion transporting pathways. The resulting ionomers displayed excellent conductivities, up to 144 mS/cm at 80 °C, and only minor degradation in rigorous alkaline stability testing. Ionomers were tested in a working alkaline fuel cell.

Hibbs *et al.* produced a quaternary aminated tetramethyl phenylated anion exchange membrane homopolymer (AMPP), and a phenylated - aminated tetramethyl phenylated anion

exchange membrane random copolymer (ADAPP-ATMPP), for the application of alkaline fuel cells.[66] The materials was synthesized by Diels-Alder polymerization, followed by bromination. The brominated material was cast from chloroform, and the thin film submerged in 45% w/w aqueous solution of trimethylamine. Ion conductivities were obtained as high as 50 mS/cm, and showed greater water uptakes and conductivities than polysulfone-based anion exchange membranes. This was attributed to bulky side groups which prevent efficient packing of the polymer. The ionomers exhibited no degradation in 4 M KOH solutions at 60 °C for up to 28 days. It was these initial findings that has inspired much of the work described in this dissertation.

2.3.3 Summary

Synthesis of ammonium cationomers is performed either by the polymerization of monomers already in the cationic form, or post polymerization modification. Post polymerization modification typically involves polymer amination, followed by either protonation or quaternization, often achieved via the Mannich reaction. Parent materials were initially prepared by chloromethylation, however due to concerns with reactant toxicity, recent studies have utilized bromination of a methyl moiety. It has been shown that both IEC and water content significantly increase with increasing amination time, temperature and concentration. In addition the position of the functional group, the amination procedure, and the extent of amination have large implications on ionomer performance and state of water. Block copolymerization of anion exchange membranes has afforded mixed results. In some reports, block copolymerization has done little to appreciably increase the ion conductivity of the ionomers. In other reports, well defined morphologies have been achieved, however electrochemical properties remain lower than PEM competitors.

2.4 Ion Exchange Membranes in VRB's

2.4.1 Anionomers in VRB's

Ion exchange membranes are needed to maintain the ion balance between the two electrolytes in a redox flow battery. These materials require functionality that allows them to facilitate selective ion transport, as well as sufficient chemical and mechanical stability to last long life cycles. An ideal IEM should have low vanadium ion permeation rates to minimize self-discharge, and low area resistivity to minimize internal losses. A thorough review of IEM's in VRB's has been reported.[67]

Perfluoronated membranes have been used most frequently in all-vanadium redox flow batteries. The chemical stability, high ion conductivity, and commercial availability of Dupont's Nafion® 117 (Nafion) has made it the standard when performing comparative studies. Many sources indicate that Nafion's VRB efficiencies are around 90% for the coulombic efficiency (CE), and 85% for the energy efficiency (EE). Work using different thicknesses of Nafion has revealed how thinner membranes may have larger ion permeability's.[54] Although Nafion shows potential in VRB systems, the material suffers from high cost and high ion permeability. This has inspired work to either reduce Nafion's vanadium ion permeability, or find more cost-competitive alternatives.

One method of modifying Nafion is to introduce inorganic particles to block the hydrophilic domains within the polymer matrix to reduce the materials ion and molecular permeability. Jingyu *et al.* used the in-situ sol-gel method to create Nafion/SiO_2 hybrid membranes.[68] These materials presented higher CE and EE values at current densities between 10-

80 mA cm^{-2}, and had considerably lower vanadium ion permeability. Properties were maintained after 100 charge-discharge cycles at 60 mA cm^{-2}. Cell efficiencies were further improved in following work where tetraethoxysilane (TEOS) and diethoxydimethylsilane (DEDMS) mixtures were used to create Nafion/ORMOSIL hybrids by in situ sol-gel reactions.[69] Nafion/TiO_2 hybrid membranes have been fabricated via the hydrothermal method and tested in VRB systems.[70] Although coulombic and energy efficiencies were only marginally higher in the hybrid material, vanadium ion permeability was significantly reduced.

Another method used to modify the transport properties of Nafion has been to create Nafion/organic hybrid membranes. Luo *et al.* modified Nafion using interfacial polymerization to form a polyethylenimine (PEI) cationic charged surface-layer.[71] Increased PEI concentration caused significant drops in VO^{2+} permeability and an increase in coulombic efficiency. However, at higher concentrations there were also higher area resistances, causing energy efficiencies to decline. Another method used to modify the surface of Nafion is an alternate adsorption method. This has been demonstrated using polycation poly(diallyldimethylammonium chloride) (PDDA) and polyanion poly(sodium styrene sulfonate) (PSS)[72]. The Nafion-[PDDA-PSS] hybrid showed decreased ion permeability. Despite a lower proton conductivity, significant improvements were observed in coulombic efficiency, and energy efficiency, open circuit voltage and charge-discharge cycling. A Nafion/organic hybrid blends have been used to similar ends. Mai *et al.* prepared a Nafion/polyvinylidene fluoride (PVDF) polymer blend in order to take advantage of PVDF's crystallinity and hydrophobicity.[73] The hybrid membrane had high compatibility and reduced swelling. A blend membrane of 20 wt% PVDF had an OCV decay twice as long as Nafion and showed an improved energy efficiency of 85% at 80 mA cm^{-2}, as well as significantly reduced VO^{2+} permeability.

Shortly after the all-vanadium cell was patented, several commercial non-fluoronated materials were used in all-vanadium redox flow batteries. Skyllas-Kazacos *et al.* used a sulfonated polyethylene and obtained energy efficiencies over 90%.[74] Although stability tests with different oxidation states led to no significant decomposition, prolonged use within the cell did cause deterioration of the positive electrode and membrane. A sulfonated polystyrene membrane was shown to have a coulombic efficiency of 90%, but a low energy efficiency of 73% due to high membrane resistivity.[75] Cycling for 2000h revealed no signs of membrane degradation.

Since the initial work done on the commercially available non-fluorinated polymers in the 1980's, several other materials have been prepared and tested. Chen *et al* prepared sulfonated poly(florenyl ether ketone) (SPFEK) for use in VRBs.[76] SPFEK had significantly lower vanadium ion permeability and gave a coulombic efficiency of 80.3%, higher than the 77.0% obtained for Nafion 117. After immersion in 1 M VO_2^+ for 15 days at 25^{o}C, no significant decrease in efficiency was observed. In 2010, Chen *et al.* went on to synthesize two novel materials for use in VRB's, poly(arylene ether sulfone)[77,78] and poly(arylene thioether).[79] Both materials exhibited good oxidative stability and lower vanadium ion permeability than Nafion 117. Lower ion permeability's gave the materials higher coulombic efficiencies, however overall energy efficiency was variable most likely due to membrane resistance. In 2011, Mai *et al.* prepared poly(tetramethyldiphenyl ether ether ketone) for use in VRB's.[80] The material displayed lower ion permeability, and slightly superior energy efficiencies and OCV decay times over Nafion 117.

Pore filled ion exchange membranes have received some attention. These membranes consist of a porous support that provides mechanical strength, and an ion exchange resin or polyelectrolyte to facilitate ion transport. A common porous support is Daramic, which consists of ultrahighmolecular polyethylene, amorphous silica and mineral oil. Mohammadi *et al.* prepared

an IEM using Daramic filled with Amberlite CG 400, using polymerized divinylbenzene (DVB) as a crosslinker.[81,82] Results showed that the polymerized DVB network does reduce the porous nature of Daramic. The IEM had a lower area resistance and had a CE of 90% during the charge/discharge cycle, compared with 77% for the original material. In a separate paper Daramic was cross-linked with DVB, and then sulfonated to obtain a cation exchange membrane of various IEC's.[83] After crosslinking, the Daramic pore size was reduced from 0.1 to 0.02 μm. Only slight decreases in vanadium permeability were observed, however area resistance, cell performance and water transport properties were significantly improved. Similar work was done with Daramic, however using poly(sodium 4-styrene-sulfonate) (PSSS) as the crosslinker.[84] The novel IEM had reduced area resistance but increased diffusivity. In a VRB system, the EE was 77% at a current density of 40 mA cm^{-2}. In 2004, Tian et al used Daramic with the commercial fluoropolymer Nafion.[85] Incorporation of the ionomer into the composite membrane and partially blocks pores. The IEM had a reduced area resistance and reasonable IEC of 0.8 to 1.2 mmol/g. With the introduction of Daramic, the self-discharge degree was dramatically reduced.

Fujimoto *et al.* reported vanadium redox flow battery data for a series of sulfonated Diels-Alder poly(phenylene)s (SDAPP). Coulombic efficiencies were observed from 91 to 99%, and energy efficiencies between 88-90%. Rigorous cell cycling revealed stability to be a function of IEC, with the highest IEC failing after 50 cycles, and the lowest after 400 cycles. Ex-situ testing revealed darkening of the ionomer films, and loss of flexibility.[86]

Several studies have been performed on the stability of cation exchange membranes in vanadium ion solutions.[87] In a study performed by Sukkar and Skyllas-Kazacos, Nafion 112 and a series of cationic Gore Select commercial membranes were exposed to V(v) solutions.[88] On exposure to a 0.1 M V(v) solution, Nafion showed the worst performance, as indicated by a drop

in resistivity, increase in IEC. And increase in V(iv) diffusivity. In a 1.0 M V(v) solution, however, Nafion showed the best resilience. It is suspected that the membranes swell more in dilute solutions, allowing the vanadium ions to permeate into the pores of the membrane more easily. It was concluded that swelling plays a vital role in the rate of degradation of materials.

A study on the degradation of a commercial sulfonated polysulfone (s-Radel®) has been performed.[89] It was desired to understand the degradation mechanism of aromatic polymers in V(v) solutions. It was concluded that hydroxyl groups had been added to the backbone of the material, indicated by quinone groups identified by FTIR. $VOCl_3$ was found to have cause no degradation, so it is hypothesized that other reactive forms of V(v) attack the S-Radel membrane by incorporation of the hydroxyl groups onto the backbone of the material, followed by oxidation of these groups to quinone functionalities.

2.4.2 Cationomers in VRB's

Anion exchange membranes have been considered in vanadium redox flow batteries as theoretically they could induce Donnan repulsion effects, improving charge-carrier selectivity. In this membrane electrode assembly, protons and sulfate or sulfuric acid based electrolytes would behave as charge carriers.

Hwang and Ohya crosslinked the commercial anion exchange New-Selemion membrane by electron radiation.[90] At a dose of 5 Mrad, the material exhibited improved coulombic and voltage efficiencies, with an energy efficiency over 80%. The material experienced no loss in efficiency after eight cycles. A novel quaternized poly(phthalazinone ether ketone) has been prepared for use in VRB's.[55,91] The materials experienced only small changes in dimension when

submerged for 30 days in a 2M $VOSO_4$/3M H_2SO_4 solution. The materials exhibited higher coulombic efficiencies than Nafion 117, however had marginally lower energy efficiencies.

A quaternary ammonium poly(pthalazinone ether ketone) has been prepared for VRB's at IEC's from 0.96 to 1.64, with a high water content of 23%, and low area resistivity of 0.94 Ω cm^2.[91] The materials displayed IEC independent CE's of 97.7-98.7%, and voltage efficiencies increasing with IEC, up to 87.3%. A quaternized poly(2,2,2-trifluoroethyl methacrylate-co-N-vinylimidazole) has been prepared for VRB's by Fang *et al.*[92] The material displayed a conductivity of 18 mS/cm at 30°C, and a low vanadium ion permeability compared to Nafion. VRB testing gave a CE of 99.5% and VE of 75.3%. Although the VE was well below the 82.6% of Nafion, the high CE gave an overall better energy efficiency. Testing on similar materials has afforded comparable results.[56,93] A study was performed observing the effect of amine agent on VRB performance.[54] An optimal treatment method for the amination of materials was proposed. Both TMA and EDA/TMA materials displayed superior energy efficiency to that of Nafion, however the capacity of the battery (or electrolyte volume) was not explicitly stated.

Chen *et al.* prepared a quaternized poly(fluorenyl ether) for use in VRB's.[94] The conductivity of the AEM and Nafion 212 were tested after submersion in a 1 M $VOSO_4$ + 2.5 M H_2SO_4 solution overnight. Nafion 212 displayed a conductivity of 40 mS/cm, half of that reported for pure water, and a conductivity of 20 mS/cm for the AEM. This analysis indicates material property changes during VRB operation. The coulombic efficiency maintained near 100%, while the voltage efficiency dropped sharply from 90% to 60%, with increasing current density from 20 to 80 mA/cm^2. The materials displayed no drop in VE or capacity after cycling for 15 cycles at 80 mA/cm^2.

In a study performed by Sukkar and Skyllas-Kazacos, the anionic commercial New Selemion Type 3H and Tokuyama membranes were exposed to V(v) solutions.[88] The membranes experienced quite severe degradation, indicated by an increase in resistivity and IEC. Interestingly, the cationomers displayed a decrease in permeability. It was concluded that degradation is slowed in more concentrated solutions, due to lower degree of swelling. This was later supported by a study involving the dimensional stability of a quaternized poly(phthalazione ether sulfone) in a 2 M $VOSO_4$ in 3 M H_2SO_4.[55] It was found that material exhibited lower levels of swelling in the electrolyte than water. It was concluded that, in water, the high concentration of ions increases the osmotic pressure and therefore, as the solution increases in electrolyte concentration, the osmotic pressure declines.

Sun *et al.* performed cycling and stability measurements for quaternary ammonium Diels-Alder poly(phenylene)s (QDAPPs).[95] The materials displayed performance as a function of IEC, whereby there existed a trade-off between voltage loss and capacity loss. Moderate IEC's were found to be optimal. Degradation studies revealed superior chemical stability to sulfonated DAPP membranes.[95]

2.4.3 Summary

Ongoing efforts in the development and optimization of ion exchange membranes for the application of vanadium redox flow batteries has revealed many challenges. The ideal membrane requires good mechanical and chemical stability, high proton conductivity, and vanadium ion rejection. Nafion, the commercial standard, displays highly competitive properties due to a high proton conductivity and chemical stability, however the material has poor charge carrier selectivity

and therefore suffers from low coulombic efficiencies. Many aromatic cationic and anionic exchange membranes that display low conductivities have been shown to improve coulombic efficiency through a lower vanadium permeability, however reveal greater internal resistances. The optimization of such materials has therefore proven challenging, and additional efforts are required to understand the role of ionomer chemistry, morphology, and electrochemical properties in the performance of VRB's.

2.5 Vanadium Redox Flow Batteries

2.5.1 Introduction to Redox Flow Batteries

A redox flow battery (RB) is a system that stores chemical energy and generates electricity via redox reactions. A major advantage of RB systems is that they have modular power outputs and energy capacities, and so can be optimized for specific applications. A typical redox flow battery (**Figure 2 - 4**) consists of an electrochemical cell stack, a proton exchange membrane, two electrolyte tanks, two pumps to allow for electrolyte circulation, and a power source or sink. During charging, reversible reduction and oxidation reactions occur on either side of the cell, allowing the battery to store chemical energy. During discharge the reverse occurs, generating electrical energy and returning the ions to their original oxidation state.

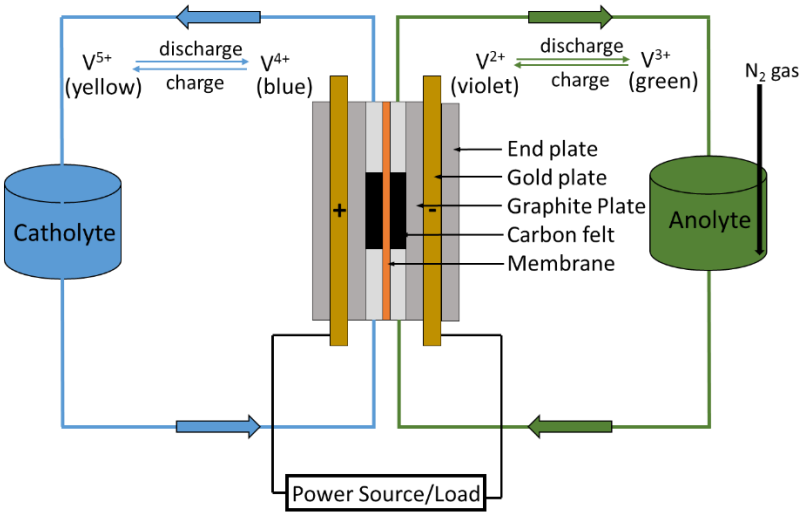

Figure 2 - 4. A typical redox flow battery, consisting of two electrolyte tanks and a single electrochemical cell.

The all Vanadium redox flow battery (VRB) was patented in 1986 by the University of New South Wales in Australia[96]. In previous systems, opposing electrolyte solutions were highly incompatible. Ion crossover had the potential to drastically lower efficiencies as electrolytes were irreversibly consumed, which would cause expensive electrolyte recoveries. Ion crossover in the all vanadium system may lower efficiencies, but irreversible electrolyte consumption is unlikely and electrolyte recovery can be accomplished through simple electrochemical oxidation. It is for these reasons much work has been focused on the development and optimization of these systems.

2.5.2 Electrochemistry of VRBs

A thorough review of the electrochemistry and transport within a vanadium redox flow battery has been reported.[97] The all vanadium redox flow battery consists of the V(II)/V(III) redox

couple at the negative electrode, and the V(IV)/V(V) redox couple at the positive electrode. During charge, electrons move from the catholyte through an external circuit to the anolyte. During discharge, the reverse occurs. The redox reactions during charge and discharge are:

$$VO_2^+ + 2H^+ + e^- \rightleftharpoons VO^{2+} + H_2O \qquad 2 - 1$$

$$V^{2+} \rightleftharpoons V^{3+} + e^- \qquad 2 - 2$$

Giving the overall redox equation:

$$V^{2+} + VO_2^+ + 2H^+ \rightleftharpoons VO^{2+} + V^{3+} + H_2O \qquad 2 - 3$$

As can be seen by the equation, water and protons are required to maintain the charge balance. This is the purpose of the semi-permeable ion exchange membrane. A high concentration of

Table 2 - 1. Salts formed by the interaction of vanadium oxidation states with sulfuric acid.

Cell State	Electrode	Species Produced	Corresponding Salt of Species
Charge	Negative	V^{2+}	VSO_4
Charge	Positive	$V^{5+}(VO_2^+)$	$0.5(VO_2)_2SO_4$
Discharge	Negative	V^{3+}	$0.5V_2(SO_4)_3$
Discharge	Positive	$V^{4+}(VO^{2+})$	$VOSO_4$

protons is present as the system is run in concentrated sulfuric acid. The salts formed by the interaction of vanadium oxidation states with sulfuric acid are shown in **Table 2 - 1**. As mentioned previously, the size of a VB cell stack will determine the batteries power. The stack voltage can be defined as the equilibrium voltage minus internal losses. This is given by:

$$U_{cell}(t) = U_{equ}(t) - U_{loss}(t) \qquad 2 - 4$$

Where U_{cell} the voltage of the cell, U_{equ} is the voltage of the cell at equilibrium, and U_{loss} are internal losses within the cell. To describe the voltage within one cell, the Nernst equation, which relates the potential of a cell to the standard electrode potential, can be written as:

$$E = E^{0\prime} + \frac{RT}{nF} \ln \frac{C_O}{C_i} \qquad 2 - 5$$

Where E is the potential of one cell, $E^{0\prime}$ is the standard potential, R is the gas constant, T is the temperature, and C_O and C_i are the concentrations of species *o* and *i* respectively. When applied to the all-vanadium electrolyte system, we obtain:

$$E = E^{0\prime} + \frac{RT}{nF} \ln[(\frac{C_{VO_2^+} * C_{H^+}^2}{C_{VO^{2+}}})(\frac{C_{V^{2+}}}{C_{V^{3+}}})] \qquad 2 - 6$$

The standard potential is defined as the potential at which the cell is operating at standard conditions. At ambient temperatures and specie concentrations of one molar, the second term in equation 2 - 6 is equal to zero. This sets the standard potential equal to the real potential. At these conditions the standard potential can be estimated using standard thermodynamic parameters. Standard Gibbs free enthalpy is defined as:

$$\Delta G^0 = \Delta H_r^0 - T\Delta S_r^0 \qquad 2 - 7$$

Where ΔH_r^0 is the difference between the product and reagent enthalpies of formation, and ΔS_r^0 is the difference between the product and reagent entropies of formation. The change in the standard Gibbs free energy can be related to the difference in the standard potential energy using the conservation of energy. This can be written as:

$$\Delta G^0 = -nFE^{0'} \qquad 2 - 8$$

Where n is the number of electrons that transfer if given potential $E^{0'}$, and F is the Faraday's constant defined as the magnitude of electric charge per mole of electrons (9.649 x 10^4 C mol^{-1}). By combining equations 2 - 7 and 2 - 8, the standard potential becomes:

$$E^{0'} = -\frac{\Delta H_r^0 - T\Delta S_r^0}{nF} \qquad 2 - 9$$

The enthalpy of formation is the difference between the sum of the product enthalpies of formation and the sum of the reagent enthalpies of formation. This gives the equation:

$$\Delta H_r^0 = \sum H_{f,product}^0 - \sum H_{f,reagent}^0 \qquad 2 - 10$$

And equivalently for the entropy of formation as:

$$\Delta S_r^0 = \sum S_{f,product}^0 - \sum S_{f,reagent}^0 \qquad 2 - 11$$

The entropies and enthalpies of formation for various vanadium oxidation states have been determined experimentally, or estimated, and can be seen in **Table 2 - 2**. By inserting these values into equations 2-10 and 2-11, one can obtain ΔH_r^0 and ΔS_r^0. Equation 2-9 can then be used to obtain the standard potential for the full-vanadium redox reaction, equal to 1.23 V.

Table 2 - 2. Salts formed by the interaction of vanadium oxidation states with sulfuric acid.[98]

Formula	State	ΔH_f^0 (kJ mol^{-1})	ΔG_f^0 (kJ mol^{-1})	ΔS_f^0 (J mol^{-1} K^{-1})
V^{2+}	aq	(-226)	(-218)	(-130)
V^{3+}	aq	(-259)	-251.3	(-230)
VO^{2+}	aq	-486.6	-446.4	-133.9
VO_2^+	aq	-649.8	-587.0	-42.3
H_2O	aq	-285.8	-237.2	69.9
H^+	aq	0	0	0

2.5.3 RB Testing and Efficiency Calculations

The standard method for analyzing the ability of a rechargeable battery to store and release energy is charge-discharge cycling. This is usually accomplished by applying a desired current and monitoring the change in cell voltage. This is often presented as a function of the batteries state of charge (SOC).The state of charge is the available capacity of a cell, expressed as a percentage. For the all-vanadium system, the state of charge is:

$$SOC = \left(\frac{C_{V^{2+}}}{C_{V^{2+}} + C_{V^{3+}}}\right) = \left(\frac{C_{VO_2^+}}{C_{VO^{2+}} + C_{VO_2^+}}\right) \qquad 2 - 12$$

Where C_x is the concentration of ionic species *x*. In a typical measurement a battery will be charged by applying a constant voltage until a set SOC, and then discharged, generally at the same current, until it reaches its initial SOC.

In order to quantify and compare a batteries ability to store and release energy, voltage, coulombic, and energy efficiency calculations can be performed. The coulombic efficiency is

defined as the ratio of the discharge capacity to the charge capacity. The equation for the average coulombic efficiency across all currents is:

$$\eta_C = \frac{Q_D}{Q_C} = \frac{\int_0^{t_d} I_d dt}{\int_0^{t_c} I_c \, dt} \qquad 2 - 13$$

Where Q_D and Q_C are the discharge and charge capacities, I_d and I_c are the discharge and charge currents, and t_d and t_c are the discharge and charge times. If the battery is charged or discharged at a constant current, the charge or discharge capacity will equal the product of the charge/discharge current and time. This simplifies 2 - 13 to:

$$\eta_C = \frac{Q_D}{Q_C} = \frac{I_d t_d}{I_c t_c} \qquad 2 - 14$$

The energy efficiency is then merely the ratio of the energy needed to charge the system to the discharged energy. This equation is:

$$\eta_E = \frac{\int_0^{t_d} U_d I_d dt}{\int_0^{t_c} U_c I_c \, dt} \qquad 2 - 15$$

This equation gives the average energy efficiency over the entire charge-discharge process. If a constant charge and discharge is applied, the equation 2 - 15 becomes:

$$\eta_E = \frac{I_d \int_0^{t_d} U_d dt}{I_c \int_0^{t_c} U_c \, dt} = \eta_C \frac{\int_0^{t_d} U_d dt}{\int_0^{t_c} U_c \, dt} \qquad 2 - 16$$

The term by which the energy and coulombic efficiencies are related can be defined as the voltage efficiency. By taking the average of the charge and discharge voltages, the voltage efficiency can be written as:

$$\eta_V = \frac{\int_0^{t_d} U_d dt}{\int_0^{t_c} U_c \, dt} = \frac{\overline{U_d}}{\overline{U_c}} \qquad 2 - 17$$

Where U_d and U_c are the average voltages during discharge and charge respectively. If ignoring mechanical losses, a relationship between the three efficiencies is obtained. This relationship can be written as:

$$\eta_E = \eta_V \eta_C \qquad 2 - 18$$

2.5.4 Internal Resistance of a RB Cell

Typically during the charge-discharge process, significant ohmic losses can be observed due to a phenomena known as cell resistance. The cell resistance is a combination of all component resistances in the membrane electrode assembly. This includes contact resistance, grain-boundary resistance, bulk membrane resistance, and electrode resistances.[99] Ohmic loss can be simply described as:

$$U_{loss} = iA_{cell}R_{cell} \qquad 2 - 19$$

Where A_{cell} is the cell area and R_{cell} is the cell resistance. Equation 2 - 19 shows that, at a constant internal resistance, we should observe larger ohmic losses with increasing current.

There are two common methods for measuring the internal resistance of a cell. The first is the current interruption method, which measures the voltage change that results from a sudden

change in current. For example, a constant current could be passed through a system and then suddenly dropped to zero. A sharp drop in voltage will occur, which is then followed by the gradual drop that occurs due to the electrochemical overpotential. The internal resistance can be found by dividing the sharp voltage drop by the change in current. Buchi *et al.* determined membrane resistance by fast current pulses.[100] To obtain accurate internal resistance data, voltage was monitored from zero to 500 nanoseconds and had less than five nanosecond trailing edges, regardless of the direct current.

The second method for determining internal resistance is through the use of electrochemical impedance spectroscopy (EIS). A review of EIS for use in fuel cells, that applies to RB systems, has been published.[101] It has been acknowledged that the EIS method gives internal resistances closer to that of the true value.[102] EIS can provide information regarding ohmic loss, charge-transfer resistance and mass transfer limitations. From a Nyquist plot, the membrane resistance is determined from the intercept of the real impedance and the reaction resistance is evaluated from the high frequency circular arc.

2.5.5 Summary

Redox flow batteries offer significant advantages over classical rechargeable batteries due to a modular power and capacity. The all-vanadium redox has been acknowledged as a good electrolyte system for RB's as electrolyte impurities that enter through ion crossover can be cheaply purified though electrochemical oxidation. In order to observe a vanadium redox flow batteries ability to store and release energy, charge-discharge curves are performed. These tests allow the coulombic, voltage and energy efficiencies to be monitored as a function of current

density. Charge-discharge cycling observes the long term effects on the system components in the cell. Together, these tests provide information regarding the efficiency and longevity of an all-vanadium RB and its components.

2.6 References

[1] Diels, O.; Alder, K. *Justus Liebigs Ann. Chem.* **1928**, *460*, 98–122.

[2] Kraiman, E. A. USP 2,890,206. CA 52, 1959.

[3] Chow, S.-W.; Whelan, J. J. M. US2971944 A, 1961.

[4] Chow, S.-W. US3074915 A, 1963.

[5] Mukamal, H.; Stille, J. K.; Harris, F. W.; Rakutis, R. O. *J. Polym. Sci. Part A-1 Polym. Chem.* **1967**, *5*, 2721–2729.

[6] Stille, J.; Rakutis, R. O.; Mukamal, H.; Harris, F. w. *Macromolecules* **1968**, *1*, 431–436.

[7] Stille, J.; Noren, G. *Macromolecules* **1972**, *5*.

[8] Shifrina, Z. B.; Averina, M. S.; Rusanov, A. L.; Wagner, M.; Mu, K. **2000**, 3525–3529.

[9] Berresheim, A. J.; Müller, M.; Müllen, K. *Chem. Rev.* **1999**, *99*, 1747–1785.

[10] Qu, W.; Ko, T. M.; Vora, R. H.; Chung, T. S. *Polymer (Guildf).* **2001**, *42*, 6393–6401.

[11] Oroujzadeh, M.; Mehdipour-Ataei, S.; Esfandeh, M. *Eur. Polym. J.* **2013**, *49*, 1673–1681.

[12] Kumar, U.; Neenan, T. X. *Macromolecules* **1995**, *28*, 124–130.

[13] Smirnova, N. N.; Kulagina, T. G.; Markin, A. V. *Thermochim. Acta* **2005**, *425*, 39–46.

[14] Thomson, R. *Dev. Ion. Polym.* **1986**, 1–76.

[15] Weiss, R. A.; Fitzgerald, J. J. *J. Macromol. Sci. Part C Polym. Rev.* **1988**, 99–185.

[16] Turbak, A. F. *Ind. Eng. Chem. Prod. Res. Dev.* **1962**, *1*, 275–278.

[17] Canter, N. *US Pat. 3,642,728* **1972**.

[18] Thaler, W. *Macromolecules* **1983**, *16*, 623–628.

[19] Makowski, H. *Ions …* **1980**.

[20] Thaler, W. A. *J. Polym. Sci. Polym. Chem. Ed.* **1982**, *20*, 875–896.

[21] Thaler, W. A. .; Dubreuil, C. *J. Polym. Sci. Polym. Chem. Ed.* **1984**, *22*, 3905–3919.

[22] LaConti, A.; Chludzinski, P.; Fickett, A. *Reverse Osmosis Membr. …* **1972**, 263–284.

[23] Patent, U. S. *Current* **2011**, *3870841*, 1–19.

[24] Bishop, M.; Karasz, F.; Russo, P.; Langley, K. *Macromolecules* **1985**, *18*, 86–93.

[25] Weiss, R. A.; Lundberg, R. D. *J. Polym. Sci. Polym. Chem. Ed.* **1980**, *18*, 3427–3439.

[26] Siadat, B. *Ph. D. Thesis* **1979**.

[27] Siadat, B; Lenz, R. W. *J. Polym. Sci. Polym. Chem. Ed.* **1980**, *18*, 3273–3287.

[28] Siadat, B. .; Oster, B.; Lenz, R. *J. Appl. Polym. …* **1981**, *26*, 1027–1037.

[29] Weiss, R. A.; Turner, S. R.; Lundberg, R. D. *J. Polym. Sci. Polym. Chem. Ed.* **1985**, *23*, 525–533.

[30] Turner, S. *J. Polym. …* **1985**, *23*, 535–548.

[31] Ponrathnam, S.; Milas, M.; Blumstein, A. *Macromolecules* **1982**, *15*, 1251–1255.

[32] Weiss, R. *J. Polym. …* **1985**, *23*, 7–23.

[33] Merle, G.; Wessling, M.; Nijmeijer, K. *J. Memb. Sci.* **2011**, *377*, 1–35.

[34] Zschocke, P.; Quellmalz, D. *J. Memb. Sci.* **1985**, *22*, 325–332.

[35] Pan, J.; Lu, S.; Li, Y.; Huang, A.; Zhuang, L.; Lu, J. *Adv. Funct. Mater.* **2010**, *20*, 312–319.

[36] Wang, J.; Wang, J.; Li, S.; Zhang, S. *J. Memb. Sci.* **2011**, *368*, 246–253.

[37] Abuin, G. C.; Nonjola, P.; Franceschini, E. a.; Izraelevitch, F. H.; Mathe, M. K.; Corti, H. R. *Int. J. Hydrogen Energy* **2010**, *35*, 5849–5854.

[38] Lu, S. F.; Pan, J.; Huang, a B.; Zhuang, L.; Lu, J. T. *Proc. Natl. Acad. Sci. U. S. A.* **2008**, *105*, 20611–20614.

[39] Hossein Ghassemia, Ram Subbaramana, Christopher Brockmana, B. P. and T. Z. *ECS Trans.* **2008**, *16*, 689–697.

[40] Li, X.; Liu, Q.; Yu, Y.; Meng, Y. *J. Mater. Chem. A* **2013**, *1*, 4324.

[41] Wang, G.; Weng, Y.; Chu, D.; Chen, R.; Xie, D. *J. Memb. Sci.* **2009**, *332*, 63–68.

[42] Park, J. S.; Park, G. G.; Park, S. H.; Yoon, Y. G.; Kim, C. S.; Lee, W. Y. *Macromol. Symp.* **2007**, *249-250*, 174–182.

[43] Park, J. S.; Park, S. H.; Yim, S. D.; Yoon, Y. G.; Lee, W. Y.; Kim, C. S. *J. Power Sources* **2008**, *178*, 620–626.

[44] Wang, J.; Li, S.; Zhang, S. *Macromolecules* **2010**, *43*, 3890–3896.

[45] Wang, J.; Zhao, Z.; Gong, F.; Li, S.; Zhang, S. *Macromolecules* **2009**, *42*, 8711–8717.

[46] Xu, T.; Weihua, Y. *J. Memb. Sci.* **2001**, *190*, 159–166.

[47] Xu, T.; Liu, Z.; Yang, W. *J. Memb. Sci.* **2005**, *249*, 183–191.

[48] Xu, T.; Liu, Z.; Li, Y.; Yang, W. *J. Memb. Sci.* **2008**, *320*, 232–239.

[49] Yuan Li, T. X. *Polym. Polym. Compos.* **2009**, 3017–3025.

[50] Li, Y.; Xu, T.; Gong, M. *J. Memb. Sci.* **2006**, *279*, 200–208.

[51] Lin, X.; Wu, L.; Liu, Y.; Ong, A. L.; Poynton, S. D.; Varcoe, J. R.; Xu, T. *J. Power Sources* **2012**, *217*, 373–380.

[52] Lin, X.; Liang, X.; Poynton, S. D.; Varcoe, J. R.; Ong, A. L.; Ran, J.; Li, Y.; Li, Q.; Xu, T. *J. Memb. Sci.* **2013**, *443*, 193–200.

[53] Fang, J.; Shen, P. K. *J. Memb. Sci.* **2006**, *285*, 317–322.

[54] Xing, D.; Zhang, S.; Yin, C.; Zhang, B.; Jian, X. *J. Memb. Sci.* **2010**, *354*, 68–73.

[55] Xing, D.; Zhang, S.; Yin, C.; Yan, C.; Jian, X. *Mater. Sci. Eng. B* **2009**, *157*, 1–5.

[56] Jian, X. G.; Yan, C.; Zhang, H. M.; Zhang, S. H.; Liu, C.; Zhao, P. *Chinese Chem. Lett.* **2007**, *18*, 1269–1272.

[57] Xiong, Y.; Fang, J.; Zeng, Q. H.; Liu, Q. L. *J. Memb. Sci.* **2008**, *311*, 319–325.

[58] Komkova, E. N.; Stamatialis, D. F.; Strathmann, H.; Wessling, M. *J. Memb. Sci.* **2004**, *244*, 25–34.

[59] Hao, J. H.; Chen, C.; Li, L.; Yu, L.; Jiang, W. *Desalination* **2000**, *129*, 15–22.

[60] Wu, L.; Xu, T.; Wu, D.; Zheng, X. *J. Memb. Sci.* **2008**, *310*, 577–585.

[61] Mansourpanah, Y.; Madaeni, S. S.; Rahimpour, a.; Kheirollahi, Z.; Adeli, M. *Desalination* **2010**, *256*, 101–107.

[62] Hwang, G. J.; Ohya, H. *J. Memb. Sci.* **1998**, *140*, 195–203.

[63] Hwang, G.-J.; Ohya, H. *J. Memb. Sci.* **1998**, *149*, 163–169.

[64] Yan, J.; Hickner, M. a. *Macromolecules* **2010**, *43*, 2349–2356.

[65] Tanaka, M.; Fukasawa, K.; Nishino, E.; Yamaguchi, S.; Yamada, K.; Tanaka, H.; Bae, B.; Miyatake, K.; Watanabe, M. *J. Am. Chem. Soc.* **2011**, *133*, 10646–10654.

[66] Hibbs, M.; Fujimoto, C.; Cornelius, C. *Macromolecules* **2009**, *42*, 8316–8321.

[67] Li, X.; Zhang, H.; Mai, Z.; Zhang, H.; Vankelecom, I. *Energy Environ. Sci.* **2011**, *4*, 1147.

[68] Xi, J.; Wu, Z.; Qiu, X.; Chen, L. **2007**, *166*, 531–536.

[69] Teng, X.; Zhao, Y.; Xi, J.; Wu, Z.; Qiu, X.; Chen, L. *J. Power Sources* **2009**, *189*, 1240–1246.

[70] Wang, N.; Peng, S.; Lu, D.; Liu, S.; Liu, Y.; Huang, K. *J. Solid State Electrochem.* **2011**, *16*, 1577–1584.

[71] Luo, Q.; Zhang, H.; Chen, J.; Qian, P.; Zhai, Y. *J. Memb. Sci.* **2008**, *311*, 98–103.

[72] Xi, J.; Wu, Z.; Teng, X.; Zhao, Y.; Chen, L.; Qiu, X. *J. Mater. Chem.* **2008**, *18*, 1232.

[73] Mai, Z.; Zhang, H.; Li, X.; Xiao, S.; Zhang, H. *J. Power Sources* **2011**, *196*, 5737–5741.

[74] Skyllas-Kazacos, M.; Rychcik, M.; Robins, R. G.; Fane, A. G.; Green, M. A. *Electrochem. Soc. J.* **1986**, *133*, 1057–1058.

[75] Skyllas-Kazacos, M.; Grossmith, F. *J. Electrochem. Soc.* **1987**, 2950–2953.

[76] Chen, D.; Wang, S.; Xiao, M.; Meng, Y. *J. Power Sources* **2010**, *195*, 2089–2095.

[77] 孟跃中, **王拴**紧, **敏 肖**, 陈栋阳韩东梅. CN 200910040808, 2010.

[78] Chen, D.; Wang, S.; Xiao, M.; Meng, Y. *Energy Convers. Manag.* **2010**, *51*, 2816–2824.

[79] Chen, D.; Wang, S.; Xiao, M.; Meng, Y. *Energy Environ. Sci.* **2009**, *3*, 622.

[80] Mai, Z.; Zhang, H.; Li, X.; Bi, C.; Dai, H. *J. Power Sources* **2011**, *196*, 482–487.

[81] Chieng, S. C. .; Kazacos, M. .; Skyllas-Kazacos, M. *J. Membr. Sci.* **1992**, *75*, 81–91.

[82] Mohammadi, T.; Skyllas-Kazacos, M. *J. Memb. Sci.* **1995**, *98*, 77–87.

[83] Mohammadi, T.; Skyllas-Kazacos, M. *J. Memb. Sci.* **1995**, *107*, 35–45.

[84] Mohammadi, T.; Skyllas-Kazacos, M. *J. Power Sources* **1995**, *56*, 91–96.

[85] Tian, B.; Yan, C. .; Wang, F. . *J. Memb. Sci.* **2004**, *234*, 51–54.

[86] Fujimoto, C.; Kim, S.; Stains, R.; Wei, X. *Electrochem. …* **2012**, *20*, 48–51.

[87] Kim, S.; Tighe, T. B.; Schwenzer, B.; Yan, J.; Zhang, J.; Liu, J.; Yang, Z.; Hickner, M. a. *J. Appl. Electrochem.* **2011**, *41*, 1201–1213.

[88] Sukkar, T.; Skyllas-Kazacos, M. *J. Appl. Electrochem.* **2004**, *34*, 137–145.

[89] Chen, D.; Hickner, M. a. *Phys. Chem. Chem. Phys.* **2013**, *15*, 11299–11305.

[90] Hwang, G.; Ohya, H. *J. Memb. Sci.* **1997**, *132*, 55–61.

[91] Zhang, S.; Yin, C.; Xing, D.; Yang, D.; Jian, X. *J. Memb. Sci.* **2010**, *363*, 243–249.

[92] Fang, J.; Xu, H.; Wei, X.; Guo, M.; Lu, X.; Lan, C.; Zhang, Y.; Liu, Y.; Peng, T. *Polym. Adv. Technol.* **2013**, *24*, 168–173.

[93] Zhang, B.; Zhang, S.; Xing, D.; Han, R.; Yin, C.; Jian, X. *J. Power Sources* **2012**, *217*, 296–302.

[94] Chen, D.; Hickner, M. a.; Agar, E.; Kumbur, E. C. *Electrochem. commun.* **2013**, *26*, 37–40.

[95] Sun, C. N.; Tang, Z.; Belcher, C.; Zawodzinski, T. a.; Fujimoto, C. *Electrochem. commun.* **2014**, *43*, 63–66.

[96] Skyllas-Kazacos, Maria; Miron, Rychick; Robins, R. ALL-VANADIUM REDOX FLOW BATTERY. 4,786,567, 1988.

[97] Blanc, C.; Rufer, A. *Lab. d'Electronique Ind. Ec. …* **2010**.

[98] Bard, Allen J.; Parsons, Roger; Jordan, J. *Standard Potentials in Aqueous Solutions*; 6th ed.; CRC press, 1985.

[99] Abe, T.; Shima, H.; Watanabe, K.; Ito, Y. *J. Electrochem. Soc.* **2004**, *151*, A101–A105.

[100] Büchi, F.; Marek, A.; Scherer, G. *J. Electrochem. …* **1995**, *142*, 1895–1901.

[101] Yuan, X.-Z.; Song, C.; Wang, H.; Zhang, J. *Electrochemical Impedance Spectroscopy in PEM Fuel Cells*; 1st ed.; Springer-Verlag: London, 2010.

[102] Andreaus, B. *Solid State Ionics* **2004**, *168*, 311–320.

Chapter 3 Experimental Methods

3.1 Materials

3.1.1 Solvents

All solvents were used as received unless otherwise specified.

Methanol	
Supplier:	*Fisher Scientific*
Purity:	*≥ 99.8%*
Empirical Formula:	*CH_4O*
CAS Number:	*67-56-1*

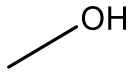

Ethanol	
Supplier:	*Decon Laboratories, Inc*
Purity:	*200 Proof*
Empirical Formula:	*C_2H_6O*
CAS Number:	*64-17-5*

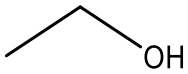

Heptane	
Supplier:	*Fisher Scientific*
Purity:	*96%*
Empirical Formula:	*C_7H1_6*
CAS Number:	*142-82-5*

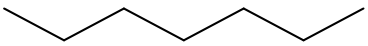

1,3-Diphenylacetone	
Supplier:	*Fisher Scientific*
Purity:	*99%*
Empirical Formula:	*$C_{15}H_{14}O$*
CAS Number:	*102-04-5*

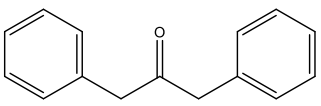

Diphenyl ether

Supplier:	*Acros Organics*
Purity:	*99%*
Empirical Formula:	*$C_{12}H_{10}O$*
CAS Number:	*101-84-8*

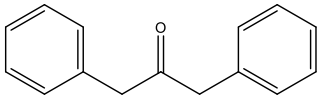

Acetone

Supplier:	*Fisher Scientific*
Purity:	*≥ 99.5%*
Empirical Formula:	*C_3H_6O*
CAS Number:	*67-64-1*

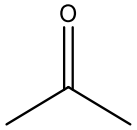

Dichloromethane

Supplier:	*Acros Organics*
Purity:	*99.9%*
Empirical Formula:	*CH_2Cl_2*
CAS Number:	*75-09-2*

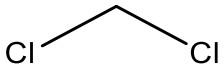

Chloroform

Supplier:	*Fisher Scientific*
Purity:	*≥ 99.8%, 0.75% Ethanol*
Empirical Formula:	*$CHCl_3$*
CAS Number:	*67-66-3*

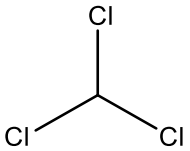

Acetonitrile

Supplier:	*Fisher Scientific*
Purity:	*≥ 98.5%*
Empirical Formula:	*C_2H_3N*
CAS Number:	*75-05-8*

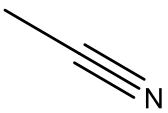

Dimethylacetamide

Supplier:	*Acros Organics*
Purity:	*≥ 99.8%*
Empirical Formula:	*C_4H_9NO*
CAS Number:	*127-19-5*

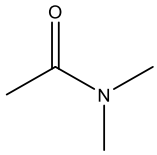

Toluene

Supplier:	*Fisher Scientific*
Purity:	*≥ 99.5%*
Empirical Formula:	*C_7H_8*
CAS Number:	*108-88-33*

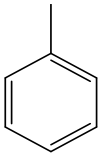

1,1,2,2-Tetrachloroethane

Supplier:	*Acros Organics*
Purity:	*98.5%*
Empirical Formula:	*$C_2H_2Cl_4$*
CAS Number:	*79-34-5*

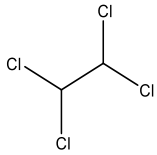

Tetrahydrofuran

Supplier:	*Fisher Scientific*
Purity:	*99.9%*
Empirical Formula:	*C_4H_8O*
CAS Number:	*109-99-9*

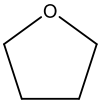

Sulfuric Acid

Supplier:	*Fisher Scientific*
Purity:	*95.0-98.0 w/w%*
Empirical Formula:	*H_2SO_4*
CAS Number:	*7664-93-9*

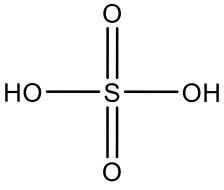

3.1.2 Reagents

1,4-Bis(phenylethynyl)benzene underwent ruthenium catalyzed oxidation to form 1,4-bis(phenylglyoxaly)benzene, a necessary step in the preparation of the poly(phenylene) monomer. The material was received in poor purity, and was purified by recrystallization in toluene prior to use.

1,4-Bis(phenylethynyl)benzene	
Supplier:	*3B Pharmachem*
Purity:	*≥ 97%*
Empirical Formula:	$C_{22}H_{14}$
CAS Number:	*1849-27-0*

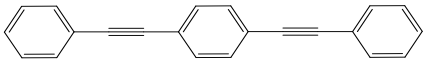

Sodium periodate was used, as received, for the regeneration of ruthenium(VIII) oxide in the oxidation of 1,4-bis(phenylenethynyl)benzene.

Sodium meta-Periodate	
Supplier:	*Fisher Scientific*
Purity:	*≥ 99.8%*
Empirical Formula:	$INaO_4$
CAS Number:	*7790-28-5*

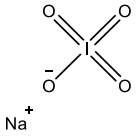

Ruthenium chloride ($RuCl_3$) was used, as received, in the oxidation of 1,4-bis(phenylethynyl)benzene. $RuCl_3$ was converted to RuO_4 in-situ for its use as an effective oxidizing agent.

Ruthenium(III) Chloride Hydrate	
Supplier:	*Acros Organics*
Purity:	*35 – 40% Ru*
Empirical Formula:	*$Cl_3Ru \cdot xH_2O$*
CAS Number:	*14898-67-0*

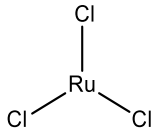

Sodium hydroxide (NaOH) was used, as received, in order to neutralize any acids that may have been formed during various reactions performed in this research. Neutralization was typically carried out by washing an organic solution with a 1 M aqueous solution of NaOH. NaOH was also critical in neutralizing the excess acids and the acidic polymer present after sulfonation.

Sodium Hydroxide	
Supplier:	*Fisher Scientific*
Purity:	*≥ 97.0%*
Empirical Formula:	*NaOH*
CAS Number:	*1310-73-2*

Potassium hydroxide (KOH) was used, as received, for the base catalyzed aldol condensation reaction of bis(phenylglyoxaly)benzene with 1,3-diphenylacetone, and with 1,3-bis(4-methylphenyl)propan-2-one.

Potassium Hydroxide	
Supplier:	*Fisher Scientific*
Purity:	*≥ 85.0%*
Empirical Formula:	*KOH*
CAS Number:	*1310-58-3*

Sodium chloride (NaCl) was used, as received, for the neutralization of cation exchange membranes from the acid to the sodium salt form, and neutralization of anion exchange membranes from the basic to the chloride form.

Sodium Chloride	
Supplier:	*Fisher Scientific*
Purity:	*≥ 99.0%*
Empirical Formula:	*NaCl*
CAS Number:	*7647-14-5*

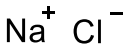

Sodium phosphate tribasic was used, as received, for the neutralization of anion exchange membranes from the basic to the phosphate form.

Sodium Phosphate Tribasic Dodecahydrate	
Supplier:	*Fisher Scientific*
Purity:	*98-102%*
Empirical Formula:	*$Na_3PO_4 \bullet 12H_2O$*
CAS Number:	*10101-89-0*

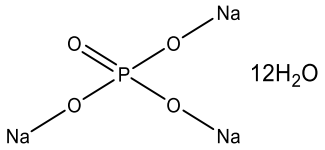

1,4-diethynylbenzene was used in the Diels-Alder reaction with a bis(tetracyclone) to form poly(phenylene) or methylated poly(phenylene). The reagent was received in poor purity, and was effectively purified by sublimation prior to use.

1,4-Diethynylbenzene	
Supplier:	*Fisher Scientific*
Purity:	*95%*
Empirical Formula:	$C_{10}H_6$
CAS Number:	*935-14-8*

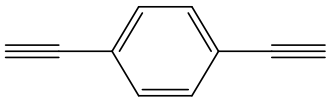

Chlorosulfonic acid was used, as received, in the post-modification sulfonation of poly(phenylene).

Chlorosulfonic Acid	
Supplier:	*Fisher Scientific*
Purity:	*97%*
Empirical Formula:	$HClO_3S$
CAS Number:	*7790-94-5*

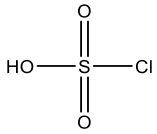

p-Tolylacetic acid was used, as received, in the synthesis of 1,3-bis(4-methylphenyl)propan-2-one by Steglich esterification.

p-Tolylacetic Acid	
Supplier:	*Acros Organics*
Purity:	*99%*
Empirical Formula:	$C_9H_{10}O_2$
CAS Number:	*622-47-9*

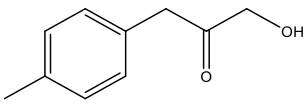

N,N'-Dicyclohexylcarbodiimide (DCC) was used, as received, in the Steglich esterification of *p*-Tolylacetic.

N,N'-Dicyclohexylcarbodiimide	
Supplier:	*Acros Organics*
Purity:	*99%*
Empirical Formula:	$C_{13}H_{22}N_2$
CAS Number:	*538-75-0*

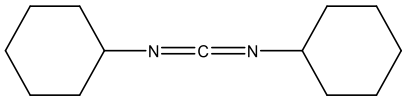

4-Dimethylaminopyridine (DMAP) was used, as received, as a catalyst with acetic anhydride in the Steglich esterification of *p*-Tolylacetic with DCC.

4-Dimethylaminopyridine	
Supplier:	*Acros Organics*
Purity:	*99%*
Empirical Formula:	$C_7H_{10}N_2$
CAS Number:	*1122-58-3*

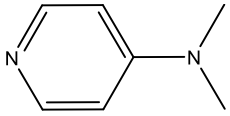

Glacial acetic acid was used, as received, as a catalyst with DMAP in the Steglich esterification of *p*-Tolylacetic with DCC.

Acetic Acid, Glacial	
Supplier:	*Fisher Scientific*
Purity:	*≥ 99.7%*
Empirical Formula:	$C_2H_4O_2$
CAS Number:	*64-19-7*

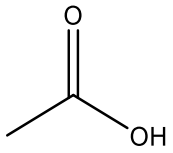

N-Bromosuccinimide (NBS) was used in the bromination of methylated poly(phenylene). NBS was received in inadequate purity, and was purified through recrystallization in water.

N-Bromosuccinimide	
Supplier:	*Acros Organics*
Purity:	*99%*
Empirical Formula:	$C_4H_4BrNO_2$
CAS Number:	*128-08-5*

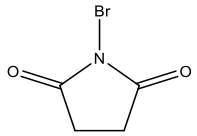

Dibenzoyl peroxide (BPO) was used in the bromination of methylated poly(phenylene). BPO was received in inadequate purity, and was purified by precipitation with methanol from chloroform.

Dibenzoyl Peroxide	
Supplier:	*Acros Organics*
Purity:	*75%, rem.* H_2O
Empirical Formula:	$C_{14}H_{10}O_4$
CAS Number:	*94-36-0*

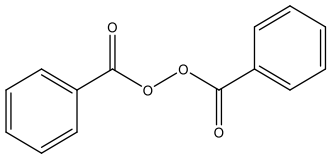

Trimethylamine in water was used, as received, in the heterogeneous quaternary amination of brominated poly(phenylene)'s.

Trimethylamine, aqu.	
Supplier:	*Acros Organics*
Purity:	*Pure, 7.3M aqu. soln*
Empirical Formula:	C_3H_9N
CAS Number:	*75-50-3*

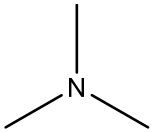

Trimethylamine in THF was used, as received, in the quaternary homogeneous amination of brominated poly(phenylene)'s.

Trimethylamine in THF.	
Supplier:	*Acros Organics*
Purity:	*1M solution in THF*
Empirical Formula:	*C_3H_9N*
CAS Number:	*75-50-3*

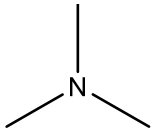

Vanadyl sulfate was used to prepare the starting electrolyte in the working vanadium redox flow battery, and in vanadium ion permeability studies.

Vanadyl(IV) Sulfate	
Supplier:	*Fisher Scientific*
Purity:	*17-23% V*
Empirical Formula:	*$VOSO_4 \bullet xH2O$*
CAS Number:	*12439-96-2*

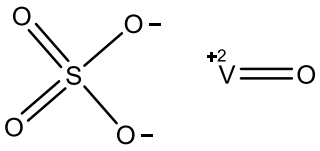

3.1.3 Commercial Polymers

Nafion® 117 (Nafion) is a sulfonated fluoropolymer developed and produced by DuPont™ Company. Due to the materials mechanical and thermal stability, high ion conductivity, and relatively low swelling, Nafion has become the benchmark for ionomer performance. The molecular weight has been recorded from estimates found in literature.[1]

DuPont™ Nafion® 117		
Supplier:	*Fuel Cells Etc*	
Thickness:	*183 micrometers*	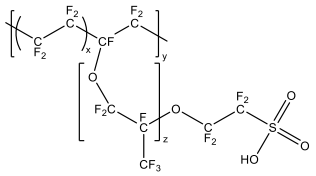
Molecular Weight:	*10^5-10^6 Da*	
IEC:	*0.95-1.01 meq/g*	
Conductivity:	*0.10 S/cm*	

3.2 Material Characterization

Various experimental techniques are required to fully characterize ionic polymeric materials. This section briefly describes the equipment and procedures utilized in this research.

3.2.1 Gel Permeation Chromatography (GPC)

The molecular weights and their distributions were obtained using an Agilent 1260 GPC/SEC System with a TL105 HPLC column heater from Timeberline Instruments®. The system consisted of a series of two linear PSS® SDV columns, with a porosity of 1000 Å and 100,000 Å and a separation range of 100 – 10,000 Da. The column combination has a separation range of 100 – 1,000,000 Da. A twelve point calibration curve, obtained within one day of data collection, was obtained using poly(styrene) standards with a molecular weight range of 474 – 2,520,000 Da from PSS® (PSS-pskitr1). The GPC was run with a tetrahydrofuran mobile phase, and a column temperature of 25 °C. The flow rate was 1 mL/min using an injection volume of 100 μL during operation. Samples were 0.1 wt. % and filtered through a 0.45 μm PTFE filters.

3.2.2 Fourier Transform Infrared Spectroscopy (FTIR)

Fourier Transform Infrared Spectroscopy (FTIR) was used to observe changes molecular structure during monomer preparation, as well as confirmation of the presence, and qualitative assessment, of functional groups in both anion- and cationomers. The instrument is a Nexus 670 ThermoNicolet FTIR with a deuterated triglycine sulfate (DTGS) detector and KBr beamsplitter. The equipment was operated an aperture diameter of 8 mm with an approximate area of 0.50 cm^2. To collect data on powders and thin films, a Smart SpeculATR single-bounce horizontal reflection accessory was used. For each sample, 30 scans were performed over a spectral range of 4000 – 400 cm^{-1}.

3.2.3 Thermal Gravimetric Analysis (TGA)

The thermal stability, weight loss, and degradation on-set temperatures of all non-functionalized and functionalized poly(phenylene) materials were assessed using a TA Instruments model Q 500 Thermo Gravimetric Analyzer. A 10 °C per minute scan rate from 50 °C to 700 °C was performed, under a 20 mL per minute N_2 purge flow rate. Thin film samples were loaded between 15-20 mg. In order to ensure no residual water was present, ionomer samples were heated to 110 °C for 30 minutes under N_2 prior to analysis.

3.2.4 Dynamic Mechanical Thermal Analysis (DMA)

A TA Instruments DMA Q800 was used to characterize the glass transition temperature and molecular transitions of the poly(phenylene)'s in this research. In a typical run, a static force of 0.010 N was applied and the temperature was equilibrated to 40.0 °C. The temperature was then

ramped at 2 °C per minute to 500 °C. Viscoelastic properties of some ionomers were obtained through a stress-strain analysis. In these tests the temperature was equilibrated at 20 °C, and the strain set to 0.01%. The displacement was then ramped from 1000 μm per minute to 25000 μm. Thin film dimensions for these tests had a length of roughly 10 mm, width of 2.5 mm, and thickness of 0.075 mm. In order to ensure a linear viscoelastic response, sample dimensions were set to ensure a length to width ratio of at least 3.

3.2.5 Differential Scanning Calorimetry (DSC) and State of Water Calculations

Thermal transitions of polymers were assessed using a TA instruments DSC Q20. For non-functionalized materials, the temperature was equilibrated at 50 °C, and then increased from 50 to 450 °C at a ramp rate of 10 °C/min under nitrogen atmosphere. This test was performed to observe high temperature phase transitions within the material.

For anion and cation exchange membranes, samples were soaked in DI-H_2O for 24 hours, blot dried, and then weighed. In a typical run, the temperature was equilibrated at -50 °C, and then increased from -50 to 75 °C at a ramp rate of 10 °C/min. This test was performed to observe the state of water within the hydrophilic regions of the materials. The data was used to determine the materials state of water. The amount of freezable water within the material was determined by the equation

$$\text{freezable w. c. } (\%) = \frac{100 \cdot \mathrm{H_{f,fw}(J\,g^{-1})}}{\mathrm{H_{f,w}(J\,g^{-1})}} \qquad 3 - 1$$

where $H_{f,fw}$ is the heat of fusion for the freezable water endotherm peak, and H_w is the heat of fusion for water (334 J/g). It follows that the percentage of bound water can be obtained using the equation.

$$\text{non} - \text{freezable w. c. (\%)} = 100 - \text{freezable w. c. (\%)}$$

3.2.6 Ion Exchange Capacity Determination by Titration

In order to observe the ion exchange capacity of the ionic polymer membranes, acid and base titrations were performed. For cation exchange membranes, the acid form of the ionomer was placed in a 1M NaCl solution. After soaking for 18 hours, the solution was titrated with a 0.01 M NaOH solution to an endpoint pH of 7 using an indicator. The IEC of the acid film, typically in milligram equivalents per gram, can then be calculated by

$$\text{IEC} = \frac{\text{v}_{\text{NaOH}}\text{C}_{\text{NaOH}}}{\text{m}_{\text{dry}} \cdot 0.001} \qquad 3 - 2$$

where v_{base} is the amount of base required during titration, C_{NaOH} is the concentration of the base, and m_{dry} is the mass of the dry polymer.

3.2.7 Water Absorption

In order to assess the nature of water in the synthesized ionomers in this research, and the role this property has on ion exchange, water absorption studies were performed. Water uptake, on a mass basis, can easily be determined gravimetrically. The acid form of membranes were allowed to soak in water for at least 24 hours. They were then removed, blot dried to remove

surface water, and weighed to obtain a wet mass (m_{wet}). The films were then placed in a vacuum at 100 °C for 24 hours, to be weighed again to determine the materials dry mass (m_{dry}). Water content can then be calculated by the equation

$$\text{w. c.} = \left(\frac{\text{m}_{\text{wet}} - \text{m}_{\text{dry}}}{\text{m}_{\text{dry}}}\right) \cdot 100\% \qquad 3 - 3$$

3.2.8 Density and Fractional Free Volume (FFV)

Density measurements were performed by using a Mettler Toledo XS205 analytical balance fitted with a Mettler density determination kit, based on Archimedes' principle. For non-functionalized materials, methanol was used as the auxiliary liquid. Fractional free volume (FFV) was determined by the equation

$$\text{FFV} = 1 - \left(\frac{\text{V}_\text{o}}{\text{V}}\right) \qquad 3 - 4$$

where V is the specific volume (i.e. the inverse of polymer density), and V_o the occupied volume. The occupied volume was determined using the group contribution method proposed by Bondi.[2] The occupied volume is given as,

$$\text{V}_\text{o} = 1.3\left(\sum_{\text{k}=1}^{\text{K}} (\text{V}_\text{w})_\text{k}\right) \qquad 3 - 5$$

where V_w is the van der Waals volume for each group contribution, *k*, for a total number of structural groups, *K*. The van der Waals volumes used in this work are presented in **Table 3- 1**.

Table 3- 1. Van der Waals volumes (V_w) for various structural groups.[3]

Group	V_w (cm^3/mol)
Phenyl	45.85
Phenyl (para/meta)	43.3
Phenyl (pentasub.)	-4.6
$-CH_3$	13.67

3.2.9 Hansen Solubility Parameters

Ionomers are typically biphasal, and therefore can display interesting solubility characteristics. Several methods have been developed to estimate polymer solubility parameters, most notably the Hoftyzer and van Krevelen solubility equations. In this work, the Hoftyzer and van Krevelen models were employed and compared to experimental observations to determine accuracy. A brief description of the theory behind these models will be discussed.

Hansen solubility parameters are governed by the assertion that total cohesion energy must equal the sum of dispersion, dipolar intermolecular and hydrogen bonding forces. This can be described as

$$E = E_d + E_p + E_h \qquad 3 - 6$$

By dividing by the molar volume, the square of the solubility parameter equals the square of the solubility of the components

$$\delta^2 = \delta_d^2 + \delta_p^2 + \delta_h^2 \qquad 3 - 7$$

In order to apply this equation, individual Hansen solubility data must be known for contributing groups within a material. Non-polar parameters were determined through a procedure outlined by Blanks and Prausnitz,[4] and were used by Hansen to determine solubility values for liquids. Based on polymer solubility in solvent systems, trial and error methods were originally used to determine cohesive energy density contributions from the polar and hydrogen bonding interactions. Later it was determined by Hansen and Skaarup that the Böttcher equation could be used to obtain an accurate estimations of the polar contribution.[5] One disadvantage of Hansen's three-component solubility parameter is that it required three dimensional representation. Many different two dimensional representations of Hansen solubility parameters have been proposed, including combining the dispersive and polar forces into a new parameter δ_v as

$$\delta_v = \sqrt{(\delta_d^2 + \delta_p^2)} \qquad 3 - 8$$

proposed by Bagley et al.[6]

Hoftyzer and Van Krevelen have developed a method, based on Hansen's assumptions, for the prediction of solubility components.[3] The equation are

$$\delta_d = \frac{\sum F_{di}}{V} \qquad 3 - 9$$

$$\delta_p = \frac{\sqrt{\sum F_{pi}^2}}{V} \qquad 3 - 10$$

$$\delta_h = \sqrt{\frac{\sum E_{hi}}{V}} \qquad 3 - 11$$

where F is a molar attraction constant originally proposed by Small.[7] Equation 3 - 10 only holds if one polar group is present, and the value of δ_p must be multiplied by a factor to account for symmetry. The factors are 0.5 for one plane of symmetry, 0.25 for two planes, and 0 for more planes. It was understood that the F-method was not applicable for the calculation of δ_h. The hydrogen bonding energy E_{hi} per structural group is approximately constant, giving equation 3 - 11. For several planes of symmetry, δ_h is equal to zero.

3.2.10 Flory-Rehner Equation

The Flory-Rehner equilibrium swelling theory observed the interaction of solvents with cross-linked network structures.[8] The theory considers the positive entropy change due to swelling equilibrium between a mixing polymer and solvent, the negative entropy change that results from polymer swelling deformation, and the heat of mixing of polymer and solvent.[9] The Flory-Rehner equation can be written as

$$-\left[\ln(1-v_2)+v_2+\chi_1 v_2^2\right] = \frac{V_1}{\bar{v}M_c}\left(1-\frac{2M_c}{M}\right)\left(v_2^{\frac{1}{3}}-\frac{v_2}{2}\right) \qquad 3 - 12$$

where v_2 is the volume fraction of polymer in the swollen mass, V_1 is the molar volume of solvent, $\bar{v}$ is the specific volume of polymer, M is the molecular mass of the polymer, M_c is the average molecular mass between cross links, and χ_1 Flory parameter that accounts for the energy of

interdispersing polymer and solvent molecules. By substituting in the number of active network chain segments per unit volume *n*, which is equal to polymer density over M_c, we obtain the equation

$$-\left[\ln(1-\mathrm{v}_2)+\mathrm{v}_2+\chi_1\mathrm{v}_2^2\right]=\mathrm{V}_1\mathrm{n}\left(\mathrm{v}_2^{\frac{1}{3}}-\frac{\mathrm{v}_2}{2}\right) \qquad 3\text{ - }13$$

Swelling and density data can be used to determine χ_1 using Equation 3 - 13. The volume fraction can be approximated by $\mathrm{v}_2=\frac{1}{1+\mathrm{Q}}$ and $\mathrm{Q}=\frac{\mathrm{W_s}\cdot\rho_\mathrm{p}}{\mathrm{W_p}\cdot\rho_\mathrm{s}}$, where *W* is the weight, and subscript *s* and *p* denote solvent and polymer respectively.

3.2.11 Liquid Diffusion

In order to assess molecular diffusion through the materials synthesized in this research, a liquid diffusion apparatus was utilized. The apparatus included a water jacketed, membrane-separated, 20 mL PermeGear® diffusion cell (**Figure 3 - 1**). Both compartments are temperature controlled, and vigorously stirred using submerged Teflon® magnetic stir bars. A 1 molar aqueous alcohol solution is placed in one compartment, and pure deionized water (DI-H_2O) in the other. In the DI-H_2O compartment, a sample stream is taken near the membrane to a Waters 410 Differential Refractometer, and recirculated back to the compartment using a Waters 515 HPLC pump at 10 mL/min. As alcohol diffuses through the membrane, the change in refractive index of the DI-H_2O compartment is monitored as a function of time. The RI signal is converted to an alcohol concentration using a predetermined calibration curve.

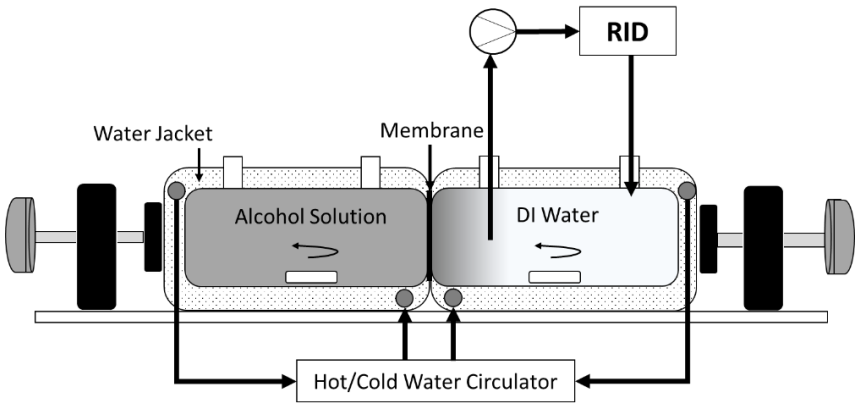

Figure 3 - 1. The apparatus used to observe liquid transport phenomena through a polymer.

The permeability of alcohol across the membrane as a function of concentration can be determined using the equation for flux, as expressed in Fick's first law

$$J_i = \frac{D_i}{l}\left(C_{i,x=0} - C_{i,x=l}\right) \qquad 3 - 14$$

where $C_{i,x=0}$ and $C_{i,x=l}$ are the concentrations of the upstream and downstream surfaces of the polymer membrane, respectively, D_i is the diffusion coefficient, and l is the polymer film thickness. The diffusion coefficient can then be obtained using the equations

$$J_i = \frac{dC_{i,x=l}}{dt}\frac{V_o}{A} \qquad 3 - 15$$

$$D_i = \frac{dC_{i,x=l}}{dt}\frac{V_o l}{C_{i,x=0} A} \qquad 3 - 16$$

3.2.12 Electrochemical Impedance Spectroscopy (EIS)

Electrochemical impedance spectroscopy, using an Autolab PGSTAT302N potentiostat/galvanostat and BT-112 conductivity cell, was utilized in order to observe in-plane proton and hydroxide ion conductivity at 100% humidity. Once the sample had been loaded, the cell was submerged in a hot water bath, accurate to 0.1 °C. In a typical impedance measurement, a small ac signal is imposed at a voltage of 10 mV across the membrane, at frequencies from 100 kHz to 100 Hz. The current response is measured and the effective resistance, or impedance, is represented in the form of a Nyquist plot. A Nyquist plot (**Figure 3 - 2**) displays the impedance as a real component (Z') on the x-axis, and an imaginary component (Z'') on the y-axis. In order to obtain the real resistance, the linear region of the Nyquist data is extrapolated to where the imaginary part is equal to zero. The ion conductivity is then

$$\kappa = \frac{l}{RA} \qquad 3 - 17$$

where R is the real impedance (at $Z'' = 0$), l is the distance between the sense electrodes, and A is the conducting membrane area.

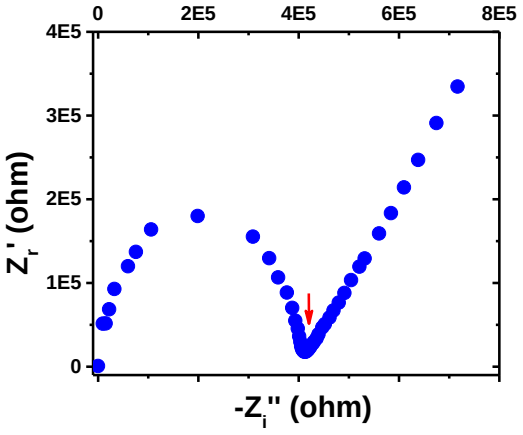

Figure 3 - 2. A Nyquist plot, showing the real (Z') and non-real (Z'') resistance.

Experiments were performed from 30 to 75 °C. The activation energy (E_a) for ion diffusion could then be calculated by fitting the Arrhenius equation

$$\sigma = \sigma^{\circ} \exp\left(-\frac{E_a}{RT}\right) \qquad 3 - 18$$

3.2.13 Nuclear Magnetic Resonance (NMR)

In order to confirm complete polymerization, determine copolymer composition, and the degree of bromination, ^{1}H NMR and ^{13}C NMR analysis were performed using a Bruker Avance III-HD 400 MHz NMR.

3.2.14 Atomic Force Microscopy (AFM)

Atomic force microscopy was performed on ionomers in this research using a Bruker ICON SPM using Peakforce Quantitative Nanomechanical Property Mapping (QNM). This feature enables high-resolution mapping of modulus and adhesion and a wide operating range. This technique was only performed on materials that were suspect of having surface structure, in order to better understand morphological impact on ion exchange properties. Thin films roughly 5 μm in thickness were prepared by dip coating onto silicon nanowafers.

3.2.15 X-Ray Scattering

Transmission small angle x-ray scattering (SAXS) was performed on a Rigaku SmartLab Diffractometer (Cu Kα, λ = 154 Å). Analysis was performed at 40kV and 44 mA. The 2θ range for X-ray scattering was 0.02-2°, where θ is the incident angle covering a *q* range of 0.014 – 1.14 nm^{-1}, where $q = 4\pi \sin\theta/\lambda$. Wide angle x-ray diffraction (WAXS) was performed under the same conditions, with a 2θ range of 2-50°, where θ is the incident angle covering a *q* range of 0.14 - 3.51 nm^{-1}.

3.2.16 Vanadium Redox Flow Battery (VRB)

A single-cell vanadium redox flow battery was used to assess how the synthesized materials perform in a VRB application, compared to a commercial standard ionomer. In this section, the equipment, cell, and software used to obtain performance data is described.

3.2.16.1 VRB Testing

The VRB system utilized in section 7.3.2 consisted of an electrochemical single-cell, a proton exchange membrane, and an Autolab PGSTAT302N potentiostat/galvanostat as a power source/sink. Each side of the cell had a borosilicate electrolyte tank, connected to the cell by Viton® tubing, and a Thermoscientific® FH100x peristaltic pump for electrolyte circulation.

In the remaining sections, a Gamry Interface 1000 potentiostat/galvanostat was used as a power source/sink, done so to allow this work to have greater autonomy and continue without

interruption. It is acknowledged that this may influence resistance measurements, and therefore data was not directly compared between systems.

3.2.16.2 VRB Cell

The VRB single-cell used in this research was the Scribner Liquid Cell Fixture, specifically designed to prevent contact between the electrolyte and the aluminum end plates. Contact between the liquid and the end plates would result in severe oxidation of the aluminum, and adversely affect data. A schematic of the single cell is presented in **Figure 3 - 3**. Each side of the cell, separate by the ion exchange membrane, consists of an aluminum endplate, a copper current collector, a graphite plate with serpentine flow, a Teflon® gasket, and a carbon felt electrode. In this study, the carbon felt electrode was 4.6 mm SIGRACELL® carbon felt (GFD4.6 EA). The gaskets used were sized to provide a nominal compression of 22%, necessary to increase contact and reduce electrode contributions to the cell ohmic resistance.

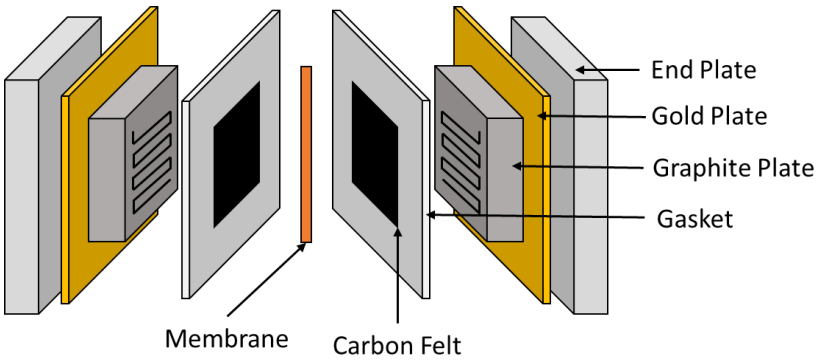

Figure 3 - 3. The components of the single cell used in the vanadium redox flow battery studies.

3.2.16.3 VRB Electrochemical Tests

A solution of 1 M $VOSO_4 \cdot xH_2O$ dissolved in 2.5 M H_2SO_4 was used as the starting electrolyte. 80 mL and 40 mL of the starting electrolyte were placed in the positive and negative electrolyte tanks, respectively. The negative half-cell tank was equipped with a nitrogen purge due to V^{2+} reactivity with air, and the electrolyte flow rate set to 20 mL min^{-1}. A constant current method with a current density of 30 mA cm^{-2} was used to charge the cell to 1.7 V. Once achieved, 40 mL of electrolyte was removed from the positive half-cell tank. Charge-discharge tests at 10-50 mA/cm^2, in 10 mA/cm^2 increments, were then performed with terminal voltages set at 1.7 V and 0.8 V respectively. An open circuit voltage (OCV) test was then performed, followed by charge-discharge cycling at 30 mA cm^{-2} to observe changes long term performance stability. On completion, the electrolyte tank volumes were measure to assess vanadium ion diffusion through the ion exchange membrane.

Since the vanadium redox flow battery is a custom set-up, tests were performed to ensure data consistency and reproducibility. In **Figure 3 - 4**, three separate Nafion 117 membranes were used in the cell. The obtained system efficiencies varied within 1%.

\

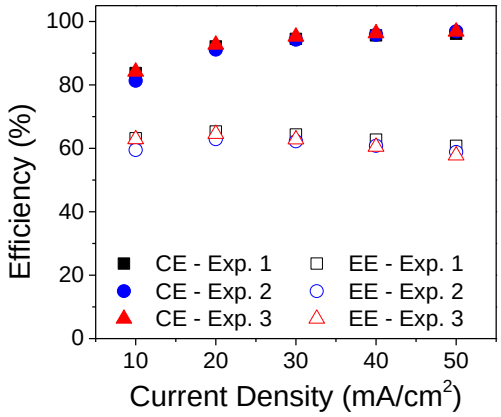

Figure 3 - 4. The working vanadium redox flow battery run three times with different Nafion 117 membranes to ensure the reproducibility of data.

3.2.17 Vanadium Ion Permeability

Vanadium ion permeability was measured using a liquid diffusion apparatus. The apparatus included a water jacketed, membrane-separated, 20 mL PermeGear® diffusion cell. Both compartments were temperature controlled, and vigorously stirred using submerged Teflon® magnetic stir bars. A 1 M $VOSO_4$ + 2.5 M H_2SO_4 solution is place in one compartment, and, to minimize the osmotic pressure effect, a 1 M $MgSO_4$ + 2.5 M H_2SO_4 in the other. Aliquots were taken near the membrane every 2 hours, and analyzed using UV-VIS spectroscopy. A predetermined calibration curve was used to determine vanadium ion concentration as a function of time.

3.2.18 Ionomer Degradation

To gain insight into degradation limitations of polymer films, a material was placed in a solution of 0.1 M V^{5+} and 5 M H_2SO_4 at 60 °C for a number of days. The V^{5+} solution is bright yellow, and changes to blue during polymer degradation, attributed to electrolyte reduction to the VO^{2+} ion during backbone degradation. This *ex-situ* method allows one to qualitatively observe gradual changes in solution and membrane color.

3.3 References

[1] Curtin, D. E.; Lousenberg, R. D.; Henry, T. J.; Tangeman, P. C.; Tisack, M. E. *J. Power Sources* **2004**, *131*, 41–48.

[2] Bondi, A. A. *Physical properties of molecular crystals liquids, and glasses.*; 1968.

[3] Van Krevelen, D. W.; Te Nijenhuis, K. *Properties of Polymers: Their Correlation with Chemical Structure; Their Numerical Estimation and Prediction from Additive Group Contributions*; 4th ed.; Elsevier: Amsterdam, 2009.

[4] Blanks, R. F.; Prausnitz, J. M. *Ind. Eng. Chem. Fundam.* **1964**, *3*, 1–8.

[5] Hansen, C.M., and Skaarup, K. *J. Paint Technol.* **1967**, *39*, 511–514.

[6] Bagley, E.B.; Nelson, T.P.; Scigliano, J. M. *J. Paint Technol.* **1971**, *43*, 35–42.

[7] Small, P. A. *J. Appl. Chem.* **1953**, *3*, 71–80.

[8] Flory, P. J.; Rehner, J. *J. Chem. Phys.* **1943**, *11*, 521–526.

[9] Sperling, L. H. *Introduction to Physical Polymer Science*; 4th ed.; John Wiley and Sons Inc.: Hoboken, New Jersey, 2006.

Chapter 4 Homopolymer and Multi-Block Diels-Alder Poly(phenylene)s: Synthesis, Physical Properties, and Structural Characterization

4.1 Introduction

Diels-Alder poly(phenylene)'s are highly amorphous and rigid polymers with elevated thermochemical and mechanical stability[1–3] that have been under consideration for numerous applications.[4–6] The materials have exhibited surprisingly high flexibility due to meta- catenation and twisting conformations around the backbone.[7,8] In this chapter mechanical and thermal properties, as well as an x-ray structural analysis of highly phenylated methylated and non-methylated poly(phenylene) homopolymers and block copolymers is reported.

4.2 Experimental

4.2.1 Poly(phenylene) Synthesis

Synthesis of 4-phenylglyoxalybenzil (bisbenzil) was performed through a modification of work by Carlsen et al (**Scheme 4- 1**).[9] In a typical procedure, a three neck flask was equipped with a mechanical mixer and condenser. 1,4-Bis(phenylethynyl)benzene (50.0g, 179.63 mmol), dichloromethane (250 mL), sodium metaperiodate (192.11g, 898.172 mmol), ruthenium chloride (0.198g, 0.955 mmol), water (240 mL), and acetonitrile (165 mL) were charged to the reaction vessel. Once mixing had begun, a small exotherm of roughly 15 °C was observed. The reaction, under rigorous mixing, was allowed to continue for 18 hours. On completion, the organic phase was decanted and filtered. The solution was neutralization with a 1M NaOH solution, washed with

water, and filtered through Celite®. Recrystallization in ethanol gave pure, bright yellow, bisbenzil. Yields were typically between 35 and 40%.

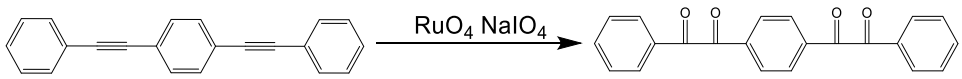

Scheme 4- 1. Ruthenium catalyzed oxidation of 1,4-bis(phenylethynyl)benzene to form 4-phenylglyoxalybenzil (bisbenzil).

Synthesis of bis(cyclopentadienone) were performed by a base catalyzed aldol condensation reaction, through a modification of work by Ogliaruso *et al*.[10] In a typical procedure, bisbenzil (10.0g, 29.21 mmol), 1,3-diphenylacetone (12.28g, 58.42 mmol), and ethanol (180 mL) were charged to a 3-neck round bottom flask. The round bottom flask was equipped with a nitrogen purge and mechanical mixing. A separate catalyst solution was prepared by dissolving KOH (3.74g, 66.60 mmol) in ethanol (10 mL) and a small amount of water. The reaction vessel was heated to 75 °C, and the catalyst solution was added droppwise. After 30 minutes the reaction was halted, cooled, and the precipitate collected via filtration. The product was washed with ethanol and water, recrystallized in toluene, and washed with ethanol again to give a dark brown solid. Yields were typically from 75-85%.

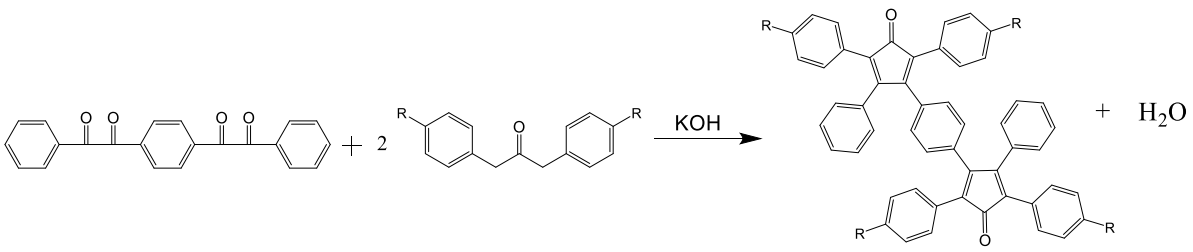

Scheme 4- 2. Aldol addition/condensation reaction between bisbenzil and 1,3-diphenyl-2-propanone to form bis(2,4,5-triphenylcyclopentadienone) (bis(cyclopentadienone)).

Poly(phenylene), methylated poly(phenylene), and block copolymers were synthesized via Diels-Alder polymerization, as reported elsewhere.[11] The described procedure is for the synthesis of the homopolymer poly(phenylene) (**Scheme 4- 3**). Bis(cyclopentadienone) (15.00 g, 18.36 mmol), 1,4-diethynylbenzene (2.316 g, 18.36 mmol), and 125 mL of diphenyl ether were charged to a reaction vessel. The reaction vessel was sealed, and the solution freeze-pump-thawed three times. The vessel was flooded with argon, and heated to 180 °C while stirred with a magnetic stir bar. The solution color typically changed from dark brown to orange after four hours, however the reaction was allowed to continue for 24 hours to maximize the molecular weight. Upon completion, the solution was precipitated into acetone, to give the tan polymer poly(phenylene) (PP). A random copolymer (RC) was formed through a Diels-Alder reaction with molar equivalents of methylated and non-methylated bis(cyclopentadienone). To form block copolymers (BC), blocks were synthesized in separate reactions, controlling molecular weight via Carothers equations. The blocks were then purified, analyzed, and subsequently copolymerized (**Figure 4 - 1**).

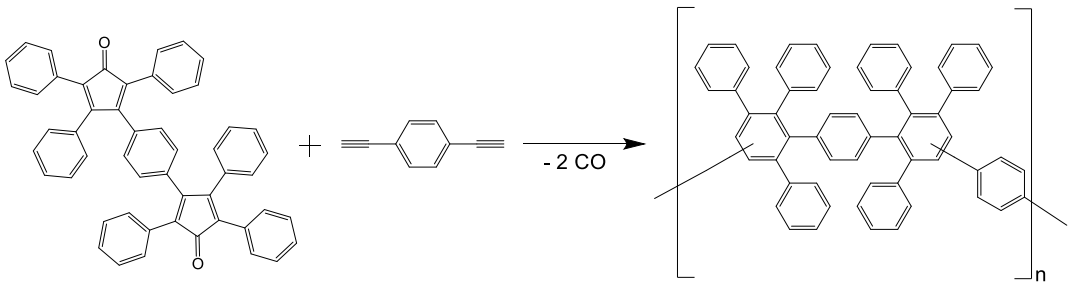

Scheme 4- 3. Polymerization reaction between bis(cyclopentadienone) and diethynyl benzene to form poly(phenylene).

The polymers and copolymers were dissolved in methylene chloride 2% by weight, and pipetted into a glass mold. The rate of solvent evaporation was controlled by covering the mold with a glass slide, and the solvent was allowed to slowly evaporate over 24 hours. Films were placed in a vacuum oven to ensure complete removal of solvent. The orange, transparent, and creasable films had thicknesses that were controlled to 85-90 μm.

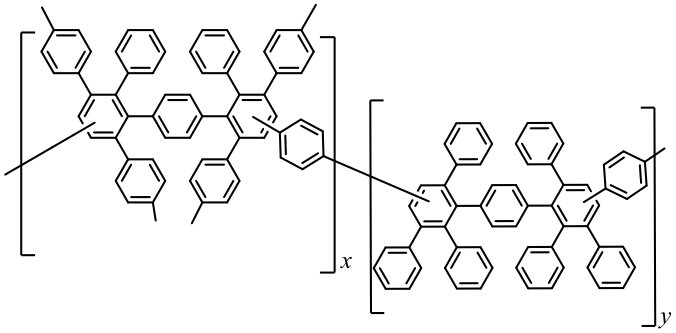

Figure 4 - 1. Chemical structure of MPP-PP block copolymers.

4.3 Results and Discussion

4.3.1 Molecular Weight Analysis

Several Diels-Alder poly(phenylene) (PP) polymerizations were performed with different reaction times, giving various molecular weight distributions (**Table 4 - 1**). There existed a somewhat linear increase in the number average molecular weight (M_n) as a function of reaction time. The weight average molecular weight (M_w) plateaued after 38 hours to give a final M_w of 192,000 g/mol. The polydispersity index (PDI), although showed no fixed trend, appeared to increase with increasing reaction time, indicating increasing heterogeneity. Despite numerous precautions, larger PDI's may be due to the presence of water, air, or chemical impurities in the system.

Table 4 - 1. The weight average (M_w), number average (M_n) and *z*-average (M_z) molecular weight distributions, and peak molecular weight (M_p) and polydispersity index (PDI), for poly(phenylene)'s obtained after various polymerization reaction times.

Sample	Reaction Time (h)	M_n (g/mol)	M_w (g/mol)	M_z (g/mol)	M_p (g/mol)	PDI
PP - 1	18	7.40E+04	1.44E+05	2.54E+05	1.21E+05	1.94
PP - 2	28	7.96E+04	1.71E+05	3.53E+05	1.31E+05	2.14
PP - 3	38	7.50E+04	1.89E+05	4.42E+05	1.42E+05	2.52
PP - 4	48	8.10E+04	1.94E+05	3.78E+05	1.53E+05	2.40
PP - 5	48	7.87E+04	1.92E+05	4.03E+05	1.37E+05	2.43

The poly(phenylene) homopolymers and block copolymers were analyzed using ^{1}H NMR to determine polymer structure, and the fraction of methylated to non-methylated repeat units. As shown in **Figure 4 - 2**, the ^{1}H NMR spectra consisted of two regions of interest (A and B). In every spectra the aromatic protons were evident from 7.5 to 6.0 ppm, and a methyl proton triplet at 2.5-2.0 ppm was observed in the methylated poly(phenylene) and block copolymers. The reason a triplet is detected is not entirely certain, but has been observed in other studies surrounding MPP and has been attributed to irregularities of the regiochemistry of the polymer backbone.[4] The integration of regions A and B were used to determine the fraction of methylated to non-methylated repeat units.

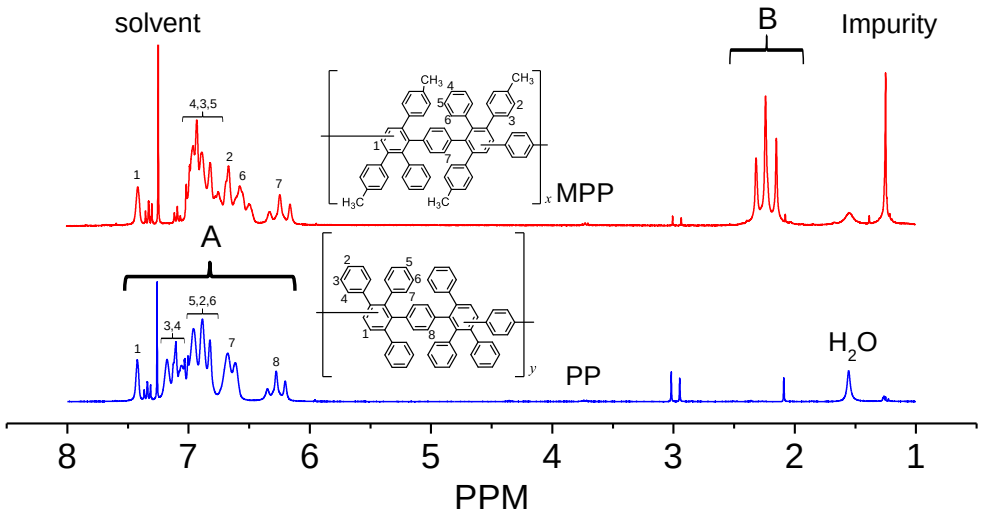

Figure 4 - 2. ^{1}H NMR spectra of poly(phenylene) (PP) and methylated poly(phenylene) (MPP).

Block compositions and molecular weight distributions (MWD) of individual blocks and polymers are shown in **Table 4 - 2**. Previous reports have shown a strong dependence between MWD and reaction time, temperature and concentration.[7,12] Weight average molecular weights

(M_w) for all Diels-Alder polymerizations ranged from 153,000 to 192,000 g/mol. The polydispersity index (PDI) of roughly two is typical for condensation reactions. A higher PDI of 2.7 was observed for MPP-PP B1, which is due to a lower number-average molecular weight (M_n) and signals a larger concentration of oligomers.

Table 4 - 2. Molecular weight distributions and repeat unit compositions for the parent homopolymers, and random and block copolymers.

	M_{nx} (10^3 g/mol)	M_{ny} (10^3 g/mol)	Composition f_{MPP}:f_{PP}	M_n (10^4 g/mol)	M_w (10^4 g/mol)	PDI -
PP	-	-	0.00:1.00	7.87	19.2	2.4
MPP-PP RC	-	-	0.44:0.56	7.52	15.3	2.0
MPP-PP B2	16.8	16.3	0.44:0.56	7.62	17.5	2.3
MPP-PP B1	11.2	8.87	0.53:0.47	5.64	15.4	2.7
MPP	-	-	0.96:0.04	8.99	18.0	2.0

4.3.2 Solubility, Density, and Fractional Free Volume (FFV)

All the polymers discussed in this chapter displayed good solubility in a wide range of common organic solvents, including toluene, chloroform, and THF. Previous reports have attributed the high degree of solubility to polymer stereochemistry. In each [4+2]-cycloaddition two distinct regioisomers are possible which leads to the possibility of both para- and meta- couplings within

the main polymer chain (**Figure 4 - 1**). Stille and Noren, using a model reaction under similar conditions, reported that no more than 50% of meta-isomers were produced.[7] However, a later study concluded that 83% of isolated polymer was of the m,m-isomer.[12] Therefore the high degree of solubility has been attributed to meta-catenation, as well as significant twisting conformations that limit or block conjugation.[8] Meta linkages, reducing polymer symmetry and increasing entropy, have also been shown to decrease the glass transition temperature, a phenomenon that has been widely documented in other polymer systems.[13,14]

Table 4 - 3 shows polymer density and calculated fractional free volume (FFV). Fractional free volumes were obtained that lie between that of poly(sulfone)s and poly(phenylene oxide)s.[15,16] The values vary over a narrow range, and do not appear to the correlated to physical properties of the materials. It is suspected that Bondi's group contribution method, used to determine a theoretical value for the occupied volume, does not accurately describe changes in chain conformation induced by block and random copolymerization in this study. Therefore the specific volume ($V = 1/\rho$) will be discussed. PP and MPP display the lowest and highest specific volumes, of 646 and 738 $cm^3\ mol^{-1}$, respectively. Despite similar chemical compositions, the random copolymer specific volumes lies between that of the homopolymers, and differs to that of block copolymers. This increase in specific volume suggests that the presence and increase of the methyl block length disrupts chain packing. This may indicate that block copolymerization is affecting the packing of polymer chains, whereby V increases with chain length.

Table 4 - 3. Density, occupied volume (V_o), specific volume (V) and fractional free volume (FFV) of the parent polymers.

	M (g/mol)	ρ (g/cm^3)	V_o ($cm^3\ mol^{-1}$)	V ($cm^3\ mol^{-1}$)	FFV	Composition f_{MPP}:f_{PP}
PP	761.0	1.178	458	646	0.291	0.00:1.00
MPP-PP RC	785.7	1.139	484	690	0.299	0.44:0.56
MPP-PP B2	785.7	1.130	484	695	0.304	0.44:0.56
MPP-PP B1	790.8	1.152	489	687	0.288	0.53:0.47
MPP	817.0	1.107	516	738	0.301	0.96:0.04

4.3.3 Thermal Transitions and Degradation

Dynamic thermal mechanical analysis (DMA) and differential scanning calorimetry (DSC) under nitrogen were used to identify thermal transitions and are listed in **Table 4 - 4**. DSC for Diels-Alder poly(phenylene)'s has been shown to give poorly resolved curves.[2] Although this was observed, the second run yielded no thermal transitions below the glass transition temperature (Tg). DSC reveals that homopolymers PP and MPP and the highest and lowest Tg's, respectively. This suggests that the methyl moiety disrupts chain packing, hindering phenyl ring entanglements. Tg of the random and block copolymers increased with increasing non-methylated (PP) block length.

Table 4 - 4. Glass transition temperatures obtain by DSC and DMA, tan delta at 200 °C, and the temperature at 5% weight loss for the parent polymers.

	DSC Tg (°C)	DMA Tg (°C)	tanδ at 200 °C	$T_d^{5\%}$ (°C)
PP	390	400[a]	0.043	581
MPP	365	382	0.037	552
MPP-PP RC	379	384	0.041	601
MPP-PP B1	380	400	0.036	600
MPP-PP B2	384	403	0.036	589

[a] *Polymer failure.*

The glass transition temperatures (Tg) obtained by DMA is defined by a drop in storage modulus and a tan delta peak, as shown in **Figure 4 - 3**. The Tg's obtained using DSC and DMA differed by up to 20 °C. The loss modulus of some samples display a broad low temperature β transition between 250 and 350 °C suggesting increased segmental mobility, likely due to reorientation of pendant aromatic rings. This transition was also evident in the first run of the DSC thermograms (**Figure 4 - 3c**), however was not present on subsequent temperature cycles. It is clear that the methylated materials display far less chain relaxation in this region. In addition, tanδ at 200 °C decreases with the addition of the methyl moiety, indicating a higher elastic response to deformation. These observations suggest that despite lowering the Tg via disruption of chain packing, the addition of the methyl moiety hinders low temperature pendant ring rotation that restricts low temperature segmental mobility. Although well below the degradation temperature,

the methylated materials display a sharp upturn in storage modulus, as well as a second peak in the loss modulus, at roughly 400 °C. This indicates some degree of crosslinking, increased by the presence of the methyl moiety. To support this hypothesis it was observed that all DSC samples that were briefly heated to 450 °C would swell, but were insoluble, in chloroform. This behavior has not yet been investigated and will be explored further.

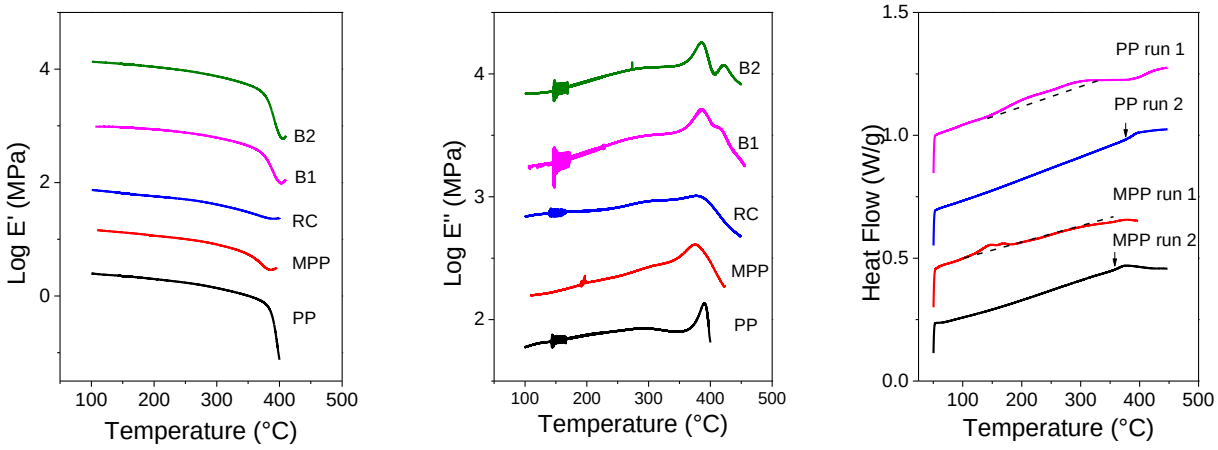

(a) (b) (c)

Figure 4 - 3. The DMA temperature effects upon the (a) storage modulus and (b) loss modulus of PP, MPP, and PP-MPP multi-blocks. The (c) first and second DSC thermograms for the homopolymers PP and MPP.

Thermal gravimetric analysis (TGA) was performed to determine material temperature stability (**Figure 4 - 4**). All materials displayed a sharp one-step degradation. MPP had the lowest onset of degradation at 539 °C, and five percent weight loss ($T_d^{5\%}$) occurring at 552 °C, suggesting high temperature methyl group instability. The block copolymers displayed increasing stability with increasing block length. The onset of degradation for MPP-PP B1 and MPP-PP B2 was 576 and 569 °C, respectively. Finally, poly(phenylene) displayed the greatest stability, with an onset

of degradation of 581 °C, and a $T_d^{5\%}$ of 576 °C. The amount of residue (char) increased with the addition of the methyl moiety, from 67% for PP to 83-85% for the block copolymers. This observation further supports evidence of crosslinking in the methylated materials, observed by less stripping of volatiles and more char.[17] The degradation of these materials is still under investigation.

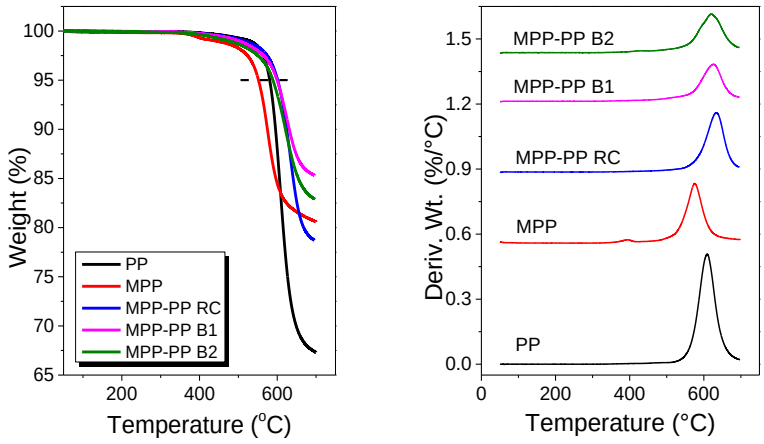

(a) (b)

Figure 4 - 4. Thermal gravimetric properties of PP, MPP, and PP-MPP multi-blocks.

4.3.4 Structural Analysis

The x-ray diffraction patterns for all materials, obtained by wide-angle x-ray scattering, are shown in **Figure 4 - 5**, and summarized in **Table 4 - 5**. Despite only small changes in polymer chemistry, the homopolymers PP and MPP display significantly different x-ray spectra. Three peaks are evident, correlating to diffraction plane distances (d-spacing's) of roughly 11.2, 5.5, and 2.1 Å. Large peak breadths are the result of the amorphous nature of the materials. Peak d-2 is the pervasive "amorphous halo", that is observed in polymer melts, glasses and rubbers. Peak d-1 has been most commonly observed in atactic polystyrene, and is referred to as the "polymerization

peak".[18–20] This peak is not observed in most other glassy polymers, and despite great efforts it is still not well understood. In a molecular dynamics simulation of atactic polystyrene, peak contributions were determined that were in agreement with experimental observations.[21] The study concluded that the "polymerization peak" (d-1) was the true amorphous peak, as it reflected inter chain packing. The higher *q* peak (d-2) was found to be mainly due to side chain (phenyl-phenyl) correlations, while peak d-3 can be attributed to side chain-backbone intramolecular interactions.

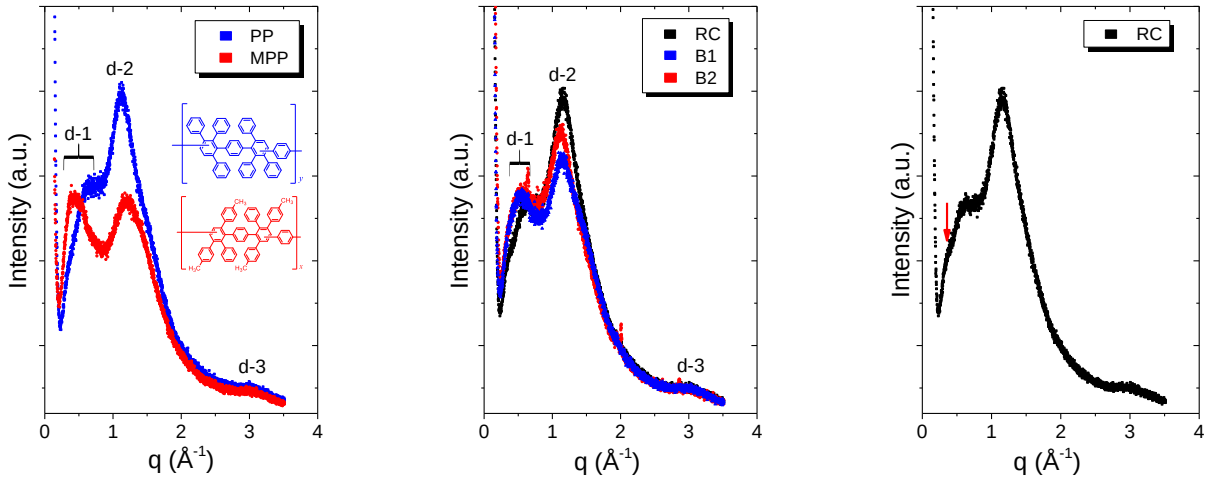

(a) (b) (c)

Figure 4 - 5. The raw x-ray diffraction patterns of the parent polymers.

Table 4 - 5. Parameters for diffraction peaks for polymers.

	d-1	d-2	d-3
PP			
2-theta	9.2	15.7	42.6
q ($Å^{-1}$)	0.65	1.12	3.00
d-spacing (Å)	9.6	5.6	2.1
MPP			
2-theta (θ)	6.3	16.8	42.0
q ($Å^{-1}$)	0.45	1.20	2.96
d-spacing (Å)	14.1	5.2	2.1
MPP-PP RC			
2-theta (θ)	8.8	16.3	41.8
q ($Å^{-1}$)	0.63	1.16	2.95
d-spacing (Å)	10.0	5.4	2.1
MPP-PP B1			
2-theta (θ)	8.1	15.8	42.7
q ($Å^{-1}$)	0.58	1.12	3.01
d-spacing (Å)	10.8	5.6	2.1
MPP-PP B2			
2-theta (θ)	7.7	16.2	41.5
q ($Å^{-1}$)	0.55	1.15	2.93
d-spacing (Å)	11.4	5.5	2.1

In **Figure 4 - 6** the distance between diffraction planes (d-spacing) of the d-1 feature was plotted as a function of the methylated block *-mer* length, specific volume (V), and fractional free volume (FFV). This large feature is of particular interest as it is suggests ordering in the amorphous region of the material. As discussed, the calculated FFV displays little variation between polymers, and therefore reveals no correlation. A strong relationship is observed between methylated *–mer* length and d-spacing, signifying the importance of both block length and chemistry. The amorphous feature is well correlated to an increase in specific volume (**Figure 4 - 6b**), except for that of the random copolymer. As highlighted in **Figure 4 - 6c**, the random copolymer appears to have a low-q shoulder in the amorphous peak, which may account for the discrepancy.

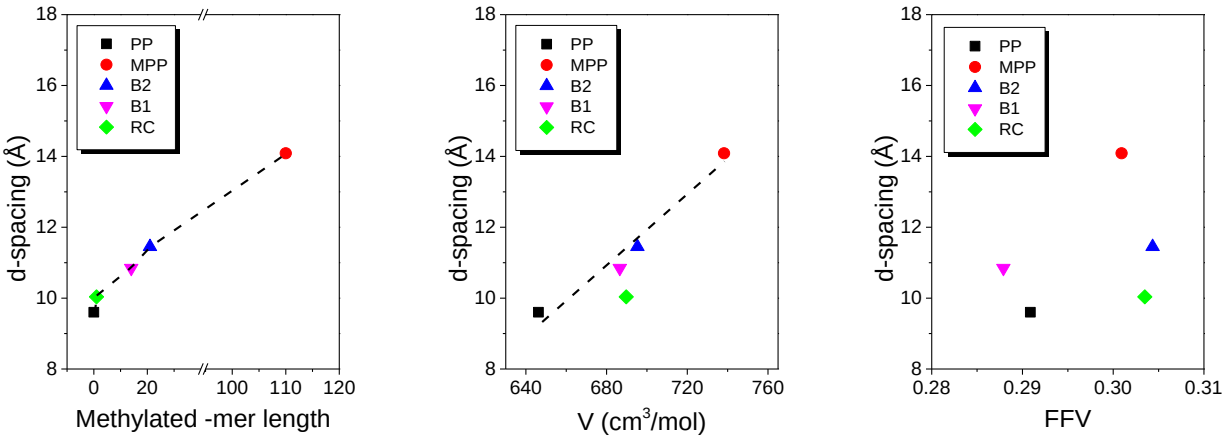

(a) (b) (c)

Figure 4 - 6. The distance between diffraction planes (d-spacing) of the d-1 feature as a function of (a) methylated block *–mer* length, (b) specific volume (1/ρ) and (c) fractional free volume (FFV).

4.4 Conclusions

The physical properties and an x-ray structural analysis is reported for Diels-Alder methylated poly(phenylene) (MPP) and non-methylated poly(phenylene) (PP) homopolymers, a random copolymer, and MPP-PP block copolymers synthesized using Diels-Alder chemistry. Glass transition temperatures of the random and block copolymers decreased with increasing methyl block length, from 390 °C to 365 °C. In addition, a low temperature relaxation was observed from 250 °C to 300 °C, particularly prominent in the non-methylated poly(phenylene). It was concluded that the presence of the methyl moiety not only lowers the Tg via disruption of chain packing, but hinders phenyl ring rotation that restricts low temperature segmental mobility. Materials displayed high thermal stability, with a sharp one-step degradation. MPP had the lowest onset of degradation at 539 °C, and five percent weight loss ($T_d^{5\%}$) occurring at 552 °C, suggesting high temperature methyl group instability. It has been demonstrated that methylation and block copolymerization of Diels-Alder poly(phenylene)'s have significant effect on the conformation of the membrane, as indicated by changes in the x-ray diffraction amorphous peak ("polymerization peak"). The amorphous peak that describes inter chain packing was directly correlated to polymer chemistry, chain mobility, and found to be proportional to the specific volume.

4.5 References

[1] Mukamal, H.; Stille, J. K.; Harris, F. W.; Rakutis, R. O. *J. Polym. Sci. Part A-1 Polym. Chem.* **1967**, *5*, 2721–2729.

[2] Stille, J.; Rakutis, R. O.; Mukamal, H.; Harris, F. w. *Macromolecules* **1968**, *1*, 431–436.

[3] Kumar, U.; Neenan, T. X. *Macromolecules* **1995**, *28*, 124–130.

[4] Hibbs, M.; Fujimoto, C.; Cornelius, C. *Macromolecules* **2009**, *42*, 8316–8321.

[5] Stanis, R. J.; Yaklin, M. a.; Cornelius, C. J.; Takatera, T.; Umemoto, A.; Ambrosini, A.; Fujimoto, C. H. *J. Power Sources* **2010**, *195*, 104–110.

[6] Fujimoto, C.; Kim, S.; Stains, R.; Wei, X. *Electrochem. …* **2012**, *20*, 48–51.

[7] Stille, J.; Noren, G. *Macromolecules* **1972**, *5*.

[8] Berresheim, A. J.; Müller, M.; Müllen, K. *Chem. Rev.* **1999**, *99*, 1747–1785.

[9] Carlsen, P.; Katsuki, T. *J. Org. …* **1981**.

[10] Ogliaruso, M. *J. Org. …* **1963**.

[11] Kumar, U.; Neenan, T. *Macromolecules* **1995**, *28*, 124–130.

[12] Shifrina, Z. B.; Averina, M. S.; Rusanov, A. L.; Wagner, M.; Mu, K. **2000**, 3525–3529.

[13] Qu, W.; Ko, T. M.; Vora, R. H.; Chung, T. S. *Polymer (Guildf).* **2001**, *42*, 6393–6401.

[14] Oroujzadeh, M.; Mehdipour-Ataei, S.; Esfandeh, M. *Eur. Polym. J.* **2013**, *49*, 1673–1681.

[15] Bhole, Y. S.; Karadkar, P. B.; Kharul, U. K. *Eur. Polym. J.* **2007**, *43*, 1450–1459.

[16] Aitken, C. L.; Koros, W. J.; Paul, D. R. *Macromolecules* **1992**, *25*, 3651–3658.

[17] Wall, L. a. *J. Elastomers Plast.* **1973**, *5*, 36–65.

[18] Schubach, H. R.; Nagy, E.; Heise, B. *Colloid Polym. Sci.* **1981**, *259*, 789–796.

[19] Katz, J. R. *Rubber Chem. Technol.* **1936**, *9*, 357–372.

[20] Mitchell, G. R.; Windle, A. H. *Polymer (Guildf).* **1984**, *25*, 906–920.

[21] Ayyagari, C.; Bedrov, D.; Smith, G. D. *Macromolecules* **2000**, *33*, 6194–6199.

Chapter 5 Transport in Sulfonated Poly(phenylene)s: The Effect Membrane Morphology, Ion Conductivity, Liquid Permeability, and the State of Water

5.1 Introduction

Cation exchange membranes (CEMs) have received much attention due to growing interest in applications for energy generation and storage, namely proton exchange membrane fuel cells (PEMFCs) and redox flow batteries. Ongoing efforts are made to produce low cost PEMs with high proton conductivity, mechanical strength, and thermochemical stability.[1] Sulfonated phenyl-containing ionomers have revealed highly competitive properties. Significant efforts have been made regarding the understand of the chemical and morphological dependence on ion transport for sulfonated poly(ether ether ketone)s,[2–4] poly(fluorenyl ether ketone)s,[5–7] poly(sulfone)s,[8–10] and many others. In order to optimize materials for a given application, the understand of the interrelationships between an ionomers chemical, physical, and electrochemical transport properties is required.

Recently, a phenylated sulfonated Diels-Alder poly(phenylene) was synthesized that revealed highly competitive properties.[11–13] In this work, these materials were synthesized and studied to better understand the interrelationship of ionomer properties, and, in Chapter 7, to be used in the analysis of vanadium redox flow battery performance. In this chapter, the effect of membrane morphology and ion content on proton conductivity, liquid permeability, and the state of water for a series of random sulfonate Diels-Alder poly(phenylene)'s is investigated.

5.2 Experimental

5.2.1 Poly(phenylene) Sulfonation

Poly(phenylene)s were functionalized by sulfonation using chlorosulfonic acid in chloroform (**Scheme 5- 1**), as described elswhere.[11] Materials were prepared with varying degrees of sulfonation. The procedure described is for a degree of sulfonation of 3. Poly(phenylene) (9.00g, 11.8 mmol) was dissolved in 135 mL of methylene chloride and charged to a flame dried, mechanically stirred, reaction vessel. The vessel was put under an argon purge, and the temperature set to roughly -79 ^{o}C (dry ice and acetone bath). A solution of chlorosulfonic acid (4.13g, 35.48 mmol) in 5 mL of chloroform was added drop-wise over 5 minutes. After 30 minutes the reaction mixture was warmed to room temperature and the organic phase decanted, to leave a black solid precipitate. 300 mL of 0.5 M sodium hydroxide solution was introduced into the reaction vessel, which, under stirring, was allowed to react overnight to ensure complete neutralization. The precipitate was then collected and washed with water to give a tan solid.

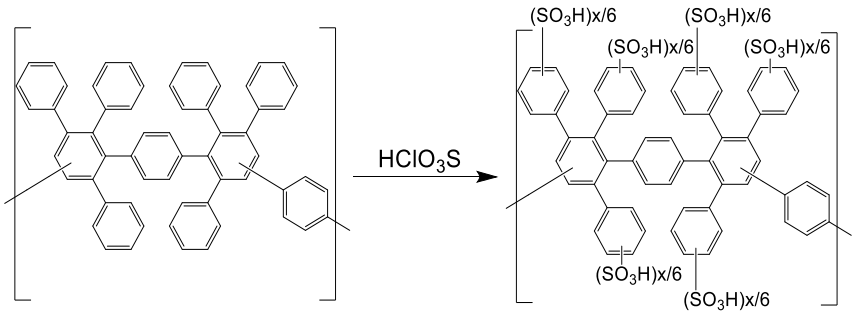

Scheme 5- 1. Homogeneous post-sulfonation of poly(phenylene) via cholorosulfonic acid.

Sulfonated poly(phenylene) membranes were cast in dimethylacetamide (5 wt. % polymer). The solutions were filtered using a 45 micron PTFE syringe filter and poured onto a glass plate in a vacuum oven. Films were allowed to form for 24 hours, under vacuum, at 50 ^{o}C. The polymer membranes were removed from the glass plate by submerging the plate in deionized water.

5.3 Results and Discussion

5.3.1 Chemistry and Morphology

In order to assess the structural changes in the polymer before and after functionalization, infrared spectroscopy was performed. The stretching and bending vibrations of covalent bonds, caused by radiation from the infrared region of the electromagnetic spectrum, can confirm the presence of particular functional groups. A quantitative assessment on the magnitude of functionalization can also be achieved, due to the relationship between covalent bond quantity and peak intensity. A morphological assessment was achieved through the use of atomic force microscopy (AFM) and x-ray scattering. Ionomers have been shown to exhibit a wide array of morphologies, which can have drastic implications on polymer properties.[14]

IR spectra was performed on the parent polymer to confirm complete conversion and polymer structure (**Figure 5- 1a**). Phenyl carbon-carbon stretching typically occurs around 1500-1400 cm^{-1} for phenylated molecules, and can be seen at 1490 cm^{-1} and 1440 cm^{-1}. Carbon-hydrogen out of plane bending peaks are evident at 692 cm^{-1} and 758 cm^{-1}. IR spectra for the sulfonated materials were normalized over the 1440 cm^{-1} C-C phenyl peak. IR spectra confirmed the presence of sulfonic acid functional groups within the structure of the polymer. As expected

there was little change in the stable aromatic carbon-carbon bonds located from 1400-1600 cm^{-1}. The phenyl out of plane C-H peak at 758 cm^{-1} is diminished in the sulfonated polymer as hydrogen is lost during the sulfonation reaction. The S=O sulfonate group assymetric and symmetric stretching can be seen at 1124 cm^{-1} and 1169 cm^{-1}, respectively. The S-O stretch can be seen by a strong band at 1008 cm^{-1}. In **Figure 5- 1b**, peaks corresponding to sulfonic acid groups increase in intensity with increasing ion exchange capacity, while the phenyl C-H OOP peaks decrease in intensity, confirming sulfonation on the pendant phenyl rings.

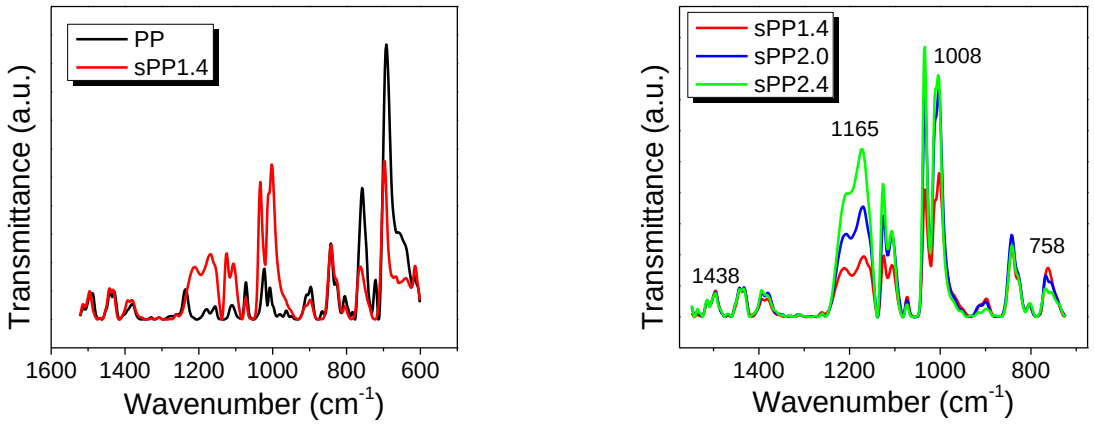

(a) (b)

Figure 5- 1. FTIR spectra of (a) the parent polymer poly(phenylene) (PP) and sulfonated material sPP 1.4, and (b) FTIR spectra of all sulfonated poly(phenylene)s.

In order to observe if quantification of the extent of functionalization was possible using IR, the ratio of the intensities of the 1438cm^{-1} and 1124cm-^{1} peaks were taken, and plotted against the experimental ion exchange capacities of sPP (**Figure 5- 2**). A linear correlation was observed, providing further confirmation of successful sulfonic acid incorporation into the backbone of the polymer, and indication of good synthetic control over polymer ion content.

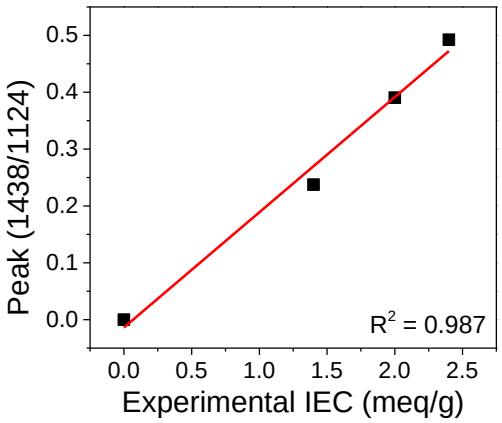

Figure 5- 2. The ratio of the intensities of the 1438 cm^{-1} and 1124 cm^{-1} peaks vs. the experimental ion exchange capacities (IEC) of sPP.

Typically morphological studies of ionic polymers can be challenging. Some success has been achieved through transmission electron microscopy, although the technique cannot be performed on hydrated materials and requires pretreatment with a stable neutralizing cation (i.e. Pb^{+2}). In this work, a morphological assessment has been performed on the surface of the ionomer membranes using an atomic force microscopy feature, peakforce quantitative nanomechanical property mapping (AFM-QNM). This feature enables high-resolution mapping of modulus and adhesion over a wide operating range. One challenge accosted with this technique is ensuring films are completely flat, and surface defects are minimized.

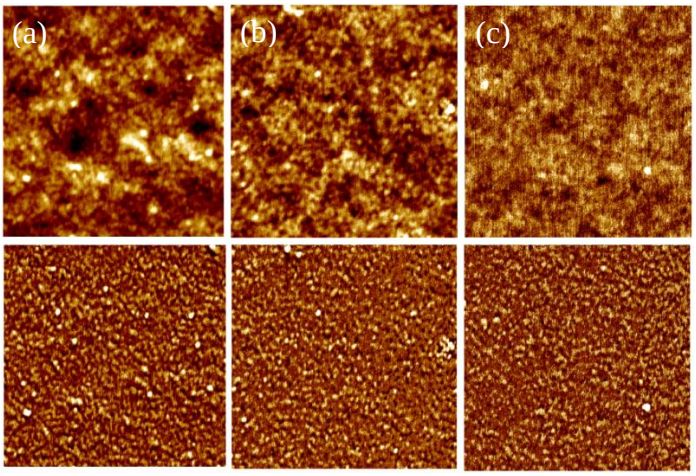

Figure 5- 3. 1μm x 1μm AFM surface images of sPP 1.4, 2.0 and 2.4 (a-c) obtained by dip coating. Height (top) and adhesion (bottom) sensors.

In **Figure 5- 3**, 1μm x 1μm AFM images are shown for the adhesion and height sensors for sPP, cast by dip coating on glass plates. It is clear from these images that although some phase separation is occurring, the materials are surprisingly uniform (homogeneous). Domain size cannot be accurately measured using this technique, but it can be observed that the frequency of these domains increases with increasing IEC. **Figure 5- 4** displays the surface morphology of Nafion 117 (Nafion). As well reported in literature, Nafion displays a high degree of phase separation, allowing for large, well-defined, hydrophilic domains.[15] sPP2.0 displays a significantly lower degree of ionic aggregation, and therefore less-distinct ionic and intermediate phases.

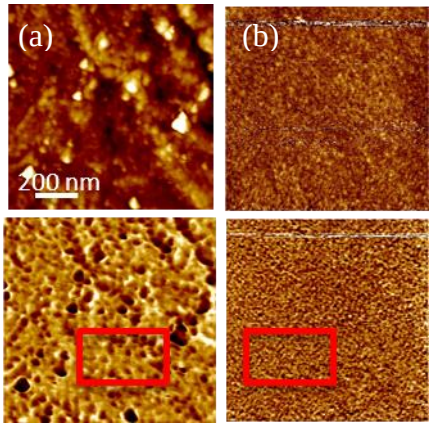

Figure 5- 4. 1µm x 1µm AFM surface images of hydrated (a) Nafion 117 (200 µm) and (b) sPP2.0 (85 µm) membranes. Height (top) and adhesion (bottom) sensors.

Wide angle x-ray diffraction patterns for all materials are shown in **Figure 5- 5**. Large peak breadths are the result of the amorphous nature of the materials.[16–19] In most diffraction patterns, four peaks were identified labelled d-1 through d-4 from the largest to smallest features, respectively. Peak d-2 (9.6 Å) lies in a region that has been most commonly observed in atactic polystyrene, and has been referred to as the "polymerization peak".[20–22] It has been determined that this region reflects inter chain packing. The d-3 peak (5.2 Å) has been termed the "amorphous halo", and is commonly seen in polymer melts, glasses and rubbers. A molecular dynamics simulation of atactic polystyrene concluded that peak d-2 is the result of side chain (phenyl-phenyl) correlations, while peaks d-3 and d-4 attributed to side chain-backbone intra- and intermolecular interactions.[23] Peak d-1 is the ionic peak, associated with ionic aggregation and ordering within the materials.[24]

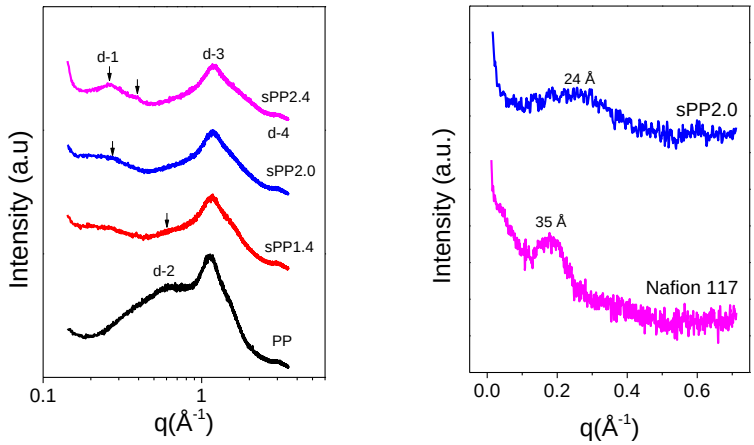

(a) (b)

Figure 5- 5. WAXS for (a) the parent poly(phenylene) and sPP (Na^+), and (b) transmission SAXS for sPP2.0 (Cs^+) and Nafion 117 (Na^+).

As seen in **Figure 5- 5a**, the presence of the sulfonic acid group largely disrupts the d-2 peak associated with interchain packing. This peak is undetectable at higher IEC's, indicating a disruption of side chain interactions, driven by the presence and aggregation of the high dielectric ion exchange groups. With increasing IEC there is an increase in relative intensity of the broad ionic peak correlating to a peak d-spacing of roughly 24 Å, similar in size to that of other amorphous sulfonate ionomers.[4,24] No significant peak shift is observed with increasing IEC. It I suspected that the ionic peak represents intra-particle scattering, whereby the aggregate size is limited by the low dielectric constant of the poly(phenylene) backbone and steric effects of the polymer chain. The increase in intensity with IEC indicates an increase in the number of scattering sites.

Transmission SAXS was performed to contrast the ionic peak of the sPP materials to that of Nafion (**Figure 5- 5b**). Nafion displays a low-q crystalline peak and a higher q ionic peak,

correlating to a d-spacing of 35 Å. The peak breadth, and therefore the aggregate size distribution, is substantially lower for Nafion than the sPP materials. This is due to reduced backbone steric hindrance resulting in a high degree of chain mobility. sPP2.0 was treated into the cesium form to increase the intensity of the ionic peak. No significant differences could be identified between transmission SAXS and WAXS for the sulfonated poly(phenylene)s in the ion peak region.

5.3.2 Ionomer Crosslinking and Solubility

Ionomers exhibit interesting solubility characteristics due to their biphasal nature. Many approaches have been used to determine the solubility parameter of Nafion. The most widely accepted theory has been that Nafion exhibits two solubility parameters, one for its non-polar backbone, and another for its ionic side chain.[25–27] In this work, brief experimental and theoretical solubility studies were performed on the sulfonated ionomers. Swelling data was used to quantify the extent of crosslinking occurring within the ionomers, and determine the interaction parameter between water and polymer ionic group. Understanding ionomer crosslinking and solubility gives insight into the cause of bulk property observations such as alcohol diffusion and mechanical properties.

The parent and sulfonated poly(phenylene)s were placed in a variety of solvents to determine material solubility (**Table 5- 1**). It was found that the parent polymer dissolved in non-polar solvents with Hildebrand solubility parameters (δ_{Hb}) from 18.16 to 19.46 $MPa^{0.5}$. As expected, the sulfonated materials exhibited more polar characteristics, and showed full dissolution in polar aprotic solvents with δ_{Hb} from 22.77-24.86 $MPa^{0.5}$. The ionomers did show some solubility

in methanol/ethanol solvent systems, however the solutions were cloudy. It is hypothesized that these solutions only displayed partial solubility due to solvent-backbone incompatibility.

Table 5- 1. PP and sPP solubility in common solvents. "-" denotes insoluble, "+" partially soluble, and "++" completely soluble.

	δ_{Hb} $MPa^{0.5}$	PP	sPP1.4	sPP2.0	sPP 2.4
Toluene	18.2	+ +	-	-	-
Chloroform	19.0	+ +	-	-	-
THF	19.5	+ +	-	-	-
DCM	20.2	+ +	-	-	-
DMAc	22.8	-	+ +	+ +	+ +
NMP	23.0	-	+ +	+ +	+ +
DMF	24.9	-	+ +	+ +	+ +
MeOH	26.5	-	+	+	+
Ethyl. Glycol	33.0	-	+	+	+
Water	47.8	-	-	-	-

The solubility parameter of sPP was also experimentally determined based on a solvent system of ethanol, ethylene glycol and water (**Figure 5- 6**). The obtained solubility parameters had a range of 27.5-30.5 $MPa^{0.5}$, which is significantly more polar than the solubility parameters of the preferred solvents DMAc and NMP. This commonly used method was inadequate in determining differences in solubility between materials of varying IEC.

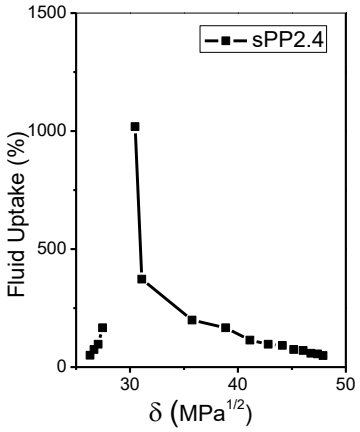

Figure 5- 6. An example of the experimental determination of the solubility parameter for sPP using solvent systems of ethanol/ethylene glycol/water.[28]

Theoretical solubility parameters were determined using tabulated group contribution parameters and the Hoftyzer and Van Krevelen method.[29,30] The most effective method for the analysis of sPP solubility was to compare the solubility contribution due to hydrogen bonding with the overall solubility parameter. It can be seen in **Figure 5- 7** that the sulfonated materials require solvents that have overall solubility parameters greater than 22.5 $MPa^{0.5}$, but low hydrogen-bonding solubility contributions. It is concluded that the solvents that have large hydrogen bonding solubility contributions do cause the ionic groups to dissociate, however are too polar to dissolve the non-polar backbone. This conclusion accounts for experimental observations discussed previously.

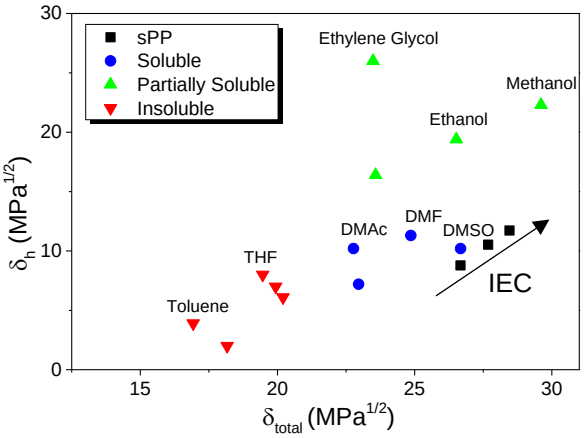

Figure 5- 7. Theoretical total solubility parameter (δ_{total}) vs. the solubility contribution from hydrogen bonding forces (δ_h) for sPP, calculated by the Hoftyzer and Van Krevelen equations. Solvent Hansen solubility parameters obtained from literature.[30]

The ion exchange capacity, ionomer density, and water content were used to obtain solubility and crosslinking data for the sulfonated ionomers (**Table 5- 2**). The crosslink density (n) was obtained under the assumption that two ionic groups are needed to form an ionic crosslink. The Flory interaction parameter (χ) and solubility for ionic group-water interactions were calculated from the Flory-Rehner and Flory-Huggins equations respectively. As expected, crosslink density and ionic group solubility increased with increasing IEC. The two materials of most similar ionic conductivity are sPP2.0 and Nafion 117. The material sPP2.0 has a higher crosslink-density, yet a significantly lower molecular weight between crosslinks. A large water content and IEC gives a lower χ parameter for sPP2.0. Despite large differences in swelling and crosslinking properties, the materials have a very similar overall solubility.

Table 5- 2. Crosslinking and ionic-group solubility data for sPP and Nafion, calculated using swelling properties, and the Flory-Rehner and Flory-Huggins equations.

	IEC	Density	W.U.	M_c	n	χ	$\delta_{Flory-R}$
	meq/g	g/cm^3	%	g/mol	mol/cm^3		MPa$^{0.5}$
sPP1.4	1.4	1.247	30.1	1391.2	9.0E-04	1.064	35.8
sPP2.0	2.0	1.308	61.1	1007.1	1.3E-04	0.786	37.5
sPP2.4	2.4	1.314	105.0	837.5	1.6E-03	0.620	38.7
Nafion 117	1	1.960	38	2000.0	9.8E-04	0.817	37.3

Table 5- 3 displays the solubility data calculated or experimentally determined in this work. Since the above mentioned solubility parameter obtained using the Flory-Rehner equation is for the ionic group alone, an adjusted parameter was calculated using the volume fraction of ionic groups to ionomer backbone. The solubility parameters are all within the solubility parameters of effective solvents. Therefore, it appears that all methods used to determine ionomer solubility have been somewhat successful. Due to ionomer insolubility in pure alcohols, it can be concluded that the most effective analysis required observing contributing Hansen solubility parameters, calculated in this work using the Hoftyzer and Van Krevelen method (**Figure 5- 7**). This method displayed the importance of considering the hydrogen-bonding contributions to the overall solvent parameters when evaluating ionomer solubility.

Table 5- 3. Solubility data for sPP obtained by the Flory-Rehner equation (adj-$\delta_{Flory-R}$), theoretical Hoftyzer and Van Krevelen calculations (δ_{H-VK}), and experimental data (δ_{Exp}).

	adj-$\delta_{Flory-R}$	δ_{H-VK}	δ_{Exp}
	$MPa^{0.5}$	$MPa^{0.5}$	$MPa^{0.5}$
sPP1.4	25.08	26.67	-
sPP2.0	25.59	27.68	-
sPP2.4	26.04	28.46	27.46-30.47

5.3.3 Thermal Stability

Thermal gravimetric analysis (TGA) can give insight into a materials thermal stability, rate of weight loss, and degradation on-set temperature. This information is particularly important for understanding ionomer performance in high temperature applications.[31] Under N_2, thermal gravimetric analysis (**Figure 5- 8**) reveals that poly(phenylene) has a single step degradation with five percent weight loss occurring at 581 °C. The functionalized polymers have a three stage degradation, with the thermal stability being limited by the degradation of the sulfonate group. An initial step, seen around 100 ℃, is due to the emission of moisture trapped within the membrane. A large amount of this moisture was accounted for by increasing the temperature, under N_2, to 110 °C for 30 minutes prior to each experiment.

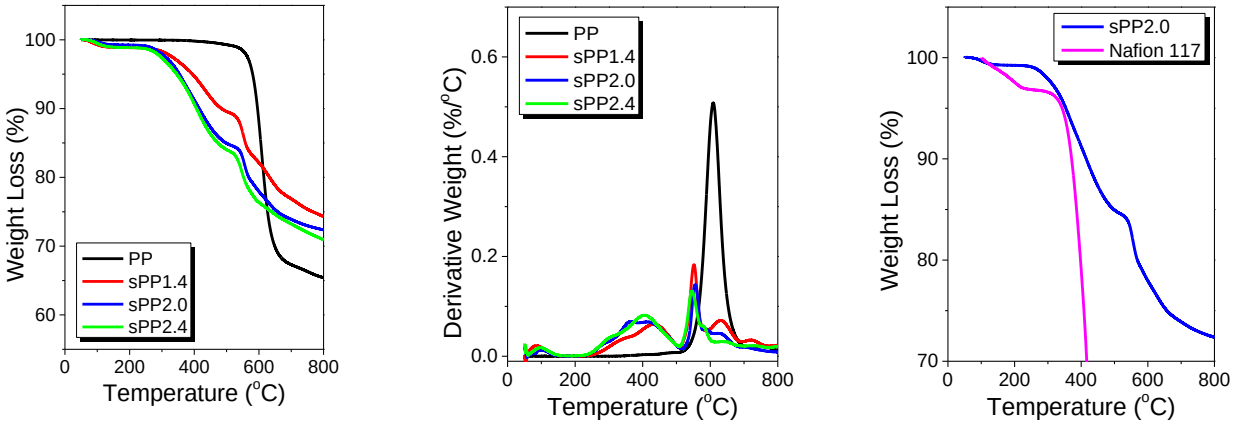

(a) (b) (c)

Figure 5- 8. (a) Weight loss and (b) derivative weight loss vs. temperature for the parent poly(phenylene) and the sulfonated poly(phenylene)'s. (c) Weight loss vs. temperature for sPP2.0 and Nafion 117.

Table 5- 4 reveals increasing residue at lower IEC's, however this is suspected to be influenced by the release of trapped water in the material. Both 5% weight loss ($T_{95\%}$) and onset degradation temperatures (T_{onset}) decrease with increasing ion exchange capacity. As can be seen in **Figure 5- 8c**, It has been reported that Nafion also has a three step degradation, with the first step between 35-280 °C presenting the loss of H_2O, SO_2 and CO_2.[32] This low temperature degradation is less prominent in the sPP materials. The second and third step, reported at 280-355 °C and above 355 °C respectively, are indication of both sulfonic acid group and backbone degradation. Due to the stability of the parent polymer, it can be assumed only SO_2 and H_2O loss occurs in sPP until backbone degradation begins at around 580 °C. The backbone stability of sPP appears to offer significant advantages over Nafion.

Table 5- 4. Onset degradation temperatures (T_{onset}), temperature at 5% weight loss, and percent residue at 700 °C for the parent and sulfonated poly(phenylene)s, and Nafion 117.

	T_{onset}	5% Wt. Loss	Residue
	C°	C°	%
PP	575.9	580.7	65.4
sPP1.4	336.5	394.5	74.3
sPP2.0	303.7	353.8	72.4
sPP2.4	316.4	345.9	70.9
Nafion 117	365.6	342.9	0.0

5.3.4 Dynamic Mechanical Analysis

Dynamic mechanical analysis gives insight into a materials rheological properties. This technique can be used to understand how the presence of polar functional groups affect a materials mechanical strength. The glass transition temperature can also be determined using thermal DMA, an important property necessary for understanding chain interactions and bulk ionomer behavior.

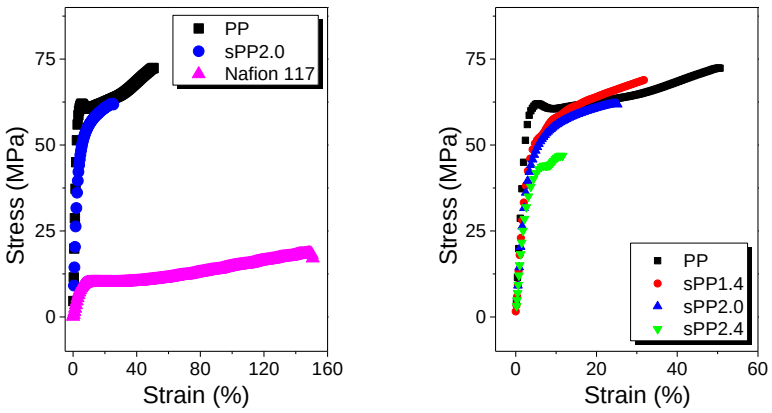

(a) (b)

Figure 5- 9. (a) Stress strain graph for the parent poly(phenylene), sPP2.0 and Nafion 117. (b) Stress strain graph for the parent poly(phenylene), and sPP.

In **Figure 5- 9a** stress strain data is shown for sPP2.0, PP and Nafion 117. Nafion 117 behaves like that of an elastomer, with a large elongation to break of 174%, and low Young's modulus of 3.24 x 10^6 Pa. This behavior is significantly different to both PP and sPP samples, who behave as thermoplastics. **Figure 5- 9b** displays stress strain data for sPP materials. These materials had far lower elongations to break, which decrease with increasing IEC from 50.6% for the parent polymer, to 11.6% for sPP2.4. Young's modulus decreases with increasing IEC, which may give an indication of increasing disruption of chain interactions, coinciding with WAXS data.

Table 5- 5. Young's modulus and elongation to break for the parent poly(phenylene), sPP, and Nafion 117.

	Young's Modulus (Pa)	Elongation to Break (%)
PP	2.50×10^9	50.6
sPP1.4	1.82×10^9	31.8
sPP2.0	1.59×10^9	25.3
sPP2.4	1.48×10^9	11.6
Nafion 117	2.02×10^8	173.7

5.3.5 Ion Transport and the State of Water

Table 5- 6 displays the proton conductivity (σ_{H+}) and water content of sulfonated poly(phenylene)s and Nafion 117. The ion exchange capacities of sPP range from 1.44 to 2.39. sPP2.0 has a conductivity most similar to Nafion 117, however Nafion 117 has significantly lower water content and IEC. The source of this drastic difference in ion exchange properties must lie in chemistry driven differences in morphology. It has been shown that Nafion exhibits ion aggregation and clustering, causing the formation of polar microchannels. These channels have been determined to be complete, allowing for effective water assisted ion diffusion.[33,34] In this study, AFM and WAXS have confirmed that the sPP materials display ionic aggregation limited in size by backbone rigidity, with no evidence of bulk phase separation. Since the ionic domain clusters in sPP are smaller and more disperse, its intermediate phase must contain a greater

concentration of ion exchange units, increasing the total water content. Therefore, a higher ion content is required to reach the percolation threshold, defined as the concentration of ionic groups needed to facilitate effective ion exchange via proton hopping and water-assisted ion diffusion.[35,36]

Table 5- 6. The ion exchange capacity (IEC), proton conductivity (σ_{H+}), water content, and proton activation energy ($E_{a,\sigma}$) for sulfonated poly(phenylene)s and Nafion 117.

	IEC (meq/g)	σ_{H+} (mS/cm^2)	Water content (%)	$E_{a,\sigma}$[2] (kJ/mol)
sPP1.4	1.4	34.8	30.1	2.7
sPP2.0	2.0	88.4	61.1	2.1
sPP2.4	2.4	122.1	105.0	1.9
Nafion 117	0.95-1.01[a]	100.4	38.0	2.4

Figure 5- 10 displays water content as a function of ion exchange capacity (IEC), and proton conductivity (100% humidity, 30 °C) as a function of water content. Sulfonated poly(ether ether ketone) (SPEEK)[37] and a sulfonate naphthalene dianhydride based polyimide (BAPS)[38] have been included for comparison. In sPP and the reference materials, water content reveals an exponential relationship to ion exchange capacity. This occurs due to the increasing polarity of the material with increasing IEC, which gradually approaches infinite swelling causing adverse effects on ion exchange properties, as well as eventual mechanical failure and ionomer dissolution. The trend indicates that sPP2.4 lies near the upper conductivity limit. An inverse exponential relationship is observed for the conductivity of BAPS and sPP versus water content (**Figure 5-**

10b). This points to a dilution effect, whereby increased water content lowers the local concentration of ion exchange groups, decreasing the effectiveness of ion exchange.

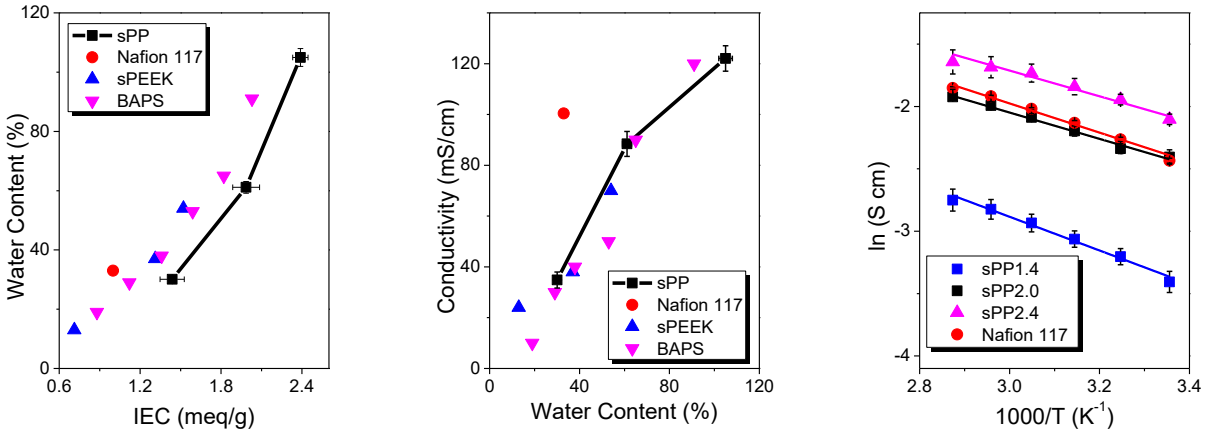

(a) (b) (c)

Figure 5- 10. (a) Water content as a function of ion exchange capacity, and (b) proton conductivity (100% humidity, 30 °C) as a function of water content. (c) Proton conductivities as a function of temperature. Data for sPEEK and BAPS obtained from literature.[37,38]

For the sulfonated poly(phenylene)s and Nafion 117 an Arrhenius relationship was observed for conductivity versus temperature (**Figure 5- 10c**). In **Table 5- 6** it can be seen that the activation energy for proton exchange increases with increasing IEC. The difference between sPP2.0 and sPP1.4 is substantial, however almost no difference is seen between sPP2.0 and sPP2.4. This indicates that sPP2.0 is somewhat optimal. Contributing factors are the low ion conductivity of sPP1.4, and an indication of a dilution effect occurring within sPP2.4. In addition it is of importance that, despite a lower ion conductivity, sPP2.4 displays a lower activation energy than Nafion 117.

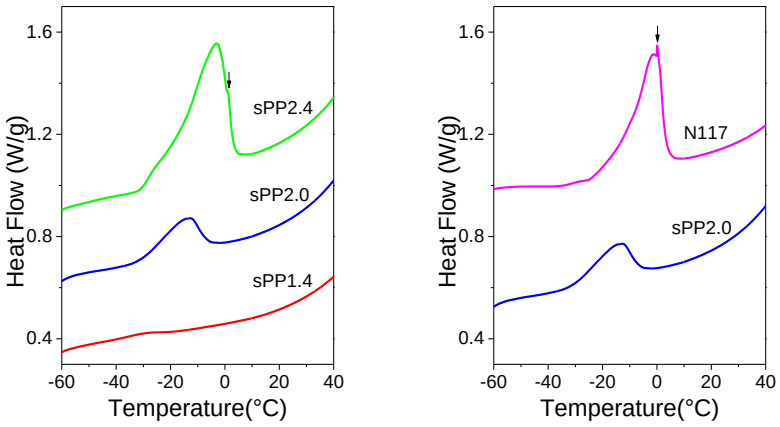

(a) (b)

Figure 5- 11. DSC thermograms for adsorbed water melting endotherms for sPP and Nafion 117 (endo up).

Calorimetric studies on the freezing of water in PEMs has been extensively studied.[39–42] Three states have been identified, a bulk-like water that freezes at roughly 0 °C, loosely bound water that displays a broad heat of fusion at lower temperatures, and nonfreezing strongly bound water. As seen in **Figure 5- 11** of the sulfonated poly(phenylene)s, only sPP2.4 displays clear freezable bulk water, indicated by a sharp peak at 0.9 °C. The width of the freezeable endotherm peak can be correlated to molecules in a range of energetic states that cannot escape the binding environment near the ionic groups.[41] An increase in the width of the peak indicates an increase in the number of energetic states the water molecules can occupy, and is therefore likely to correlated to the size of the hydrophilic domains. Because the freezable bulk water peak overlapped with the loosely bound peak, these peaks are evaluated together as “freezing/free water”, and all remaining water is considered “bound water”. In **Table 5- 7** the hydration number, which is the number of water molecules per sulfonic acid group, is listed, as well as the percentage of the water content that coincides with freezing or bound water. Surprisingly, sPP1.4 has 11 water molecules bound

to a single sulfonic acid group, yet displays almost no free water. We subsequently see large increases in free water for sPP2.0 and sPP2.4, that have hydration numbers of 17 and 24, respectively. The morphological differences between Nafion and sPP reveal large differences in the materials state of water, and is clearly observed by the bound to free water molecule ratio ($N_{bound/free}$).

Table 5- 7. The hydration numbers (λ), and freezing and bound water (%) content within the sPP and Nafion 117 materials.

	λ	$\Delta H_{f,lb}$	Water content	Free Water	Bound Water	$N_{bound/free}$
	($n H_2O/SO_3H$)	(J/g)	(%)	(%)	(%)	-
sPP1.4	12	4.0	30.1	0.4	29.7	82
sPP2.0	17	31.1	61.1	5.7	55.4	10
sPP2.4	24	96.5	105.0	30.4	74.6	2
Nafion 117	18	121.8	38.0	12.1	20.9	2

It is revealed that sPP2.0 and Nafion 117 do not greatly differ in the number of water molecules per sulfonic acid group. As discussed, Nafion's chemistry allows for larger ionic domains, in addition to a well ordered microstructure, giving better accessibility for water molecules to interact with acidic groups. This allows Nafion to have a high degree of free water in the hydrophilic domains, without the need for a high overall ion content. It is concluded that the bound water in the sPP materials is due to a large number of ionic groups in the intermediate phase. **Figure 5- 12** displays the conductivity versus total water content and free water content. Free water

appears to be highly necessary for ion transport, and is likely a function of ion aggregate frequency and interconnectivity.

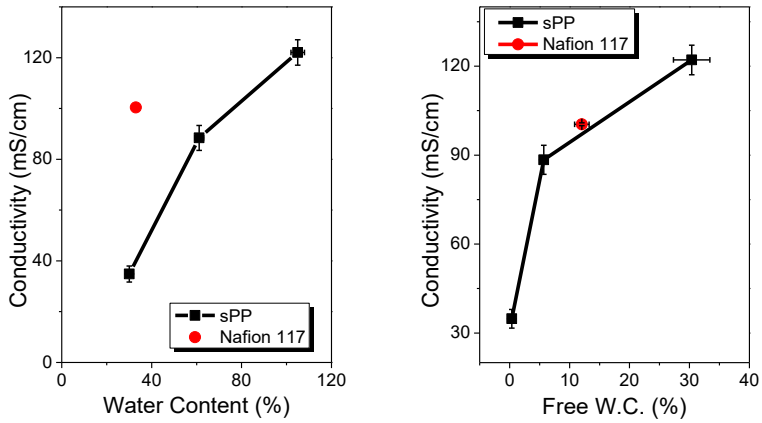

(a) (b)

Figure 5- 12. Ion conductivity as a function of (a) total water content and (b) free/freezable water content.

5.3.6 Liquid Transport Properties

Table 5- 8 displays alcohol permeability data for the sulfonated poly(phenylene)'s and Nafion 117. The alcohol diffusion coefficients for sulfonated poly(phenylene) increase with increasing IEC. The increased presence of sulfonate groups on the polymer backbone increases the number of ionic aggregates within the material, increasing water content and in turn liquid diffusion. Permeability decreases with increasing alcohol size, giving some indication of an increase in hydrophillic channel size and connectivity. sPP2.0 has an ion conductivity most similar to that of Nafion, a property shown to be closely related to the availability of free water within the material. Despite somewhat similar free water, Nafion 117 displays significantly higher alcohol

permeability. This observation emphasizes a major drawback of the high conductivity induced by Nafion's bicontinuous morphology.

Table 5- 8. The methanol, ethanol and 2-propanol permeability's through sulfonated poly(phenylene)s and Nafion 117 at 30 °C.

	Permeability (10^8 cm^2/s)		
	Methanol	Ethanol	2-Propanol
sPP1.4	57	27	12
sPP2.0	108	73	40
sPP2.4	184	134	89
Nafion 117	159	135	113

A similar but opposite trend can be observed for the activation energies (E_x) needed for liquid and proton diffusion through the membranes (**Table 5- 9**). Alcohol activation energies decrease with increasing IEC and increase with increasing alcohol size. That is, more energy is required for larger molecules to diffuse across the membrane, and less energy is required with increasing membrane polarity. It was noted that sPP2.0 had lower alcohol permeability than Nafion 117, however sPP2.0 has lower alcohol activation energies. This may be the result of improved domain connectivity at high temperatures in sPP due to increased swelling. This observation is supported by the proton activation energy, previously discussed.

Table 5- 9. Methanol, ethanol and 2-propanol activation energies for alcohol diffusion through sulfonated poly(phenylene) and Nafion 117.

	Activation Energy (kcal/mol)			
	Methanol	Ethanol	2-Propanol	H^+
sPP1.4	3.3	6.0	9.1	2.7
sPP2.0	4.2	4.7	6.1	2.1
sPP2.4	4.2	4.7	5.5	1.9
Nafion 117	4.9	5.0	6.1	2.4

In **Figure 5- 13** the methanol permeability is displayed as a function of total water content and free water content. The data for Nafion 117 is more closely correlated to that of the sPP trend when considering free water. The relationship between free water, and ion conductivity and methanol permeability highlights the difficulty in obtaining materials with high ion selectivity. From **Figure 5- 13c** it is clear that 2-propanol permeability is a poor function of free water, and is more likely correlated to channel size. Therefore, despite similar methanol permeability, it is suspected that sPP will display superior ion selectivity due to smaller and less-interconnected ionic channels.

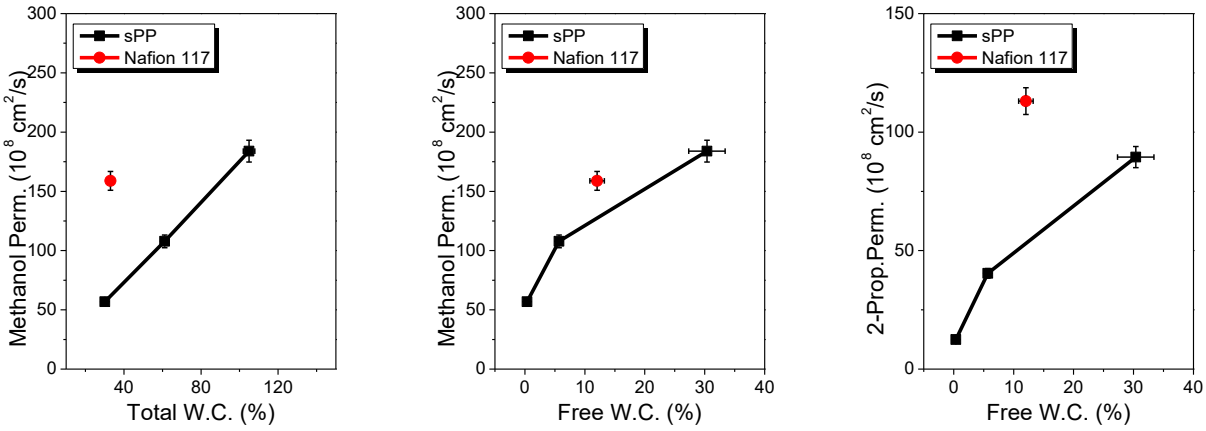

(a) (b) (b)

Figure 5- 13. Methanol permeability as a function of (a) total water content and (b) free/freezable water content, and (c) 2-propanol permeability as a function of free water content for sPP and Nafion 117.

In ion exchange applications such as fuel cells and redox flow batteries, ion selectivity is desired over other larger molecular or ionic species.[43,44] A method used to determine electrochemical selectivity is to plot ion conductivity versus permeability (**Figure 5- 14**).[45] An ideal membrane with high proton conductivity and alcohol rejection would lie to the upper left of the graph. sPP offers better selectivity than Nafion for all alcohols, improving with alcohol size. As discussed, sPP has smaller ionic domains than Nafion, however Nafion has more-complete, uniform, interconnectivity that allows for the diffusion of large molecules. The high conductivity and superior selectivity of sPP is a vital property for many industrial applications.

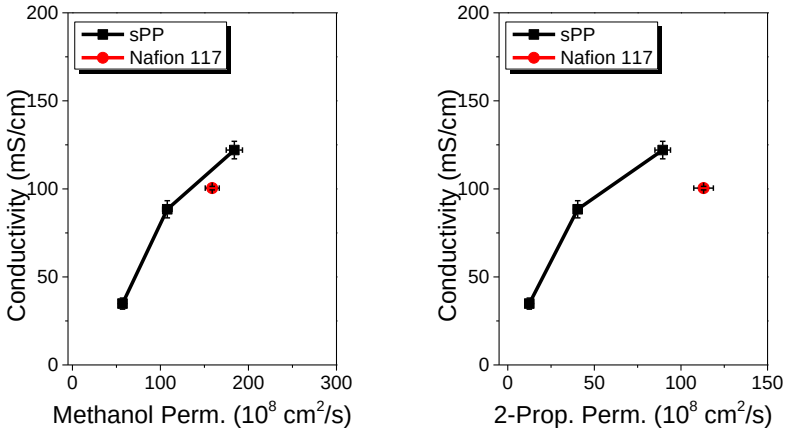

(a) (b)

Figure 5- 14. Conductivity of sPP and Nafion 117 as a function of (a) Methanol and (b) 2-propanol permeability.

5.4 Conclusions

The effect of membrane morphology and ion content on proton conductivity, permeability, and the state of water for a series of random sulfonate Diels-Alder poly(phenylene)s was performed. A WAXS analysis revealed an ionic peak correlating to a d-spacing of 24 Å. The peak displayed no shift with increasing IEC, however did increase in intensity. It is therefore suspected that IEC has little impact on domain size, but rather domain frequency. AFM confirmed that, compared to the commercial standard Nafion 117, sPP displays a highly homogeneous morphology. Materials were synthesized up to an IEC of 2.4, displaying a conductivity of 120 mS/cm, and water content of 105%. sPP required greater water content to achieve electrochemical properties competitive to Nafion 117. A state of water analysis revealed that free/freezable water was roughly equivalent in both sPP2.0 and Nafion 117, and therefore is considered the main factor for the facilitation of ion exchange. sPP2.0 had far greater bound water, likely residing in the

intermediate phase. For sPP, liquid permeability increased with increasing free water content, however the synthesized materials had far better ion/2-propanol selectivity. This is attributed to the smaller and less interconnected ionic domains caused by a highly rigid poly(phenylene) backbone.

5.5 References

[1] Smitha, B.; Sridhar, S.; Khan, a. a. *J. Memb. Sci.* **2005**, *259*, 10–26.

[2] Song, J.-M.; Shin, J.; Sohn, J.-Y.; Nho, Y. C. *Macromol. Res.* **2012**, *20*, 477–483.

[3] Silva, V.; Silva, V.; Mendes, A.; Madeira, L.; Nunes, S. *Desalination* **2006**, *200*, 645–647.

[4] Zhao, C.; Lin, H.; Shao, K.; Li, X.; Ni, H.; Wang, Z.; Na, H. *J. Power Sources* **2006**, *162*, 1003–1009.

[5] Chen, D.; Wang, S.; Xiao, M.; Han, D.; Meng, Y. *J. Power Sources* **2010**, *195*, 7701–7708.

[6] Chen, D.; Wang, S.; Xiao, M.; Meng, Y. *J. Power Sources* **2010**, *195*, 2089–2095.

[7] Chen, D.; Wang, S.; Xiao, M.; Han, D.; Meng, Y. *Polymer (Guildf).* **2011**, *52*, 5312–5319.

[8] Kim, Yu Seung; Dong, Limin; Hickner, Michael A.; Glass, T. E. *Macromolecules* **2003**, *36*, 6281–6285.

[9] Benavente, J.; García, J.; Riley, R. *J. Membr. …* **2000**, *175*, 43–52.

[10] Harrison, W. L. Synthesis and characterization of sulfonated poly(arylene ether sulfone) copolymers via direct copolymerization: candidates for proton exchange membrane fuel cells, *Dissertation* **2002**

[11] Fujimoto, C. H.; Hickner, M. A.; Cornelius, C. J.; Loy, D. A. **2005**, 5010–5016.

[12] Hickner, M.; Fujimoto, C.; Cornelius, C. *Polymer (Guildf).* **2006**, *47*, 4238–4244.

[13] He, L.; Fujimoto, C. H.; Cornelius, C. J.; Perahia, D. **2009**, 7084–7090.

[14] Yang, Y.; Holdcroft, S. *Fuel Cells* **2005**, *5*, 171–186.

[15] McLean, R. S.; Doyle, M.; Sauer, B. B. *Macromolecules* **2000**, *33*, 6541–6550.

[16] Moore, R.; Martin, C. *Macromolecules* **1989**, *22*, 3594–3599.

[17] Grady, B. P. **2008**.

[18] Page, K. a.; Landis, F. a.; Phillips, A. K.; Moore, R. B. *Macromolecules* **2006**, *39*, 3939–3946.

[19] Visser, S. a.; Cooper, S. L. *Macromolecules* **1991**, *24*, 2584–2593.

[20] Schubach, H. R.; Nagy, E.; Heise, B. *Colloid Polym. Sci.* **1981**, *259*, 789–796.

[21] Katz, J. R. *Rubber Chem. Technol.* **1936**, *9*, 357–372.

[22] Mitchell, G. R.; Windle, A. H. *Polymer (Guildf).* **1984**, *25*, 906–920.

[23] Ayyagari, C.; Bedrov, D.; Smith, G. D. *Macromolecules* **2000**, *33*, 6194–6199.

[24] Lu, X.; Steckle, W. P.; Weiss, R. a. *Macromolecules* **1993**, *26*, 5876–5884.

[25] Yeo, R. S.; Cheng, C.-H. *J. Appl. Polym. Sci.* **1989**, *32*, 5733–5741.

[26] Yeo, R. S. *Polymer (Guildf).* **1980**, *21*, 432–435.

[27] Gebel, G.; Aldebert, P.; Pineri, M. *Polymer (Guildf).* **1993**, *34*, 333–339.

[28] Wang, D. Ionomer Morphology, Solution to Film Thermodynamics, Molecule Transport, Physical Properties, and Water Desalination via Electrodialysis, University of Connecticut, 2014.

[29] Van Krevelen, D. W.; Te Nijenhuis, K. *Properties of Polymers: Their Correlation with Chemical Structure; Their Numerical Estimation and Prediction from Additive Group Contributions*; 4th ed.; Elsevier: Amsterdam, 2009.

[30] Hansen, C. M. *Hansen Solubility Parameters A User's Handbook*; Second.; CRC Press, 2007.

[31] Peighambardoust, S. J.; Rowshanzamir, S.; Amjadi, M. *Int. J. Hydrogen Energy* **2010**, *35*, 9349–9384.

[32] Lage, L. G.; Delgado, P. G.; Kawano, Y. *J. Therm. Anal. Calorim.* **2004**, *75*, 521–530.

[33] Schmidt-Rohr, K.; Chen, Q. *Nat. Mater.* **2008**, *7*, 75–83.

[34] Orfino, F.; Holderoft, S. *J. New Mater. …* **2000**, *292*, 287–292.

[35] Carretta, N.; Tricoli, V.; Picchioni, F. *J. Memb. Sci.* **2000**, *166*, 189–197.

[36] Gebel, G. *Polymer (Guildf).* **2000**, *41*, 5829–5838.

[37] Gil, M.; Ji, X.; Li, X.; Na, H.; Eric Hampsey, J.; Lu, Y. *J. Memb. Sci.* **2004**, *234*, 75–81.

[38] Einsla, B.; Kim, Y.; Hickner, M.; Hong, Y.; Hill, M.; Pivovar, B.; Mcgrath, J. *J. Memb. Sci.* **2005**, *255*, 141–148.

[39] Lu, Z.; Polizos, G.; Macdonald, D. D.; Manias, E. *J. Electrochem. Soc.* **2008**, *155*, B163.

[40] Kreuer, K. D. *J. Memb. Sci.* **2001**, *185*, 29–39.

[41] Hodge, R. M.; Edward, G. H.; Simon, G. P. *Polymer (Guildf).* **1996**, *37*, 1371–1376.

[42] Yoshida, H.; Miura, Y. *J. Memb. Sci.* **1992**, *68*, 1–10.

[43] Merle, G.; Wessling, M.; Nijmeijer, K. *J. Memb. Sci.* **2011**, *377*, 1–35.

[44] Weber, A.; Mench, M.; Meyers, J. *J. Appl. ...* **2011**, 1137–1164.

[45] Pivovar, B. S.; Wang, Y. X.; Cussler, E. L. *J. Memb. Sci.* **1999**, *154*, 155–162.

Chapter 6 Transport in Aminated Random and Block Copolymer Diels-Alder Poly(phenylene)s: The Effect of Membrane Morphology, Ion Conductivity, Liquid Permeability, and the State of Water

6.1. Introduction

Anion exchange membranes (AEMs) have received much attention due to growing interest in applications such as anion exchange membrane fuel cells (AEMFCs) and redox flow batteries. AEMFCs offer a competitive alternative to PEMFCs, that offer suffer from slow kinetics, low electrical efficiency, high cost of platinum catalyst, catalyst poisoning, and high fuel permeability.[1] AEMFCs have lower operating temperatures (23-70 °C), higher reaction kinetics, and the utilization of less Pt catalyst.[2] Desired properties of an anion exchange membranes (AEM) for such applications includes good mechanical and thermal stability during manufacturing and operation, a good carrier for hydroxyl transport, high ionic conductivity, low electronic conductivity, and low cost. AEMs that have been developed that show great promise include those with chemistries based on poly(sulfones),[3–6] poly(phenylene oxide)s,[7] poly(phthalazion ether ketone)s,[8,9] poly(arylene ether)s,[10–12] poly(fluorenyl ether)s,[13] and many others. Persistent issues with AEMs include inherently low hydroxyl conductivity, and subjection to nucleophilic attack by the hydroxide anion. A better understanding of the interrelationship between AEM morphology, ion conductivity, liquid permeability, and the state of water is required to further optimize the materials for practical use.

In this chapter, the effect of membrane morphology and ion content on ion conductivity, liquid permeability, and the state of water for a series of quaternary ammonium Diels-Alder poly(phenylene)s is investigated. The effect of random copolymerization and block length is assessed. Two amination methods were employed, a solid state “heterogeneous” amination

technique, and a solution cast "homogeneous" amination technique. This in depth analysis offers insight into effect of amination technique and polymer chemistry on anion exchange membrane performance.

6.2 Experimental

6.2.1 Bromination and Membrane Formation

Bromination of Diels-Alder poly(phenylene)s was performed by allylic bromination using N-bromosuccinimide (NBS), with dibenzoyl peroxide (BPO) as a radical initiator, as described elsewhere.[14] Described is the procedure for the bromination of the methylated homopolymer (mPP) with a degree of bromination of 1. The methylated polymer (3.5g, 4.28 mmol) was dissolved in 1,1,2,2-tetrachloroethane, 5% by weight. The solution was placed in a flame dried reaction vessel, and fitted with a nitrogen purge and mechanical stirrer. The solution was heated to 85 °C, whereby the stoichiometric amount of NBS (0.762g, 4.28 mmol) and a small amount of BPO (0.052g, 0.214 mmol) was added. After 3 hours, the solution was cooled to room temperature, and the brominated polymer was precipitated by pouring into ethanol, filtered, and washed with water. The films were dried at 30 °C in a vacuum oven overnight. Caution was taken during drying, as high temperatures would initiate crosslinking and render the material insoluble.

Brominated polymers were cast in chloroform (5 wt%). Solutions were filtered through 5 µm PTFE syringes onto a glass mold. A slow rate of evaporation was ensured by covering the mold with a glass plate. After 24 hours, the polymer films were placed in a vacuum oven at room temperature to ensure the membranes were completely dry. The orange brominated films were transparent, robust, and creasable.

6.2.2 Method 1: Heterogeneous Amination

Heterogeneous aminated polymers were formed by placing brominated films in an airtight vessel containing a 1 M solution of trimethylamine in water. The materials were allowed to soak for 48 hours to ensure complete amination. Membranes were then removed, washed with water, and placed into an aqueous 1 M solution of sodium hydroxide for 48 hours. The films were then removed and soaked in deionized water for 48 hours in an open cup, replenishing the water at least twice, to ensure complete conversion from the hydroxyl to the carbonate form.

6.2.3 Method 2: Homogeneous Amination

To from homogeneous anion exchange membranes, it was desired to obtain a solution of the aminated polymer. To achieve this, brominated membranes were placed in an airtight vessels containing a 1 M solution of trimethylamine in THF and soaked for 48 hours to ensure complete amination. The TMA/THF solution was then decanted, and the vessel was filled with DMF. The polymer was stirred for 24 hours; achieving complete dissolution. The dissolved aminated polymer was cast under vacuum at 65 °C overnight. The films were treated in a 1 M solution of sodium hydroxide for 48 hours. Membranes were soaked in deionized water for 48 hours in an open cup, replenishing the water at least twice, to ensure complete conversion from the hydroxyl to the carbonate form.

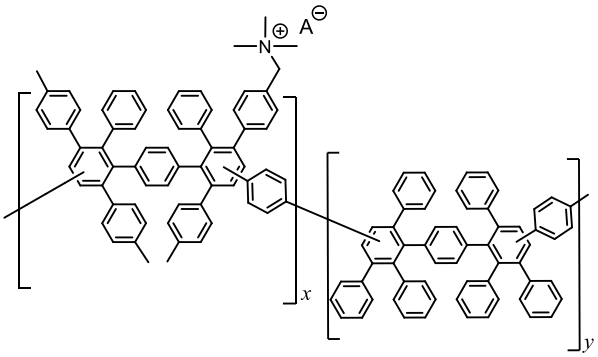

Scheme 6- 1. Chemical structure of aminated AmPP-PP random and block copolymers.

6.3 Results and Discussion

6.3.1 Chemistry and Solubility

The molecular weight distributions of the homopolymer (mPP), random copolymer (mPP-PP) and block copolymers (B1mPP-PP and B2mPP-PP) are displayed in **Table 6- 1**. Two block copolymers were synthesized, with each having methylated and non-methylated block lengths of roughly equal size. The parent Diel-Alder poly(phenylene)s displayed good solubility in a wide range of common organic solvents, including toluene, chloroform, and THF. The high degree of solubility has been attributed to meta-catenation, as well as significant twisted conformations that limit or block conjugation.[15–19] The parent copolymers were analyzed using NMR to determine polymer chemistry and the ratio of methylated to non-methylated repeat units.

Table 6- 1. Molecular weight distributions and repeat unit compositions for parent methylated polymers.

	M_{nx} (10^3 g/mol)	M_{ny} (10^3 g/mol)	Composition f_{MPP}:f_{PP}	M_n (10^4 g/mol)
mPP	-	-	0.96:0.04	8.99
mPP-PP	-	-	0.44:0.56	7.52
B1mPP-PP	11.2	8.87	0.53:0.47	5.64
B2mPP-PP	16.8	16.3	0.44:0.56	7.62

FT-IR spectroscopy was performed on the parent polymer to confirm complete conversion and polymer structure (**Figure 6- 1a**). Phenyl carbon-carbon stretching typically occurs around 1500-1400 cm^{-1} for phenylated molecules, and can be seen at 1435 cm^{-1} and 1402 cm^{-1}. Carbon-hydrogen out of plane bending peaks are evident at 698 cm^{-1} and 812 cm^{-1}. FTIR was performed on the brominated materials, normalized around the C=C phenyl peak at 1435 cm^{-1}. As expected there was little change in the stable aromatic carbon-carbon bonds located from 1400-1600cm^{-1}. IR spectra confirmed the presence of bromine group, seen as a sharp peak at 605 cm^{-1}. In **Figure 6- 1b**, the peak corresponding to the bromine group increased in intensity with increasing degree of bromination.

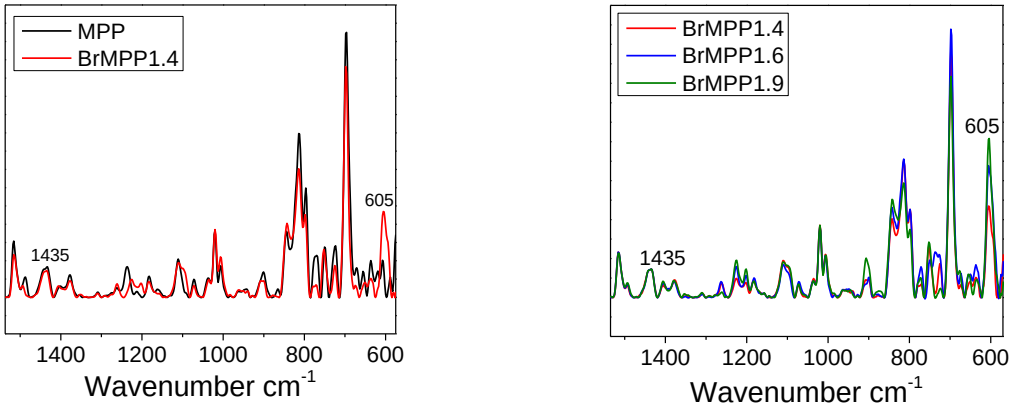

(a) (b)

Figure 6- 1. FTIR spectra of (a) the parent polymer methylated poly(phenylene) (MPP) and brominated material BrMPP1.4, and (b) FTIR spectra of all brominated poly(phenylene)s.

As shown in **Figure 6- 2**, the NMR spectra of the materials displayed aromatic protons peaks from 7.5-6.0 ppm ("a"), and a benzylic proton triplet at 2.5-2.0 ppm ("c"). The ratio of methylated to non-methylated repeat units was determined by the ratio of the integration of these two peaks. Brominated materials displayed a bromomethyl peak at 4.4 ppm ("b"), used to determine a theoretical IEC. Brominated materials displayed no noticeable change in solubility, however were subject to crosslinking if heated above ambient temperatures. Although soluble in pure THF, the brominated materials were insoluble in TMA/THF solutions. This is likely due to both the higher polarity of the solution, and the rapid change in characteristic solubility of the polymer as the amination reaction proceeds. Upon amination the membrane was soluble in several polar aprotic solvents, such as DMAc, DMSO and DMF. After high temperature casting materials were only able to be partially redissolved, and so was avoided.

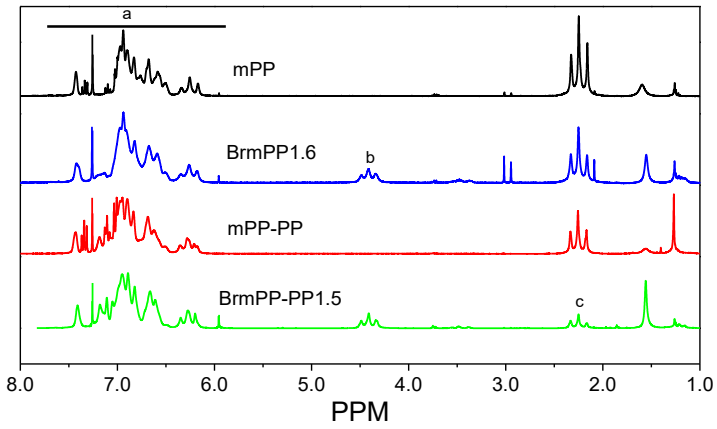

Figure 6- 2. NMR spectra of the parent polymers mPP and mPP-PP, and brominated polymers BrmPP16 and BrmPP-PP15.

6.3.2 Morphology

Amination method I, accomplished by modification of a preformed thin film, has been most commonly used in the study of anion exchange membranes.[4,7,8,10] In this study, this method was used to aminate the methylated homopolymer (aMPP) and the random copolymer (aMPP-PP). This method is somewhat undesirable as it does not allow for reorientation of polymer chains. Chain mobility during processing allows for improved ionic aggregation and, with certain chemistries, well defined morphologies.[20] The main challenge in obtaining a castable solution of cationomer is the large change in characteristic solubility of the polymer upon functionalization. Attempts have been made using solvent systems,[3] but it is suspected that this influences film homogeneity. Amination method II produces castable homogeneous solutions in aprotic polar solvents, and is particularly effective for the solution amination of material chemistry that undergo large increases in polarity, such as during quaternary amination of Diels-Alder poly(phenylene)s.

This method was used to produce the random copolymer hAmPP-PP, and block copolymers B1hAmPP-PP and B2hAmPP-PP.

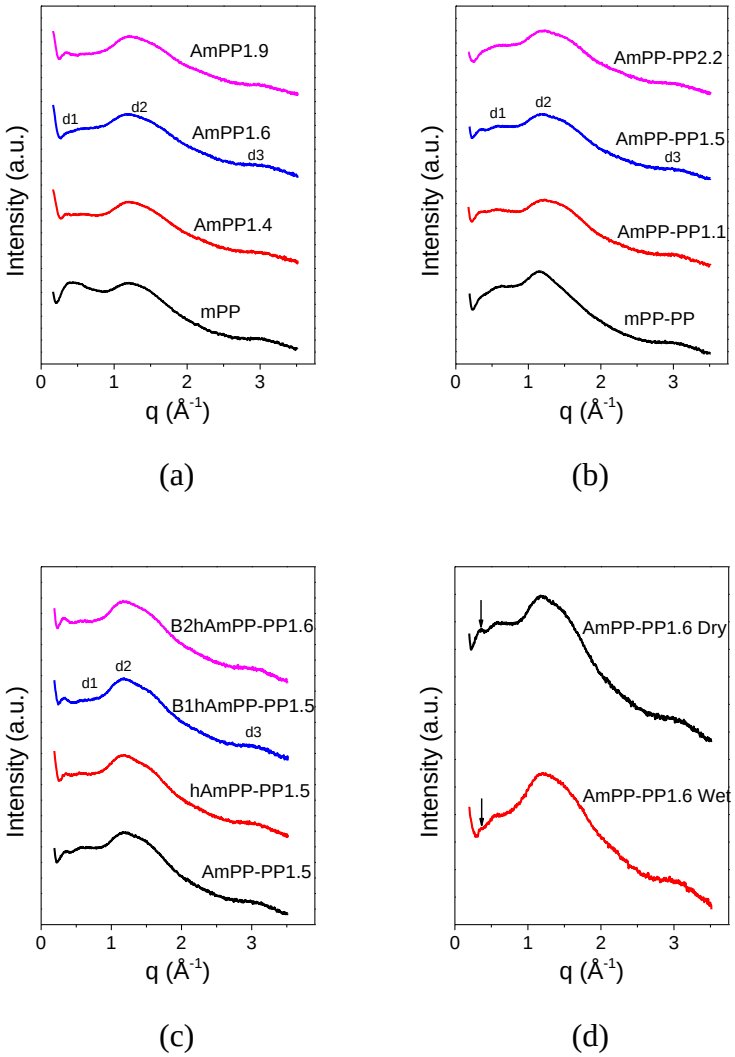

Figure 6- 3. Wide angle x-ray diffraction patterns for the heterogeneously aminated (a) AmPP and (b) AmPP-PP materials, the (c) homogeneously aminated random and block copolymers, and (d) the effect of hydration.

Wide angle x-ray diffraction patterns for all materials are shown in **Figure 6- 3**. Large peak breadths are the result of the amorphous nature of the materials. In most diffraction patterns, three peaks were identified labelled d-1 through d-3 from the largest to smallest features, respectively. The first and second peaks lie in a region that has been most commonly observed in atactic polystyrene, and has been referred to as the "polymerization peak".[21–23] It has been determined that this region reflects inter chain packing.[24] The region in which peak d-2 has been termed the "amorphous halo", and has is seen in polymer melts, glasses and rubbers. A molecular dynamics simulation of atactic polystyrene concluded that peak d-3 is attributed to side chain-backbone intra- and intermolecular interactions. Unlike cation exchange membranes, anion exchange membranes do not exhibit a feature due to ion group interactions such as ionic clusters.[25]

In all diffraction patterns, quaternary amination had the most significant effect on the d-1 region. This feature for mPP decreased in relative intensity and width with increasing IEC (**Figure 6- 3a**). The reduction in d-1 intensity may indicate a disruption in chain packing due to the presence of quaternary ammonium groups. In **Figure 6- 3d** the hydrated AmPP1.6 membrane displays a drop in intensity of the d-1 peak, signifying further disruption of chains interactions on this order due to the accommodation of water molecules. A similar conclusion can be made for the functionalization of mPP-PP (**Figure 6- 3b**), however the reduction in intensity of the "polymerization peak" region is lessened due to the presence of non-functionalized, non-methylated, repeat units. This is most clear in the comparison of the diffraction patterns for AmPP1.9 and AmPP-PP2.2. The effect of homogeneous amination and block length on the x-ray spectra can be seen in **Figure 6- 3**c. Unlike the heterogeneous radom copolymers, homogeneous amination and increasing block length causes significant disruption of the inter-chain spacing

feature. This may indicate that regardless of non-functionalized chain length, ordering in this region is significantly lost post homogeneous amination.

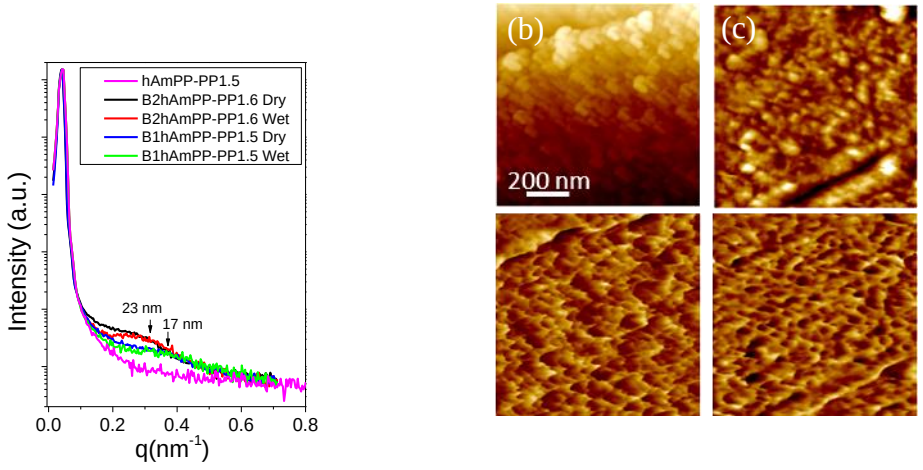

(a)

Figure 6- 4. (a) SAXS of the homogeneous materials. AFM height (top) and adhesion (bottom) surface images of hydrated (b) AmPP-PP1.5, (c) B2hAmPP-PP1.6 membranes.

In order to ascertain whether bulk microphase separation was occurring between the heterogeneous and homogeneous random and block copolymers, small angle x-ray scattering (SAXS) was performed (**Figure 6- 4a**). B1hAmPP-PP1.5 and B2hAmPP-PP1.6 display broad peaks, corresponding to 17 and 23 nm, respectively. The hydrated membranes did not display any q-shift, however did appear to narrow the d-spacing distribution and sharpen the peak. The magnitude of the separation lengths indicate that the features result from block microphase separation and not ion clusters found in statistical copolymers, which give smaller separation lengths.[25] Microphase separation of this size has been observed in AEM materials with similar block sizes. In a recent study, a microphase separation of 28 nm was achieved for a quaternary

ammonium block poly(arylene ether sulfone) with an ionic block length of 14,600 g/mol and an IEC of 2.[26] Atomic force microscopy performed on the surface of the hydrated membranes revealed that AmPP-PP1.5 (**Figure 6- 4b**) displays some degree of heterogeneity seen by a random variation in adhesion force over the area of the phase image, whereby dark and light regions indicate polar and non-polar regions, respectively. B2hAmPP-PP1.6 (**Figure 6- 4c**), however, displays more distinct phases, as seen by greater contrast between hydrophilic and hydrophobic regions.

6.3.3 Thermal Stability

The thermal stability of ionomers is important for high temperature applications. Much concern has been expressed regarding the stability of ionomers during the operation of fuel cells approaching temperatures of 100 °C.[27] Thermal gravimetric analysis (TGA) can give insight into a materials thermal stability, rate of weight loss, and degradation on-set temperature. Thermal gravimetric analysis under nitrogen was performed on all materials, displayed in **Figure 6- 5** and listed in **Table 6- 2**. The parent materials mPP and mPP-PP displayed single step degradations, with onset temperatures of 552 and 601 °C, respectively. The functionalized polymers appear to have a four stage degradation, however initial weight loss (below 180 °C) is observed due to the evaporation of free water. The AmPP and AmPP-PP materials displayed thermal properties directly correlated to IEC.

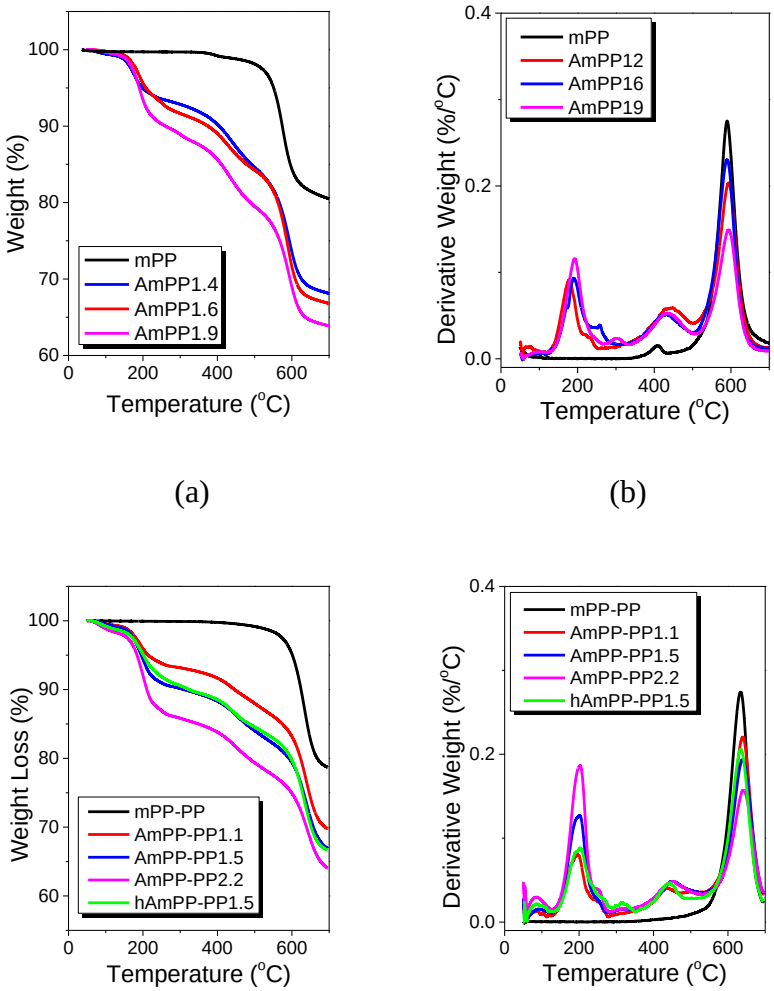

Figure 6- 5. The (a) weight loss and (b) derivative weight loss vs. temperature for heterogeneous AmPP. The (c) weight loss and (d) derivative weight loss vs. temperature for heterogeneous AmPP-PP, and homogeneous hAmPP-PP1.5.

Due to a direct correlation to ionomer chemistry (**Table 6- 2**), random and block copolymerization had little impact on thermal stability. The narrow temperature range in which all functionalized materials underwent degradation indicates that, at all IEC's, risk of degradation of

the quaternary ammonium group, and therefore loss of functionality, is to be expected above a temperature of 150 °C.

Table 6- 2. The onset degradation temperatures (T_{onset}), 5% weight loss, and percent residue at 700 °C for the parent and aminated poly(phenylene)s.

	T_{onset} C°	5% Wt. Loss C°	Residue %
mPP	545	552	81
AmPP1.4	154	198	68
AmPP1.6	164	208	67
AmPP1.9	166	190	64
mPP-PP	586	601	79
AmPP-PP1.1	160	214	70
AmPP-PP1.5	167	196	67
AmPP-PP2.2	172	184	64
hAmPP-PP1.5	169	201	67
B1hAmPP-PP1.5	176	217	67
B2hAmPP-PP1.6	172	206	63

6.3.4 Dynamic Mechanical Analysis

Dynamic mechanical analysis gives insight into a materials rheological properties. This technique can be used to understand how the presence of polar functional groups affect a materials

mechanical strength. As can be seen in **Figure 6- 6a**, quaternary amination lowered the Young's modulus and yield strength of the materials. Interestingly, the mechanical strength of the materials increased with increasing IEC. This is typically observed in ionically crosslinked polymers, however it has not been well documented for anion exchange membranes. It has been documented that counterion has a significant effect on AEM mechanical strength.[28] The divalent counterion, carbonate, may result in good mechanical properties due to ionic interactions between multiple ionic sites. Lastly, it has been acknowledged that crosslinking, as indicated by a reduced solubility in aprotic polar solvents, occurs with increased temperature or prolonged time. An increase in the extent of unintended covalent crosslinking due to a higher concentration of ion exchange units could contribute to the observed phenomena.

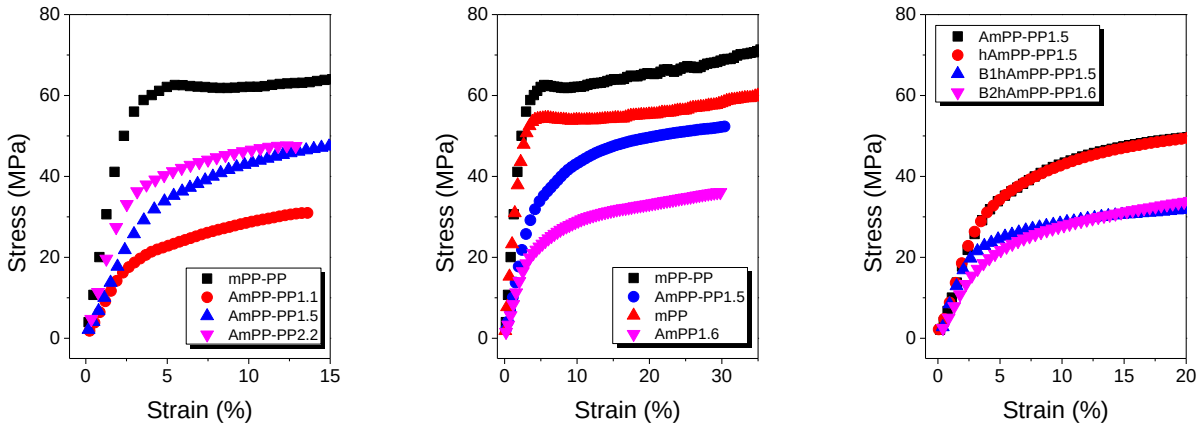

(a) (b) (c)

Figure 6- 6. Stress strain graph for (a) mPP-PP and AmPP-PP, (b) AmPP-PP1.5 and AmPP1.6, and (c) the random heterogeneous, random homogeneous, and homogeneous block anion exchange membranes.

Figure 6- 6b reveals that the aminated random copolymer, AmPP-PP1.5 displays significantly better mechanical properties than the aminated homopolymer, AmPP1.6. This in part is due to the superior mechanical properties of the parent random copolymer, mPP-PP. However, the large difference indicates other contributing factors. The morphological analysis suggested that the random aminated copolymer has larger hydrophobic domains. This conclusion coincides with the rheological analysis, whereby there exists a greater backbone contribution to the materials modulus and yield strength. **Figure 6- 6c** reveals that homogeneous preparation of the random copolymer had no impact on the mechanical properties of the material, indicating that the preparation technique is highly effective. Lastly, the block copolymers display far lower Young's moduli and yield strength than the random copolymer. It is likely that, while the random copolymer benefits from the larger hydrophobic domains, the large hydrophilic domains in the block materials cause significant disruption of the side-chain interactions, lowering the mechanical strength. This is supported by the structural x-ray diffraction analysis.

Table 6- 3. Young's modulus and yield strength for the parent and aminated materials.

	Young's Modulus (GPa)	Yield Strength (MPa)
mPP	2.22	31.5
AmPP1.6	0.44	10.2
mPP-PP	2.36	36.5
AmPP-PP1.1	0.75	11.3
AmPP-PP1.5	0.91	23.0
AmPP-PP2.2	1.50	20.3
hAmPP-PP1.5	0.95	23.3
B1hAmPP-PP1.5	0.84	17.1
B2hAmPP-PP1.6	0.60	12.2

6.3.5 Ion Transport and the State of Water

Table 6- 4 displays the amination method, ion exchange capacity, water content, ion conductivity, and ion exchange activation energy for all materials. After treatment of the material into the hydroxide form, conductivity steadily declined over the course of several days (**Figure 6-7c**), a phenomenon that has been documented elsewhere.[3] It has been discovered that on exposure to CO_2, absorption causes the rapid neutralization of hydroxide to the carbonate/bicarbonate form.[29] To ensure the membrane was at equilibrium, films were kept for one week in an open cup before testing, and assumed to be fully neutralized into the carbonate/bicarbonate form. In **Figure 6- 7a**, proton conductivity is plotted versus ion exchange capacity. For the heterogeneous materials

AmPP and AmPP-PP, water content versus IEC is somewhat linear, with consistently lower values for the random copolymer. This suggests significant differences in the distribution of ion exchange groups within the polymer matrix. Interestingly, despite large differences in chemistry and preparation technique, the homogeneous random copolymer displays properties very similar to that of the heterogeneous random copolymers.

Table 6- 4. The amination method used, theoretical anion exchange capacity (IEC_t), water content, ion conductivity (σ), and activation energy for ion transport for the aminated materials.

	Amination Method	IEC_t[1] (meq/g)	Water content (wt%)	σ[2] (mS/cm)	$E_{a,\sigma}$[2] (kJ/mol)
AmPP1.4	I	1.4	39.4	9.9	12.0
AmPP1.6	I	1.6	53.1	14.0	5.9
AmPP1.9	I	1.9	73.1	26.9	6.7
AmPP-PP1.1	I	1.1	31.6	6.4	9.5
AmPP-PP1.5	I	1.5	45.2	9.9	12.5
AmPP-PP2.2	I	2.2	57.3	17.3	12.6
hAmPP-PP1.5	II	1.5	51.1	9.2	11.8
B1hAmPP-PP1.5	II	1.5	75.7	12.0	17.5
B2hAmPP-PP1.6	II	1.6	72.3	10.5	15.3

[1]Determined by ^{1}H NMR
[2]At 100% humidity

Heterogeneous AmPP and AmPP-PP show a similar linear trend for water content versus ion conductivity (**Figure 6- 7b**). This indicates that the lower conductivity of the block copolymer AmPP-PP is directly related to the suppression of water content, limiting water assisted ion diffusion. Despite an increased water content, the homogeneous material hAmPP-PP1.5 displays no significant change in conductivity over AmPP-PP1.5. The block copolymer B1hAmPP-PP1.5 does display a higher conductivity than hAMPP-PP1.5, corresponding with, but not proportional to, the materials higher water content. This observation may indicate that microphase separation is causing a dilution of the ion exchange groups. Interestingly, the block copolymer with the higher phase separation, B2hAmPP1.6, shows marginally lower water content and conductivity. A lowering of water content has been observed with ordered block PEMs, however it is usually accompanied by an increase in conductivity.[20,30] It is possible that increased ordering is lowering water content, but the dilution effect persists. A similar dilution effect has been observed in a recent study regarding block quaternary ammonium poly(arylene ether sulfone)s.[26] All materials displayed high activation energies for ion conductivity ($E_{a,\sigma}$) due to the nature of anion exchange membranes. Lower activation energies were observed for aMPP over aMPP-PP, indicating a correlation to water content.

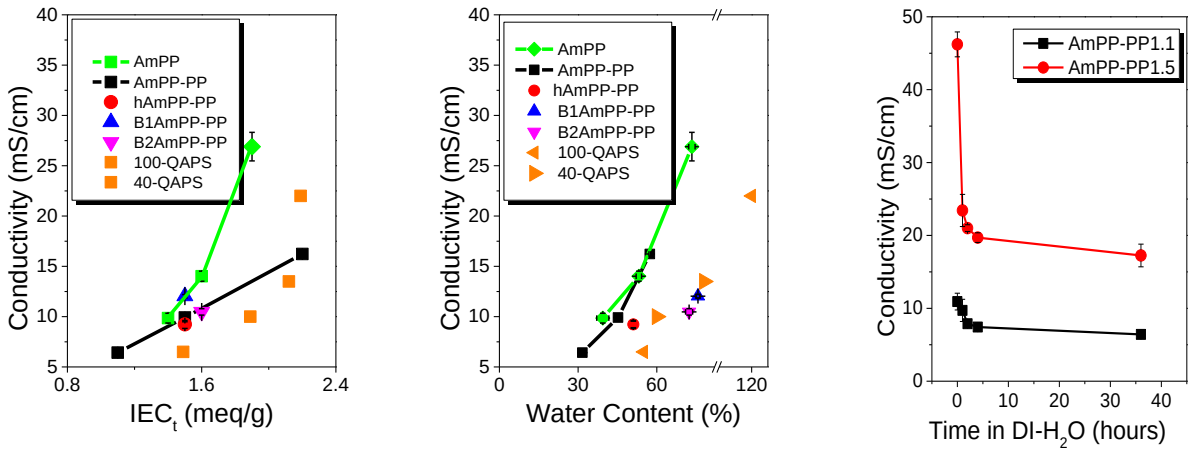

(a) (b) (c)

Figure 6- 7. Proton conductivity of AmPP, AmPP-PP and QAPS[3] as a function of (a) ion exchange capacity and (b) water content. (c) Conductivity for AmPP-PP after removal from a 1M NaOH solution as a function of DI-H2O submersion time.

Figure 6- 7a and **b** include data from a similar study for heterogeneous random (100-QAPS) and homogeneous block copolymer (40-QAPS) quaternary ammonium poly(sulfone)s.[3] The ion conductivity versus IEC of 100-QAPS and 40-QAPS have a similar trend and magnitude to those in this study. The difference in IEC may not be real, but a result of experimental versus theoretical determination. In **Figure 6- 7b**, however, it is clear that aminated poly(phenylene)s display higher conductivities for a given water content. The highly rigid poly(phenylene) backbone may restrict chain mobility, resulting in smaller hydrophilic domains. The block copolymers 40-QAPS displays a marginally higher water content resulting in a higher conductivity, a phenomena not observed for the block copolymers in this study.

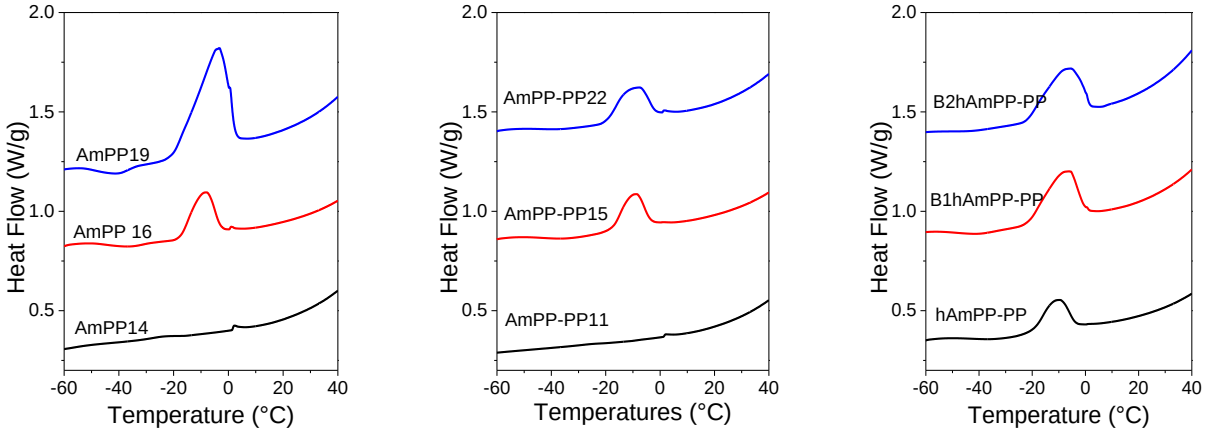

(a) (b) (c)

Figure 6- 8. DSC thermograms for adsorbed water melting endotherms for AmPP and AmPP-PP membranes (endo up).

Calorimetric studies on the freezing of water in PEMs has been extensively studied.[31–34] Three states have been identified, a bulk-like water that freezes at roughly 0 °C, loosely bound water that displays a broad heat of fusion at lower temperatures, and nonfreezing strongly bound water. All materials displayed little freezeable bulk water that, at low IEC's, were distinct from the loosely bound endotherm peak. Although a correlation is observed between free water and the IEC of AmPP and AmPP-PP, obtaining heat of fusion values for freezable bulk water proved difficult due to peak size or overlap. Despite this, it is clear AmPP1.9 has a free water peak at 0.6 °C that is significantly larger than that of the other polymers, which may indicate the importance of free water for the facilitation of ion exchange. The width of the freezeable endotherm peak can be correlated to molecules in a range of energetic states that cannot escape the binding environment near the ionic groups.[33] An increase in the width of the peak indicates an increase in the number of energetic states the water molecules can occupy, and are therefore likely to correlate to the size

and frequency of hydrophilic domains. Because the freezable bulk water peak overlapped with the loosely bound peak, these peaks are evaluated together as “freezing/free water”, and all remaining water is considered “bound water”. In **Table 6- 5** the hydration number, which is the number of water molecules per quaternary ammonium group, is listed, as well as water content that coincides with freezing or bound water. AmPP1.6 and AmPP-PP1.5 display roughly the same hydration number, of 18 and 17, respectively, however AmPP1.6 has more freezable water correlating to its increased ion conductivity. Very little difference is observed between the AmPP-PP1.5 and hAmPP-PP1.5. The homogeneous bock copolymers have large hydration numbers, well above that of AmPP1.9, however display only roughly half the free water content.

Table 6- 5. Hydration numbers, heats of fusion, total water content, free/freezable water content, and bound water content for the aminated materials.

	λ ($n H_2O/N(CH_3)_3$)	$\Delta H_{f,lb}$ (J/g)	Water content (%)	Freezing Water (%)	Bound Water (%)
AmPP1.4	16	2.5	39.4	0.3	39.1
AmPP1.6	18	35.2	53.1	5.6	47.5
AmPP1.9	21	95.2	73.1	20.9	52.2
AmPP-PP1.1	16	1.1	31.6	0.1	31.5
AmPP-PP1.5	17	32.2	45.2	4.4	40.8
AmPP-PP2.2	14	31.6	57.3	5.4	51.9
hAmPP-PP1.5	19	32.0	51.1	4.9	46.2
B1hAmPP-PP1.5	28	45.8	75.7	10.4	65.3
B2hAmPP-PP1.6	25	45.9	72.3	10.0	62.3

Figure 6- 9 displays the conductivity versus the total and free water content within the materials. The trend for total water content versus conductivity is near identical for the aminated homopolymers and random copolymers. However the importance of free water is highlighted in **Figure 6- 9b**, were a linear relationship can be observed for AmPP. The trend for AmPP-PP in this plot may indicate that this material is near the percolation limit, and may be able to be optimized at a higher ion content. As previously stated, the block copolymers show an increase in free water, yet no improvement in ion conductivity. This further indicates a dilution effect.

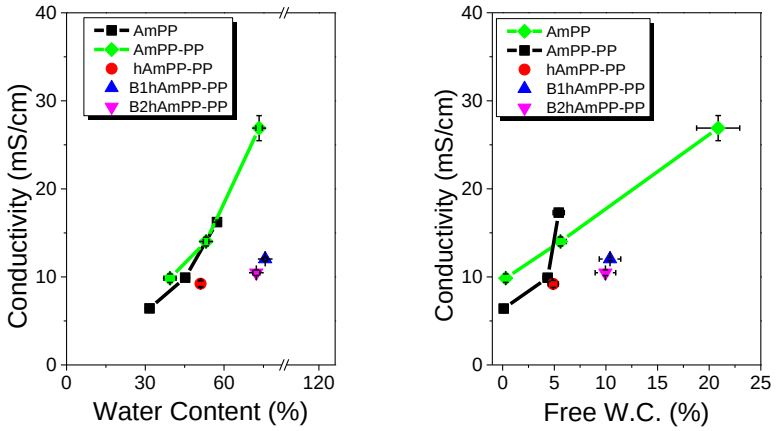

(a) (b)

Figure 6- 9. Conductivity versus (a) total water content and (b) free/freezable water content for the aminated materials.

6.3.6 Liquid Transport and Selectivity

Liquid permeability for methanol, ethanol and 2-propanol for the aminated materials is displayed in **Table 6- 6**. For heterogeneous AmPP and AmPP-PP, liquid permeability increases with increasing IEC and water content, and decreases with increasing diffusing molecule size. AmPP homopolymers display substantially greater methanol permeability's than the AmPP-PP random copolymers. This correlates well to the higher water content and ion conductivity of the AmPP homopolymers. With an increase in alcohol size, the difference in permeability between the materials is reduced indicating a lessening of the relative dimensions between the ionic channels and diffusing species. An increase in alcohol permeability is observed for hAmPP-PP1.5 over AmPP-PP1.5, with the difference widening with increasing alcohol size. This is consistent with the high degree of phase separation observed in the morphological analysis.

Table 6- 6. Liquid permeability at 30 °C of AMPP and AMPP-PP membranes.

	Permeability (10^8 cm^2/s)		
	Methanol	Ethanol	2-propanol
AmPP1.4	42.8	45.4	31.0
AmPP1.6	124.2	79.4	51.2
AmPP1.9	130.0	84.6	56.5
AmPP-PP1.1	55.1	39.1	27.4
AmPP-PP1.5	94.9	50.9	33.2
AmPP-PP2.2	108.0	74.0	53.5
hAmPP-PP1.5	102.5	73.2	55.7
B1hAmPP-PP1.5	115.5	75.9	53.1
B2hAmPP-PP1.6	112.9	68.3	46.4

In ion exchange applications such as fuel cells and redox flow batteries, ion selectivity is desired over other larger molecular or ionic species.[2,35] A method used to determine electrochemical selectivity is to plot ion conductivity versus the molecular diffusion.[36] In this analysis, an ideal ionomer with high selectivity would lie in the upper left corner. For electrochemical selectivity for methanol (**Figure 6- 10a**), AmPP1.9 and AmPP1.4 display poor selectivity, but stand out due to a high ion conductivity and high methanol resistivity, respectively. AmPP-PP1.9 appears to show the most promise, with high conductivity and moderate methanol resistivity. For the electrochemical selectivity of ion transport over 2-

propanol (**Figure 6- 10b**), AmPP1.9 and AmPP-PP1.5 reveal improved molecular resistivity. This increase in selectivity make them viable candidates for applications that require selectivity over larger molecular or ionic species. This analysis highlights the usefulness of random copolymerization in suppressing molecular diffusion in AEMs. The homogeneous materials hAmPP-PP1.5 and block copolymers B1AmPP-PP1.5 and B2AmPP-PP1.6 reveal poor electrochemical selectivity, due to high alcohol permeability and low conductivity. The understanding of property relationships such as these are of importance for the optimization of materials for particular applications.

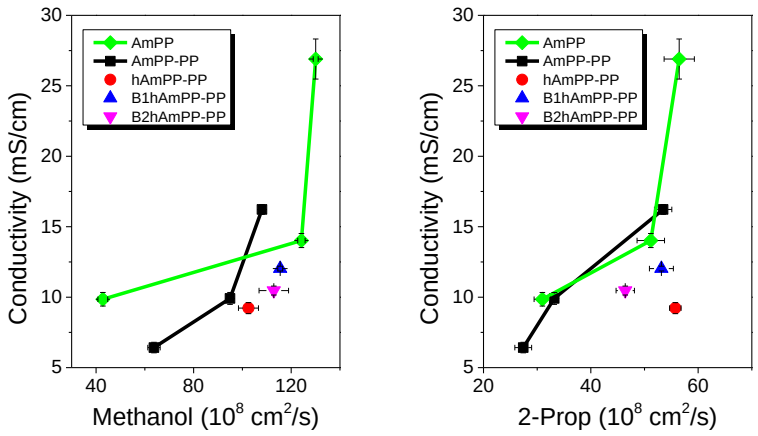

Figure 6- 10. Proton conductivity versus (a) methanol and (b) 2-propanol permeability.

6.3.7 Conclusions

The effect of membrane morphology and ion content on ion conductivity, permeability, and the state of water for a series of quaternary ammonium Diels-Alder poly(phenylene)s was investigated. Two amination methods were employed, a solid state "heterogeneous" amination technique, and a solution cast "homogeneous" amination technique. Heterogeneously aminated

homopolymers were synthesized with conductivities of up to 27 mS/cm in the carbonate form. Heterogeneously aminated random copolymerization with an equal fraction of ionic and non-ionic units improved mechanical properties, suppressed water content within the material, lowered ion conductivity, and decreased alcohol permeability. In all heterogeneous materials water content was directly related to conductivity. However, a state of water analysis revealed significantly different trends, and displayed the importance of free/freezable water for the facilitation of ion exchange.

A homogeneously aminated random copolymer displayed no change in conductivity, but expressed marginally higher water content and substantially higher alcohol permeability, indicating large microstructural changes. SAXS revealed that homogeneous block copolymers had microphase separations of up to 23 nm in size. A state of water analysis indicated that block copolymerization increased free water, yet displayed a disproportionately low conductivity and increased alcohol permeability, indicating a dilution effect.

6.4 References

[1] Alleau, T.; Barbier, F. *Actual. Chim.* **2001**, *12*, 48–57.

[2] Merle, G.; Wessling, M.; Nijmeijer, K. *J. Memb. Sci.* **2011**, *377*, 1–35.

[3] Yan, J.; Hickner, M. a. *Macromolecules* **2010**, *43*, 2349–2356.

[4] Wang, G.; Weng, Y.; Chu, D.; Chen, R.; Xie, D. *J. Memb. Sci.* **2009**, *332*, 63–68.

[5] Zschocke, P.; Quellmalz, D. *J. Memb. Sci.* **1985**, *22*, 325–332.

[6] Zhang, F.; Zhang, H.; Qu, C. *J. Mater. Chem.* **2011**, *21*, 12744.

[7] Wu, L.; Xu, T.; Yang, W. *J. Memb. Sci.* **2006**, *286*, 185–192.

[8] Zhang, S.; Yin, C.; Xing, D.; Yang, D.; Jian, X. *J. Memb. Sci.* **2010**, *363*, 243–249.

[9] Zhang, B.; Zhang, S.; Xing, D.; Han, R.; Yin, C.; Jian, X. *J. Power Sources* **2012**, *217*, 296–302.

[10] Miyake, J.; Watanabe, M.; Miyatake, K. *Polym. J.* **2014**, *46*, 656–663.

[11] Tanaka, M.; Fukasawa, K.; Nishino, E.; Yamaguchi, S.; Yamada, K.; Tanaka, H.; Bae, B.; Miyatake, K.; Watanabe, M. *J. Am. Chem. Soc.* **2011**, *133*, 10646–10654.

[12] Wang, J.; Li, S.; Zhang, S. *Macromolecules* **2010**, *43*, 3890–3896.

[13] Chen, D.; Hickner, M. a.; Wang, S.; Pan, J.; Xiao, M.; Meng, Y. *Int. J. Hydrogen Energy* **2012**, *37*, 16168–16176.

[14] Hibbs, M.; Fujimoto, C.; Cornelius, C. *Macromolecules* **2009**, *42*, 8316–8321.

[15] Stille, J.; Noren, G. *Macromolecules* **1972**, *5*.

[16] Berresheim, A. J.; Müller, M.; Müllen, K. *Chem. Rev.* **1999**, *99*, 1747–1785.

[17] Qu, W.; Ko, T. M.; Vora, R. H.; Chung, T. S. *Polymer (Guildf).* **2001**, *42*, 6393–6401.

[18] Oroujzadeh, M.; Mehdipour-Ataei, S.; Esfandeh, M. *Eur. Polym. J.* **2013**, *49*, 1673–1681.

[19] Shifrina, Z. B.; Averina, M. S.; Rusanov, A. L.; Wagner, M.; Mu, K. **2000**, 3525–3529.

[20] Yang, Y.; Holdcroft, S. *Fuel Cells* **2005**, *5*, 171–186.

[21] Schubach, H. R.; Nagy, E.; Heise, B. *Colloid Polym. Sci.* **1981**, *259*, 789–796.

[22] Katz, J. R. *Rubber Chem. Technol.* **1936**, *9*, 357–372.

[23] Mitchell, G. R.; Windle, A. H. *Polymer (Guildf).* **1984**, *25*, 906–920.

[24] Ayyagari, C.; Bedrov, D.; Smith, G. D. *Macromolecules* **2000**, *33*, 6194–6199.

[25] Lu, X.; Steckle, W. P.; Weiss, R. a. *Macromolecules* **1993**, *26*, 5876–5884.

[26] Weiber, E. A.; Meis, D.; Jannasch, P. *Polym. Chem.* **2015**, *6*, 1986–1996.

[27] Peighambardoust, S. J.; Rowshanzamir, S.; Amjadi, M. *Int. J. Hydrogen Energy* **2010**, *35*, 9349–9384.

[28] Narducci, R.; Chailan, J.-F.; Fahs, a.; Pasquini, L.; Di Vona, M. L.; Knauth, P. *J. Polym. Sci. Part B Polym. Phys.* **2016**, n/a – n/a.

[29] Yanagia, H.; Fukuta, K. *ECS Trans.* **2008**, *16*, 257–262.

[30] Choi, J.-H.; Willis, C. L.; Winey, K. I. *J. Memb. Sci.* **2012**, *394-395*, 169–174.

[31] Lu, Z.; Polizos, G.; Macdonald, D. D.; Manias, E. *J. Electrochem. Soc.* **2008**, *155*, B163.

[32] Kreuer, K. D. *J. Memb. Sci.* **2001**, *185*, 29–39.

[33] Hodge, R. M.; Edward, G. H.; Simon, G. P. *Polymer (Guildf).* **1996**, *37*, 1371–1376.

[34] Yoshida, H.; Miura, Y. *J. Memb. Sci.* **1992**, *68*, 1–10.

[35] Weber, A.; Mench, M.; Meyers, J. *J. Appl. …* **2011**, 1137–1164.

[36] Pivovar, B. S.; Wang, Y. X.; Cussler, E. L. *J. Memb. Sci.* **1999**, *154*, 155–162.

Chapter 7 Random Sulfonate Poly(phenylene) Performance and Stability in a Working Vanadium Redox Flow Battery

7.1 Introduction

The all vanadium redox flow battery (VRB) has received much attention due to a modular power output and energy capacity, as well as facile electrolyte recovery.[1] A semi-permeable ion exchange membrane is required to maintain the charge balance during charge and discharge. Obtaining an ideal ionomer for this application has proven challenging, as the ideal membrane requires high ion conductivity, high chemical stability, a low vanadium ion permeability, and low electric area resistivity.[2] Low proton conductivity decreases the voltage efficiency of the system due to a higher ohmic overpotential, and vanadium ion crossover lowers coulombic efficiency due to self-discharge. Significant work has been performed on improving the ion selectivity of highly conductive cation exchange membranes, including notable work on sulfonated poly(styrene) based ionomers,[1,3] poly(fluorenyl ether ketone)s,[4] poly(sulfone)s,[5] sulfonated poly(tetramethydiphenyl ether ether ketone)s,[6] and many others.[7] However, a greater understanding of membrane properties and how they relate to vanadium redox flow battery performance is required to improve the efficiency and cost effectiveness of the VRB system. In addition, chemical degradation of membranes has necessitated research to understand the relationship between polymer chemistry and stability in highly concentrated vanadium ion environments. This study serves to contribute to further the understanding of polymer chemistry and morphology as it relates to VRB performance, and material stability.

In Chapter 5, the synthesis and analysis of membrane morphology, ion content, ion conductivity, liquid permeability, and the state of water for a series sulfonated Diels-Alders

poly(phenylene)s (sPP) was performed. sPP membranes were developed with varying degrees of ionic character, displaying properties comparable to that of the commercial standard, Nafion 117. In this chapter, the sPP materials and Nafion 117 will be tested in a working vanadium redox flow battery, in order to contribute to the understanding of how ionomer chemistry, and electrochemical and transport properties affect VRB performance.

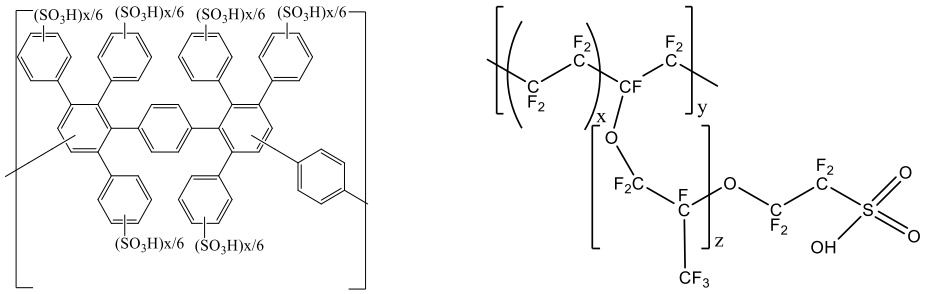

Figure 7- 1. Sulfonated Diels-Alder poly(phenylene) (left) and Nafion 117 (right).

7.2 Results and Discussion

7.2.1 Electrochemical Properties and Vanadium Ion Permeability

The ion exchange capacity, water content, conductivity and vanadium ion (VO^{2+}) permeability is listed in **Table 7- 1**. Diels-Alder cation exchange membranes (CEMs) were synthesized with a low, medium and high ion exchange capacity in order to better understand the relationship between ionomer electrochemical properties and VRB performance. Both water content and conductivity increase with increasing sPP IEC. sPP2.0 displays electrochemical properties most similar to that of Nafion 117 (Nafion), however requires significantly higher water content and ion content. In chapter 5, the interrelationships between ionomer morphology, electrochemical properties, liquid diffusion, and the state of water is discussed. Here it is observed

that despite a higher water content, sPP2.0 displays lower vanadium ion (VO^{2+}) permeability. sPP1.4 has the same water content as Nafion, however displays a vanadium ion permeability an order of magnitude lower.

Table 7- 1. The ion exchange capacity (IEC), water content, ion conductivity (σ), and vanadium ion (VO^{2+}) permeability for sPP and Nafion 117.

	IEC[1] (meq/g)	w.u. (%)	σ[2] (mS/cm)	P(VO^{2+}) (cm^2/min)
sPP1.4	1.4	30.1	34.8	3.1E-09
sPP2.0	2.0	61.1	88.4	2.1E-08
sPP2.4	2.4	105.0	122.1	5.1E-08
Nafion 117	1.0	33.0	100.4	3.2E-08

[1]Determined by titration
[2]At 100% humidity

Figure 7- 2a displays vanadium ion permeability versus free water content. As previously discussed, a large portion of the water within sPP is bound to the ion exchange units, both in the ionic and intermediate phases. However, considering only the free water gives a very similar trend for both sPP and Nafion 117. Free water gives some insight into the size, number, and/or interconnectivity of ionic aggregates, as ionic regions contain a greater number of freezable water molecules in lower energetic states. Although Nafion has a low water content, it displays a high degree of ionic aggregation that forms interconnected channels[8] which allows for a large proportion of water to be loosely bound within the ionic domains. This should theoretically lower

the energy requirement for the diffusion of vanadium ions (VO^{2+}) across the membrane. **Figure 7- 2b** displays conductivity as a function of vanadium ion permeability. This plot gives some indication of proton selectivity, whereby an ideal ionomer would lie in the upper left hand corner. Similar to that observed between free water content and VO^{2+} permeability, little difference between Nafion 117 and sPP is evident. This analysis emphasizes the difficulty in cation exchange membrane optimization for VRB's. The ionomers must also exhibit high resistivity for other more permeable ionic species, and therefore this measurement may not correlate well to ion selectivity during VRB operation. In **Figure 7- 2c**, the conductivity is given as a function of 2-propanol permeability. As discussed in Chapter 5, sPP and Nafion display drastically different permeability characteristics for this molecular species, and is attributed the difference in morphology. That is, diffusion of 2-propnaol is highly influenced by ionic channel size and connectivity. This indicates that, although sPP displays similar VO^{2+} selectivity, Nafion displays poorer proton selectivity over large molecules which may result in adverse effects during VRB operation due to the permeation of large vanadium and sulfate based ions.

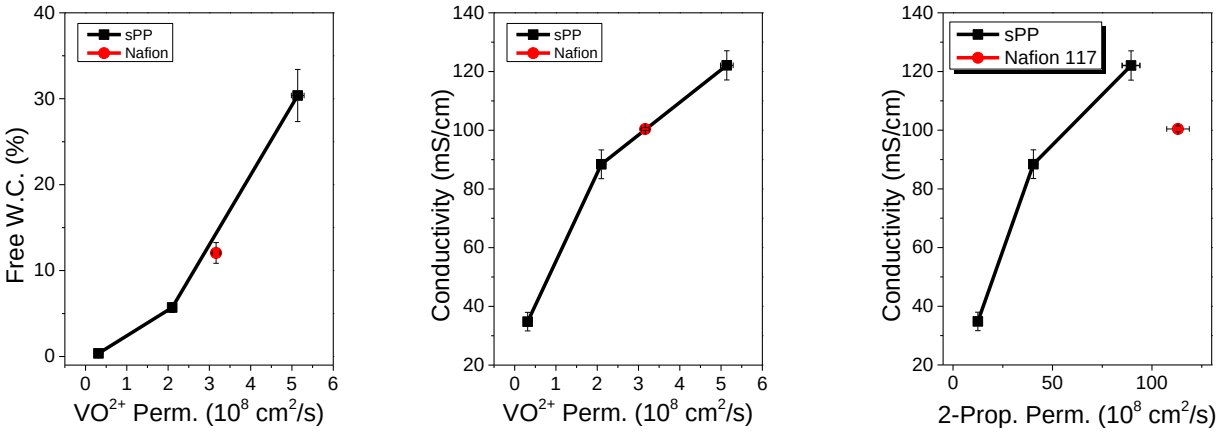

(a) (b) (b)

Figure 7- 2. The (a) free water content and (b) conductivity as a function of vanadium ion permeability for sPP and Nafion 117. The (c) conductivity as a function of 2-propanol permeability.

7.2.2 Vanadium Redox Flow Battery Performance

The random sulfonate Diels-Alder poly(phenylene)s (sPP) and Nafion were tested in a working vanadium redox flow battery. The coulombic efficiency (CE), displayed in **Figure 7- 3a**, is a measure of the capacity loss within the system. A low CE is primarily the result of energy loss due to vanadium ion crossover. It can be seen that CE increases with increasing charge/discharge current density. This is due to, at higher charge and discharge currents, less time for vanadium ions to diffuse across the membrane before the maximum voltage is reached. As discussed, VO^{2+} permeability for sPP and Nafion (**Table 7- 2**) indicated that Nafion would exhibit similar vanadium ion selectivity to sPP2.0. However, Nafion displays significantly lower ion selectivity, highlighting the importance of the consideration of larger diffusing species in permeability/selectivity studies, such as 2-propanol. As noted in **Table 7- 2**, sPP2.0 exhibits a CE

of 94.0% at 20 mS/cm^2, 1.3% higher than Nafion. sPP1.4 displays incredible vanadium ion rejection, with a CE of 97.8% at 20 mA/cm^2, approaching 100% at higher current densities.

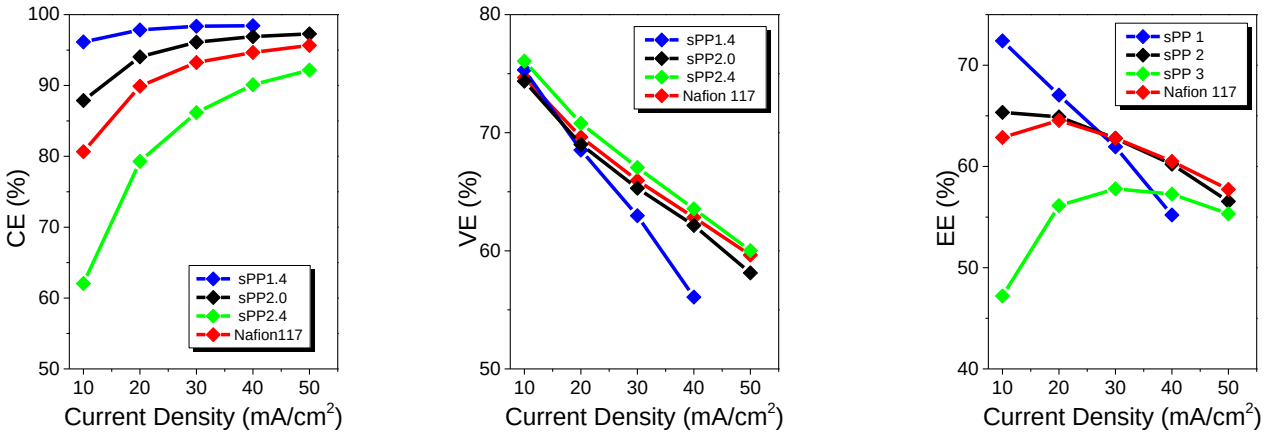

(a) (b) (c)

Figure 7- 3. The (a) Coulombic efficiency, (b) voltage efficiency and (c) energy efficiency as a function of current density for sPP and Nafion 117 materials.

Figure 7- 3b displays the voltage efficiency (VE) as a function of current density. Charge and discharge voltage is determined by the thermodynamic reduction potential of the redox couples in the half cells, and the overpotential of the cell. Membrane resistance contributes to the overpotential, and therefore higher membrane resistance will cause higher charge voltages and lower discharge voltages, lowering the VE. In addition, higher currents will increase the ohmic resistance, causing the observed decrease in voltage efficiency with increasing current density. The VE of sPP increases as a function of IEC, indicating a strong relationship to proton conductivity. Despite a highly homogeneous morphology, sPP2.4 displays higher VE than Nafion due to superior electrochemical transport properties. As shown in **Table 7- 2**, at 20 mA/cm^2, the

VE of sPP's lie within 2% of Nafion 117, correlating to ionomer conductivity, however indicating a narrowed effect likely due to high electrolyte concentration.

Table 7- 2. The vanadium ion permeability and open circuit voltage discharge time (OCV), and coulombic, voltage and energy efficiencies for sPP and Nafion 117 at 20 mA/cm^2.

	P(VO^{2+}) (cm^2/min)	OCV (hours)	CE (%)	VE (%)	EE (%)
sPP1.4	3.1E-09	>140	97.8	68.5	67.1
sPP2.0	2.1E-08	87	94.0	69.0	64.9
sPP2.4	5.1E-08	17	79.3	70.8	56.1
Nafion 117	3.2E-08	48	92.7	69.9	64.5

The energy efficiency (EE) is the product of the CE and VE, and can be used to represent the overall efficiency of the system (**Figure 7- 3c**). sPP1, does not show a local maxima in EE as a function of current density, as the materials performance is strongly dictated by its high electrochemical resistance. Both sPP2.0 and Nafion display optimal performance at 20 mA/cm^2, while sPP2.4 is most competitive at 30 mA/cm^2. As can be seen in **Table 7- 2**, sPP1.4 displays competitive properties and low current densities, 2.6% better than Nafion at 20 mA/cm^2. sPP2.0 and Nafion 117 show comparable performance, likely within the margin of error, at 64.9 and 64.5% EE, respectively. Although it is intuitive that high conductivity materials are most competitive fast charge-discharge cycles, this analysis indicates that sPP2.0 and Nafion 117 are preferred over sPP2.4 up to 50 mA/cm^2, due to superior proton selectivity.

Figure 7- 4a displays the charge and discharge curves for all materials at 10 mA/cm^2. The capacity has been normalized to highlight the differences in charge and discharge time. A self-discharge test was performed which is a measure of capacity loss of the battery when the system is not connected to any electrodes. As discussed, the primary loss of capacity is due to permeation of vanadium ion across the ion exchange membrane. The open circuit voltage plot for all materials is displayed in **Figure 7- 4b**. All plots decline slowly to 1.25 V and then suddenly drop. The OCV discharge times correlate well to the CE values at 10 mA/cm^2. Nafion and sPP2.4 displayed poor vanadium rejection, and consequently had OCV discharge times of roughly 48 and 17 hours, respectively. sPP2.0 had a discharge time of 87 hours, almost double that of Nafion. sPP1.4 displayed discharge times over 140 hours, coinciding with the materials incredible proton selectivity.

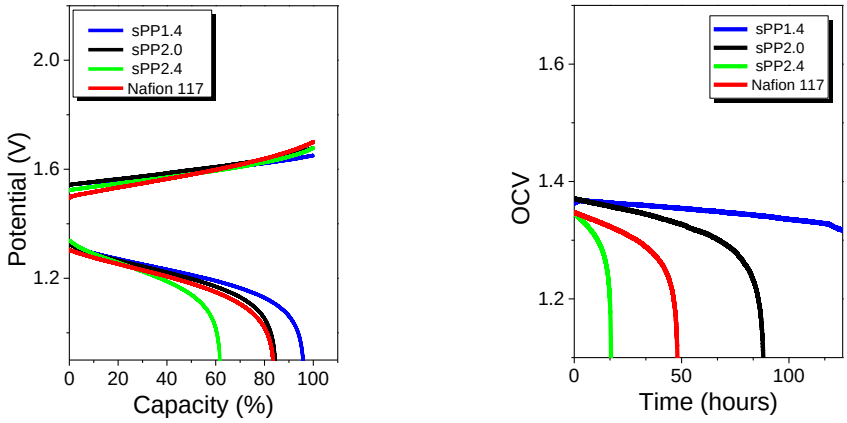

(a) (b)

Figure 7- 4. (a) Charge-discharge profile at 10 mA/cm^2 and the (b) open circuit voltage profile for sPP and Nafion 117.

7.2.3 Effect of Membrane Thickness

Although not frequently considered, it has been shown that membrane thickness plays a vital role in VRB perforamce.[9] In this section, the effect of membrane thickness of sPP2.0 on VRB performance is observed. As seen in **Figure 7- 5a**, the coulombic efficiency increases drastically with increasing membrane thickness, with a 10.6% difference at 10 mA/cm^2 between the 60 µm and 172 µm membranes. The sPP2.0 membrane with a thickness of 60 µm has a CE comparable to that of Nafion 117. It can be seen that the thicker membrane serves as a better barrier between the two electrolyte solutions, slowing the rate of diffusion of vanadium ions across the membrane and reducing self-discharge. Nafion's bicontinuous morphology necessitates a thick membrane to provide sufficient ion selectivity, while sPP's homogeneous morphology can provide the same vanadium ion resistance at 60 µm. The increased thickness, however, not only reduces vanadium ion crossover, but also the rate of diffusion of charge carrier ionic species, i.e. protons. In **Figure 7- 5b** this tradeoff is clear, as voltage efficiency decreases with thickness, implying a greater membrane resistance and resulting overpotential. It is of note that sPP2.0 – 60 µm, which displayed CE values similar to that of Nafion, displays superior VE at all current densities. In **Figure 7- 5c** it is shown that the thickness of sPP2.0 has a direct impact on the overall energy efficiency of the system. The 100 µm film appears optimal for low current applications, while the thin film better for applications that require fast charge-discharge cycles. This can be attributed to sPP2.0's incredible ion selectivity, allowing a reduction in thickness to decrease the membrane resistance and increase the VE far more significantly than it decreases the CE.

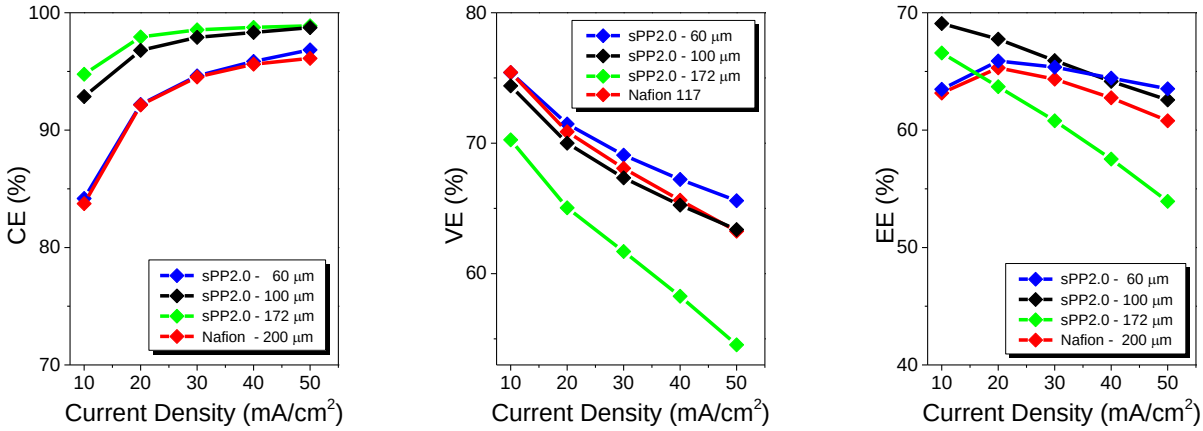

(a) (b) (c)

Figure 7- 5. The (a) coulombic efficiency, (b) voltage efficiency and (c) energy efficiency as a function of current density for sPP2.0 membranes with different thicknesses.

Figure 7- 6a displays the charge and discharge curves for sPP2.0 with different thickness at 10mA/cm^2. The capacity has been normalized to highlight the differences in charge and discharge time. The open circuit voltage plot for all materials is displayed in **Figure 7- 6b**. As previously noted, all plots decline slowly to 1.25 V and then suddenly drop. The OCV discharge times increase with increasing CE. Nafion and the sPP2.0 membrane with a thickness of 60 µm displayed poor vanadium ion rejection, and consequently had equally short discharge times of roughly 75 hours. The 100 µm membrane had a discharge time of 87 hours, almost double that of Nafion. The thickness of the 172 µm membrane afforded it with incredible proton selectivity, displaying a discharge time of over 195 hours.

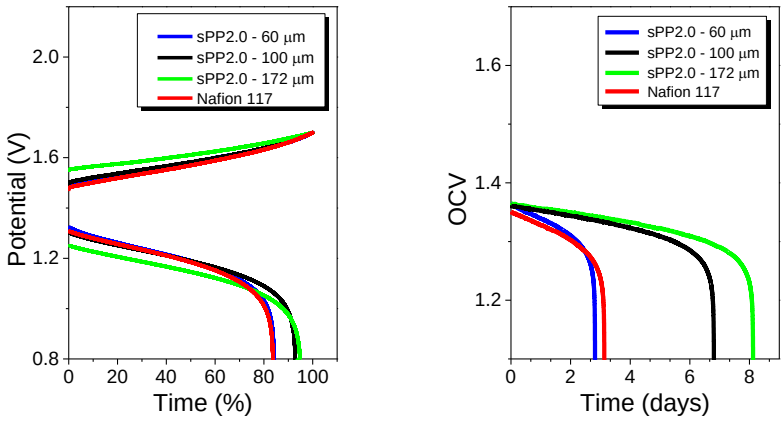

(a) (b)

Figure 7- 6. (a) Charge-discharge at 10 mA/cm^2 with a normalized capacity, and (b) open circuit voltage data for sPP2.0 of different membrane thicknesses, and Nafion 117.

7.2.4 Charge-Discharge Cycling and Membrane Stability

The most direct way in which membrane stability has been tested in VRB's has involved the *in-situ* method cell cycling. This method involves monitoring CE, VE and/or EE until a sharp drop in efficiency is observed. In **Figure 7- 7a,** the voltage and energy efficiencies are shown for membranes sPP2.0 and Nafion 117 as a function of cycle number (30 mA/cm^2). After over 40 cycles (roughly 2 week time equivalent) no failure was evident in either material. During the course of testing the materials displayed a marginal increase in coulombic efficiency, and a gradual drop in EE due to a lowering of the voltage efficiency. This rise in CE and drop in VE can be explained by observing the rate of capacity loss displayed in **Figure 7- 7b**. As discussed, sPP2.0 – 100 µm displays a coulombic efficiency just 3.4% greater than Nafion 117, however the capacity loss after 40 cycles is dramatic. This highlights the importance of coulombic efficiency on ensuring system durability. In addition, it suggests that sPP, although does suffer from degradation, outperforms in

low capacity cycling tests. This analysis does not appear to serve as a good quantitative or qualitative measurement of membrane stability.

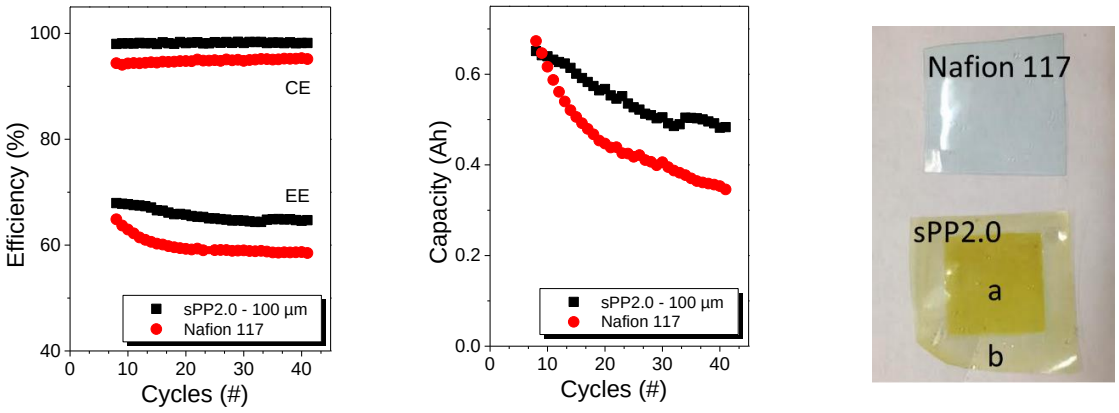

(a) (b) (c)

Figure 7- 7. The (a) cycling efficiency and (b) capacity as a function of cycle number for sPP2.0 and Nafion 117. (c) A photograph of the membranes after cycle testing.

The membranes, after more than 3 weeks of exposure to vanadium electrolyte, were removed from the system and analyzed (**Figure 7- 7c**). The entire Nafion 117 membrane appeared blue, likely due to vanadium ion substitution of the proton on the sulfonic acid group. sPP2.0 drastically darkened in the region that was in direct contact with the vanadium electrolyte (labeled "a"), however no change in thickness was observed. The conductivity of Nafion 117 and sPP2.0 region "a" was measured, and are listed in **Table 7- 3**. Nafion 117's conductivity dropped from 100.4 to 25.8 mS/cm, while sPP2.0's conductivity dropped from 88.4 to 10.1 mS/cm. These "vanadium-ion form" conductivities are comparable to the decrease in conductivity due to treatment into the sodium form (Na^+), and therefore are not a clear indication of degradation.

Table 7- 3. Conductivity of sPP2.0 and Nafion 117 in the acid and salt (Na+) forms, as well as the proton conductivity after 3 weeks of VRB system *in-situ* exposure to vanadium electrolyte.

	σ (H^+) (mS/cm)	σ (Na^+) (mS/cm)	σ_{end} (mS/cm)
sPP2.0a	88.4	14.4	10.1
Nafion117	100.4	26.2	25.8

As observed, the *in-situ* testing does not accurately describe degradation during long term operation. For this reason a procedure has been proposed to test materials in harsh vanadium ion environments.[5,10,11] In this study, a material was placed in a solution of 0.1 M V^{5+} and 5 M H_2SO_4 at 40 °C for a number of days. The V^{5+} solution is bright yellow, and changes to blue during polymer degradation, attributed to reduction to the VO^{2+} ion during backbone degradation. This *ex-situ* method allows one to qualitatively observe gradual changes in solution and membrane color, as well as membrane flexibility. After several days the parent polymer gave no indication of degradation, while the sPP solutions gradually turned from yellow to green, at a rate increasing with IEC. This observation may indicate that water content and swelling gives access to the reactive V^{5+} ion to the polymer backbone. After 10 days, the materials were removed from the vanadium solutions and rinsed with water. No degradation or color change was evident for Nafion 117, likely due to its highly fluorinated backbone. The sPP membranes experienced significant darkening and became increasingly brittle with IEC. It is clear that the sPP materials suffer from long-term degradation induced by exposure to the V^{5+} vanadium ion. A thorough investigation into the V^{5+} degradation of sulfonated Radel® membranes by Chen *et al.* gave insight into the

mechanism of the degradation of aromatic groups.[5] It was concluded that the degradation mechanism involved the addition of hydroxyl and quinone groups on the backbone of the material. WAXS (**Figure 7- 8b**) revealed a large increase in intensity of the ionic peak, likely due to the presence of the vanadium ions in the ionic phase of the material. The x-ray structural analysis did not confirm degradation in the sPP materials.

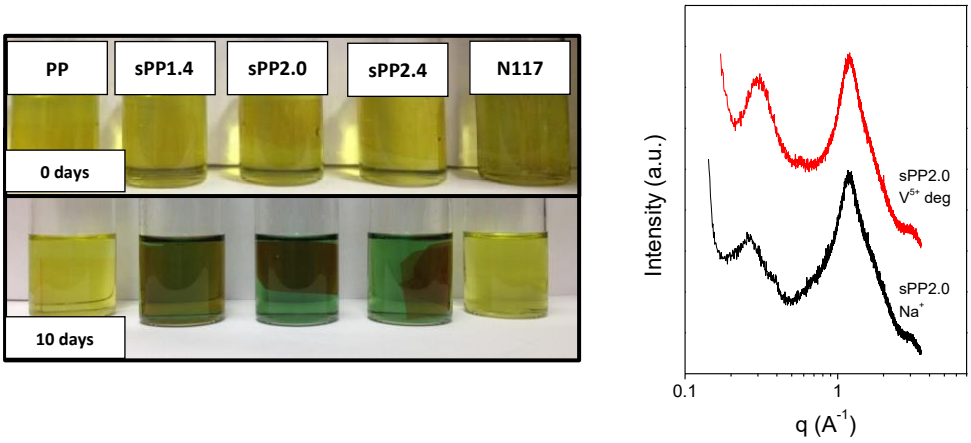

(a) (b)

Figure 7- 8. (a) The *ex-situ* degradation study of sPP and Nafion 117 films in a V^{5+} vanadium ion solution after 10 days and (b) WAXS data for sPP2.0 before and after the cell cycling test.

In **Figure 7- 9a** the FTIR spectra is shown for sPP2.0 before and after VRB testing. Although the materials exit VRB testing with complete flexibility, the color change may indicate changes in either the ionic or phenyl peaks, and so normalization proved difficult. A significant change in the shape and relative intensity of the 1178 cm^{-1} sulfonic acid group peak may indicate sulfonic acid interactions with the vanadium ion. In **Figure 7- 9b** we see the change in IR spectra after rigorous *ex-situ* stability testing. As discussed, after 5 days all materials experienced complete loss of mechanical properties and had visible signs of cracking. A thorough study on the

degradation of s-Radel revealed large changes in the FTIR spectra during degradation.[5] The most notable being a shift in a the bending O-H vibration peak, and a new peak at 1677 cm^{-1}, deemed to lie within the quinone region. In this work, a new peak is observed at 1724 cm^{-1}, corresponding to a C=O stretch. A peak at 912 cm^{-1}, not observed in the s-Radel study, lies within the mono-substituted alkene region. These findings do not contradict the proposed mechanism by Chen and Hickner, that is the incorporation of hydroxyl groups through a radical mechanism, followed by oxidation of the hydroxylated aromatic group into quinone through a redox mechanism.[5]

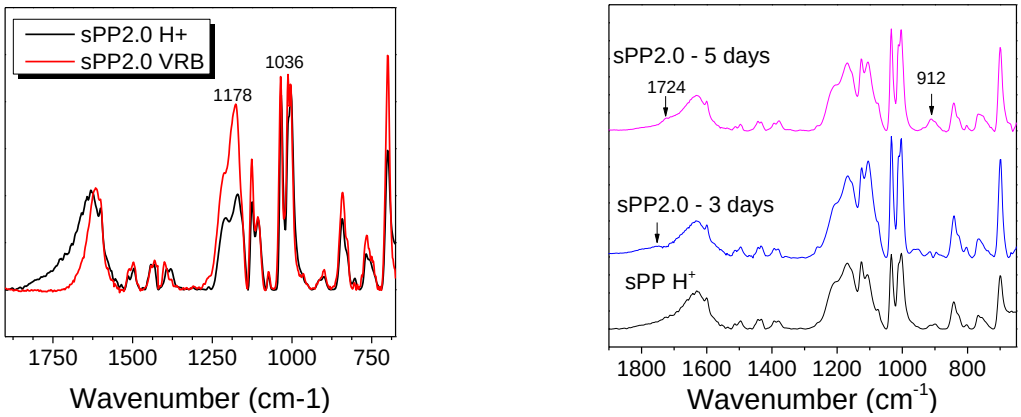

(a) (b)

Figure 7- 9. FTIR spectra of (a) sPP2.0 before and after testing in the VRB system, and (b) stages of V^{5+} degradation in the *ex-situ* study.

7.3 Conclusions

In this study, the vanadium ion permeability, battery performance, and material stability of random sulfonate Diels-Alder poly(phenylene)s (sPP) is reported. sPP thin films were tested with IEC's up to 2.4 meq/g, displaying an ion conductivity of 122.1 mS/cm and a water content of 105.0%. Nafion 117 and sPP revealed similar relationships for proton conductivity vs. VO^{2+}

permeability. Despite this, sPP2.0 displayed a CE of 94.0% at 20 mS/cm^2, 1.3% higher than Nafion. sPP1.4 displayed incredible vanadium ion rejection, with a CE of 97.8% at 20 mA/cm^2, approaching 100% at higher current densities. Voltage efficiency was directly correlated to proton conductivity, with sPP1.4 < sPP2.0 < Nafion 117 < sPP2.4. The energy efficiency of sPP2.0 exceeded that of Nafion 117 at low current densities. Film thickness was shown to be a vital factor in the optimization of a charge carrier for a VRB system. With increasing membrane thickness, the rate of diffusion of vanadium ions across the membrane was reduced, ultimately increasing the coulombic efficiency. The increased thickness, however, not only reduced vanadium ion crossover, but also the rate of diffusion of the charge carrier ionic species, lowering the voltage efficiency. For sPP2.0, a thickness of 60 μm displayed equal voltage efficiency to that of Nafion 117, yet superior coulombic efficiency. By tuning film thickness, sPP2.0 membranes were produced that exceeded the energy efficiency of Nafion at all current densities. Charge-discharge cycling did not adequately indicate membrane degradation, as changes in efficiency were driven by capacity loss due to vanadium ion crossover. An *ex-situ* experiment indicated that all sulfonated poly(phenylene) materials display degradation after 10 days in 0.5 M V^{5+} + 5 M H_2SO_4 solution at 40 °C. This was indicated by a darkening of the films, and loss of flexibility.

7.4 References

[1] Skyllas-Kazacos, Maria; Miron, Rychick; Robins, R. ALL-VANADIUM REDOX FLOW BATTERY. 4,786,567, 1988.

[2] Li, X.; Zhang, H.; Mai, Z.; Zhang, H.; Vankelecom, I. *Energy Environ. Sci.* **2011**, *4*, 1147.

[3] Mohammadi, T.; Skyllas-Kazacos, M. *J. Memb. Sci.* **1995**, *98*, 77–87.

[4] Chen, D.; Wang, S.; Xiao, M.; Han, D.; Meng, Y. *J. Power Sources* **2010**, *195*, 7701–7708.

[5] Chen, D.; Hickner, M. a. *Phys. Chem. Chem. Phys.* **2013**, *15*, 11299–11305.

[6] Mai, Z.; Zhang, H.; Li, X.; Bi, C.; Dai, H. *J. Power Sources* **2011**, *196*, 482–487.

[7] Weber, A.; Mench, M.; Meyers, J. *J. Appl. …* **2011**, 1137–1164.

[8] Mauritz, K. a; Moore, R. B. *Chem. Rev.* **2004**, *104*, 4535–4585.

[9] Liu, Q.; Grim, G.; Papandrew, A. *J. …* **2012**, *159*, 1246–1252.

[10] Sukkar, T.; Skyllas-Kazacos, M. *J. Appl. Electrochem.* **2004**, *34*, 137–145.

[11] Kim, S.; Tighe, T. B.; Schwenzer, B. **2011**, 1201–1213.

Chapter 8 Random Copolymer Quaternary Ammonium Diels-Alder Poly(phenylene) Performance and Stability in a Working Vanadium Redox Flow Battery

8.1 Introduction

In this chapter, the effect of ionic and non-ionic unit copolymerization of a quaternary ammonium Diels-Alder poly(phenylene) on vanadium ion permeability, battery performance, and material stability is reported. As discussed in the literature review, a semi-permeable ion exchange membrane is required to maintain the charge balance during charge and discharge. Obtaining an ideal ionomer for this application has proven challenging, as the ideal membrane requires high ion conductivity, high chemical stability, a low vanadium ion permeability, and low electric area resistivity.[1] Many efforts have been made regarding the optimization of cation exchange membranes, however obtaining a material with a high ion conductivity, while minimizing vanadium ion crossover, has proven challenging.[2–7] The use of anion exchange membranes (AEMs) has been proposed, as it is theorized that they will result in reduced vanadium ion permeability due to the Donnan exclusion principle.[7–10] In addition, AEMs may be able to transport multiple charge carriers to balance the redox reaction, including protons, sulfate, or sulfuric acid based electrolytes. Work regarding AEMs in VRBs include the performance of ammonium functionalized poly(fluorenyl ether)s,[11] poly(phthalazinone ether ketone)s,[8,12] and poly(sulfone)'s.[13] This study serves to contribute to further the understanding of the interrelationship between AEM polymer chemistry, VRB performance, and material stability.

8.2 Results and Discussion

8.2.1 Background

In Chapter 6, the synthesis and analysis of membrane morphology, ion content, ion conductivity, liquid permeability, and the state of water for a series quaternary ammonium Diels-Alders poly(phenylene)s was performed. This characterization was necessary as an initial assessment of ionomer properties, and used to select the most competitive materials for testing in the working vanadium redox flow battery application. In this analysis, it was discovered that quaternary ammonium Diels-Alders poly(phenylene) homopolymers (AmPP) revealed high conductivities, however displayed poor mechanical properties and insufficient ion selectivity. For an equivalent ion exchange capacity, random copolymer quaternary ammonium Diels-Alder poly(phenylene)s (AmPP-PPs) effectively reduced water content, improved mechanical properties, and increased ion selectivity. The analysis of two amination methods was discussed, a solid state "heterogeneous" amination technique, and a solution cast "homogeneous" amination technique. The less utilized homogeneous technique, applied to a random copolymer and two block copolymers, had adverse effects on all properties, indicating a dilution effect. It was concluded that the random copolymer quaternary ammonium Diels-Alder poly(phenylene)s (AmPP-PP) displayed the most competitive ionomer properties. The AmPP-PP materials were therefore selected for testing in a working VRB. A quaternary ammonium homopolymer was included in the assessment to validate this hypothesis.

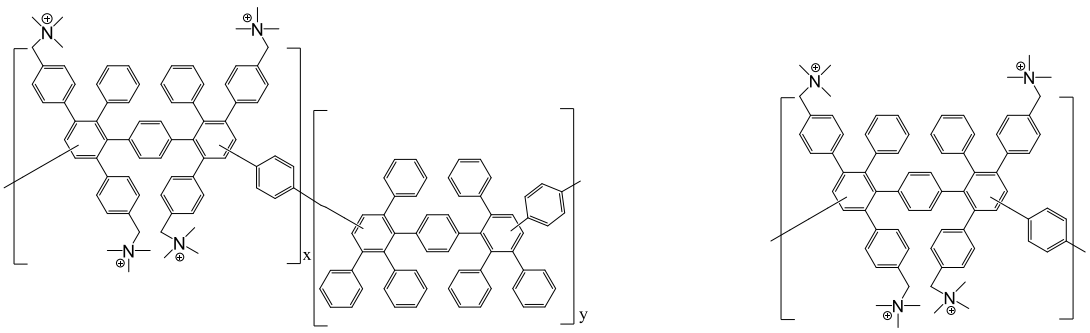

Figure 8- 1. A depiction of the chemical structure of the quaternary ammonium Diels-Alder poly(phenylene) random copolymer AmPP-PP (left) and homopolymer AmPP (right).

8.2.2 Electrochemical Properties and Vanadium Ion Permeability

The ion exchange capacity, water content, conductivity and vanadium ion (VO^{2+}) permeability for AmPP-PP, AmPP, and Nafion 117 is listed in **Table 8- 1**. As discussed in Chapter 6, when exposed to CO_2, absorption causes the rapid neutralization of hydroxide to the carbonate/bicarbonate counter ion.[14] For this reason, all films were kept for one week in an open cup before testing, and assumed to be fully stable by neutralization into the carbonate/bicarbonate form. The anion exchange membranes (AEMs) display significantly lower conductivities than the cation exchange membrane, Nafion 117 (Nafion). The carbonate/bicarbonate anion has far lower dilute solution mobility than hydroxyl or protons ions, and therefore the AEMs will predominantly facilitate water assisted ion diffusion. For AmPP-PP, with increasing IEC, we observe increasing water content, conductivity, and vanadium ion permeability. AmPP1.6 and random block copolymer AmPP-PP1.5 are similar in IEC, yet AmPP-PP1.5 displays a water content almost 8% lower. In Chapter 6, it was concluded that the random copolymer chemistry encouraged larger hydrophobic domains, suppressing water content. The drop in water content is accompanied by a lower ion conductivity and vanadium ion permeability.

Table 8- 1. The theoretical ion exchange capacity (IEC_t), water content, ion conductivity (σ), and vanadium ion (VO^{2+}) permeability for AmPP, AmPP-PP and Nafion 117.

	IEC_t[1] (meq/g)	w.u. (wt%)	σ[2] (mS/cm)	$P(VO^{2+})$ (cm^2/min)
AmPP1.6	1.6	53.1	14.0	7.7E-08
AmPP-PP1.1	1.1	31.6	6.4	3.3E-09
AmPP-PP1.5	1.5	45.2	9.9	3.2E-08
AmPP-PP2.2	2.2	57.3	17.3	4.3E-08
Nafion117	1.0	33.0	100.4	9.7E-08

[1]Determinedby NMR
[2]At 100% humidity

Figure 8- 2a displays free water content as a function of vanadium ion permeability. Although AmPP-PP and AmPP have relatively high total water content, they contain very little is free water necessary for water-assisted ion diffusion. Both graphs indicate that, despite a comparable state of water, AmPP-PP displays lower vanadium ion permeability (greater resistivity). **Figure 8- 2b** displays conductivity as a function of vanadium ion permeability, whereby an ideal ionomer would lie in the upper left hand corner. This plot reveals that, despite highly competitive electrochemical properties, Nafion displays similar vanadium resistivity to the AmPP-PP membranes. It was suspected that the anion exchange membranes would exhibit low vanadium ion diffusion due to the electrostatic interactions, or the Donnan exclusion principle, however this is not evident in this analysis. The trend of AmPP-PP lies to the left of the homopolymer, AmPP, indicating that block copolymerization has a net positive effect on the ion conductivity/vanadium permeability trade-off, potentially indicating improved VRB performance.

It is acknowledged that this experiment does not account for smaller, more permeable, vanadium ion species. As discussed in Chapter 6, for most species, the random copolymer with the highest ionic character AmPP-PP2.2 exhibits lower molecular and ion permeability than AmPP1.6. This highlights the increased ion selectivity induced by random copolymerization. This is not displayed for the ion/2-propanol selectivity (**Figure 8- 2b**), indicating lessened relative dimension between the channel size and the diffusing species. This is in contrast to Nafion 117 which displays high 2-propanol permeability due to large interconnected channels. Overall, it is concluded that the random copolymers display superior selectivity for small and large diffusing species over AmPP1.6 and Nafion 117.

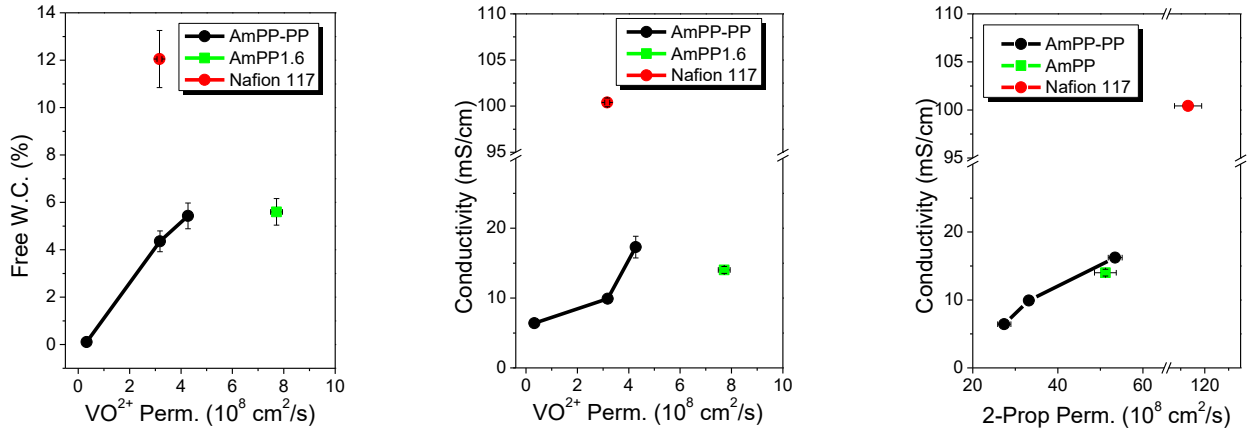

(a) (b) (c)

Figure 8- 2. The (a) free water content and (b) ion conductivity as a function of vanadium ion permeability for AmPP1.6 and AmPP-PP materials. The (c) ion conductivity as a function of 2-propanol permeability.

8.2.3 Vanadium Redox Flow Battery Performance

The quaternary ammonium homopolymer (AmPP), random copolymer Diels-Alder poly(phenylene)s (AmPP-PP), and Nafion were tested in a working vanadium redox flow battery. The coulombic efficiency (CE), displayed in **Figure 8- 3a**, is a measure of the capacity loss within the system. A low CE is primarily the result of energy loss due to vanadium ion crossover. It can be seen that CE increases with increasing charge/discharge current density. This is because, at higher charge and discharge currents, there is less time for vanadium ions to diffuse across the membrane before the maximum voltage is reached. Coinciding with a lower vanadium ion permeability (**Table 8- 2**), AmPP1.6 displays lower coulombic efficiencies than Nafion. At all current densities, despite almost twice the water content, AmPP-PP2.2 displays CE's comparable to that of Nafion. As seen in **Table 8- 2**, AmPP-PP1.5 and AmPP-PP2.2 display an improvement of 14% and 4%, respectively, versus AmPP1.6 at 10 mA/cm^2. This demonstrates the high ion selectivity of quaternary ammonium Diels-Alder poly(phenylene) random copolymers for the charge carrier in the vanadium redox flow battery application.

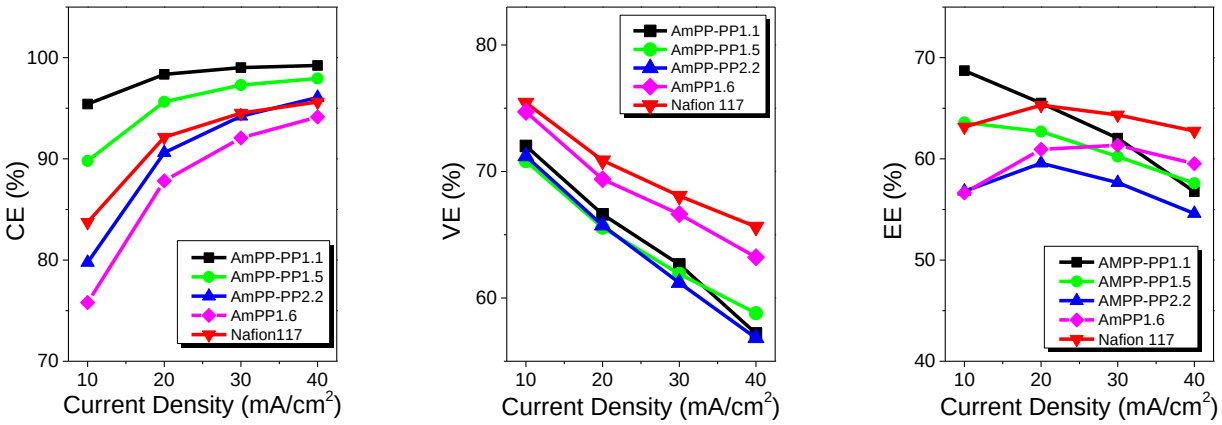

(a) (b) (c)

Figure 8- 3. The (a) coulombic efficiency, (b) voltage efficiency, and (c) energy efficiency as a function of current density for AmPP, AmPP-PP, and Nafion 117.

Figure 8- 3b displays the voltage efficiency (VE) as a function of current density. The charge and discharge voltage is determined by the thermodynamic reduction potential of the redox couples in the half cells, and the overpotential of the cell. Membrane contributions to the overpotential causes higher charge voltages and lower discharge voltages, lowering the VE. The higher currents will increase the ohmic resistance, and cause lower voltage efficiency with increasing current density. A variation in VE of only roughly 2% is observed for the AmP-PP materials despite large differences in IEC. In addition, despite an incredibly high conductivity, Nafion displays a VE of at most only 8% higher than that of the other materials. This may indicate that the high electrolyte concentration decreases the difference in ionic conductivity during operation, and therefore area resistivity, a conclusion also made elsewhere.[15–17] AmPP1.6 displays a surprisingly high voltage efficiency. The larger ionic domains of the homopolymer may allow for better transport of sulfate based anionic charge carriers, however at the expense of severe losses in coulombic efficiency.

Table 8- 2. The vanadium ion permeability, and coulombic, voltage and energy efficiencies for the aminated materials at 10 mA/cm^2.

	$P(VO^{2+})$ (cm^2/min)	CE %	VE %	EE %
AmPP1.6	7.7E-08	75.8	74.7	56.6
AmPP-PP1.1	3.3E-09	95.4	72.0	68.7
AmPP-PP1.5	3.2E-08	89.8	70.8	63.6
AmPP-PP2.2	4.3E-08	79.8	71.2	56.8
Nafion117	9.7E-08	83.7	75.4	63.2

The energy efficiency (EE) is the product of the CE and VE, and can be used to represent the overall efficiency of the system (**Figure 8- 3c**). As seen in **Table 8- 2**, at low current densities the materials with the lowest vanadium permeability display the highest EE, most notably AmPP-PP1.1 and AmPP-PP1.5. This may indicate that these highly selective materials are most useful for low current applications. At higher current densities less time is taken to achieve the maximum set voltage, lowering the CE contribution and therefore lowering the energy efficiency of the high resistance AmPP-PP membranes. AmPP1.6 and Nafion, due to high VE, display superior performance during quick charge/discharge cycles. However, due to poor ion selectivity and only moderate ion conductivity, AmPP1.6 does not display properties competitive with that of Nafion.

Figure 8- 4a displays the charge and discharge curves for all materials at 10mA/cm^2. The capacity has been normalized to highlight the differences in charge and discharge time. A self-

discharge test was performed which is a measure of capacity loss of the battery when the system is not connected to any electrodes. As discussed, the primary loss of capacity is due to permeation of vanadium ion across the ion exchange membrane. The open circuit voltage plot for all materials is displayed in **Figure 8- 4b**. All plots decline slowly to 1.25 V and then suddenly drop. The OCV discharge times correlate well to the CE values at 10 mA/cm^2. Nafion had an OCV discharge time of roughly 75 hours. AmPP1.6 and AmPP-PP2.2 display poor selectivity, with OCV discharge times of 37 and 45 hours, respectively. AmPP-PP1.5 had a discharge time of 100 hours, over double that of AmPP1.6, while AmPP-PP1.1 took 11 days, displaying high vanadium ion rejection.

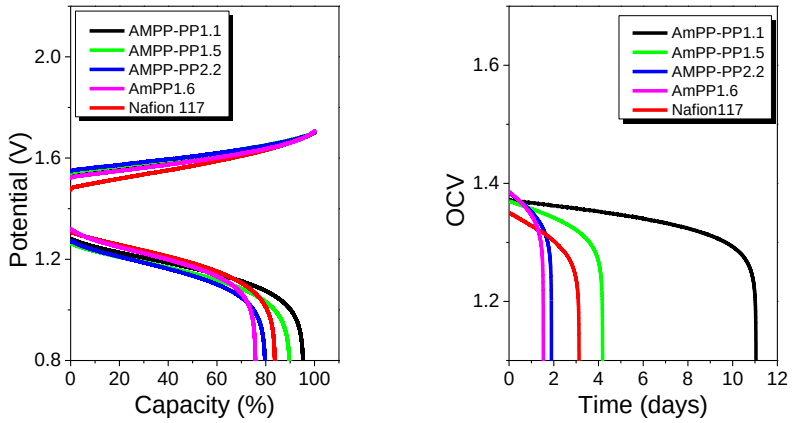

(a) (b)

Figure 8- 4. (a) The charge and discharge curves for AmPP, AmPP-PP and Nafion 117 at 10 mA/cm^2. (b) OCV decay of the VRB cell for all materials.

8.2.4 Charge-Discharge Cycling and Membrane Stability

As discussed in chapter 7, a direct way in which membrane stability has been tested in VRB's has involved *in-situ* cell cycling, observing the CE, VE and/or EE until a sharp drop in efficiency is observed. In **Figure 8- 5a,** the coulombic and energy efficiencies are shown for

membranes AmPP-PP1.5 and Nafion 117 as a function of charge-discharge cycle number. As observed for sPP, the materials display increasing coulombic efficiency, and a gradual drop in EE due to a lowering of the voltage efficiency. At 30 mA/cm^2, the CE of AmPP-PP1.5 is only 3% higher than that of Nafion 117, however the difference in capacity loss over the course of the experiment is substantial (**Figure 8- 5b**). It is this large drop in capacity that causes the sharp rise in CE of Nafion 117 with increasing cycle number. This highlights the importance of coulombic efficiency on ensuring system durability, however does not shed any light on membrane stability. In conclusion, this analysis does not serve as a good quantitative or qualitative measurement of membrane stability.

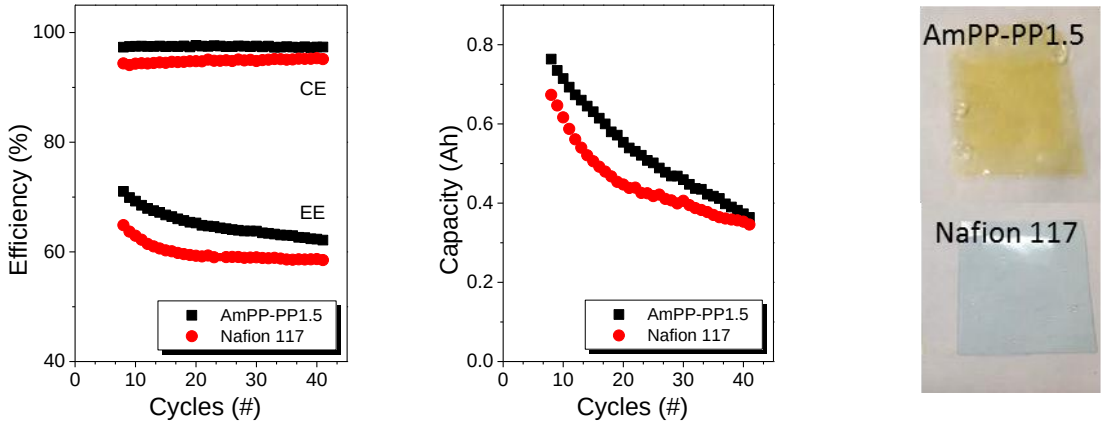

(a) (b) (c)

Figure 8- 5. The (a) cycling efficiency and (b) capacity as a function of cycle number for AmPP-PPP1.5 and Nafion 117. (c) A photograph of the membranes after cycle testing.

The membranes, after more than 3 weeks of exposure to vanadium electrolyte, were removed from the system and analyzed (**Figure 8- 5c**). The entire Nafion 117 membrane appeared

blue, likely due to vanadium ion substitution of the proton on the sulfonic acid group, however no degradation was evident. AmPP-PP1.5 displayed only slight discoloration, appearing to be far more resilient than sPP2.0. The conductivities of the degraded Nafion 117 and AmPP-PP1.5 films were measured. Nafion 117's conductivity dropped from 100.4 to 25.8 mS/cm, while the conductivity of AmPP-PP1.5 dropped from 9.9 mS/cm to 4.5 mS/cm. It is likely, just as it was reasoned that sPP and Nafion are in the "vanadium-ion form", that the AmPP-PP membranes are now in the sulfonate form. Due to comparable sodium and chloride form conductivities, no conclusion can be made regarding membrane stability.

Table 8- 3. Ion conductivity of AmPP-PP1.5 and Nafion 117 in the acid/base and Na^+/Cl^- forms, as well as after 3 weeks of VRB system *in-situ* exposure to vanadium electrolyte.

	σ (H^+/OH^-) (mS/cm)	σ (Na^+/Cl^-) (mS/cm)	σ_{end} (mS/cm)
AmPP-PP1.5	9.9	5.2	4.5
Nafion117	100.4	26.2	25.8

In rigorous *ex-situ* testing, whereby a material was placed in a solution of 0.1 M V^{5+} and 5 M H_2SO_4 at 50 °C for a number of days, AmPP-PP did display signs of degradation. The V^{5+} solution is bright yellow, and changes to blue during polymer degradation, attributed to reduction to the VO^{2+} ion during backbone degradation. After 48 hours, the parent polymer gave no indication of degradation, while the quaternary ammonium random polymer solutions gradually turned from yellow to green, at a rate increasing with IEC. The homopolymer solution had turned

blue, potentially indicating that the larger hydrophilic domains within the homopolymer accelerates degradation. After 1 week, the materials were removed from the vanadium solutions and rinsed with water (**Figure 8- 6a**). As observed in previous studies for AmPP,[9] none of the materials broke apart, and despite darkening of the film (**Figure 8- 6c**) AmPP-PP1.1 and AmPP-PP1.5 retained their flexibility. This is in contrast to the sulfonated materials, which displayed rapid loss of flexibility. The AEM's may exhibit slower rates of degradation over CEM's due to electrostatic repulsion. As was previously discussed, no degradation or color change was evident for Nafion 117, likely due to its highly fluorinated backbone. WAXS (**Figure 8- 6b**) did not confirm degradation in the materials. More work is required to further understand methods to mitigate degradation of aromatic ionomers.[18]

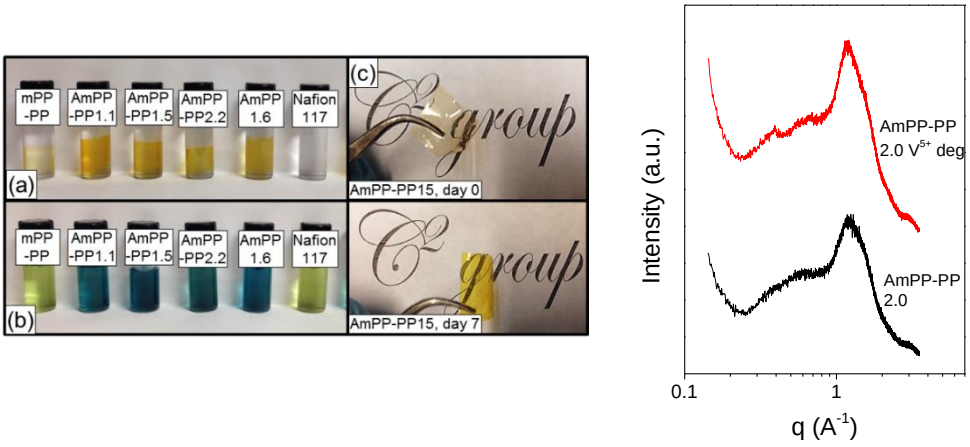

(a) (b)

Figure 8- 6. (a) The *ex-situ* degradation study of aminated and Nafion 117 films in a V^{5+} vanadium ion solution after 10 days and (b) WAXS data for sPP2.0 before and after the cell cycling test.

8.3 Conclusions

In this study, the effect of block copolymerization of quaternary ammonium Diels-Alder poly(phenylene)s on vanadium ion permeability, battery performance, and material stability was reported. Quaternary ammonium Diels-Alder random copolymers were synthesized with IEC's up to 2.2 meq/g, displaying an ion conductivity of 17.3 mS/cm and water content of 57.3%. A random copolymer of equivalent ion exchange capacity displayed lower water content than the homopolymer, accompanied by a lower ion conductivity. The random copolymers showed significantly reduced vanadium ion permeability. The homopolymer and random copolymer vanadium redox flow battery performance was compared for IEC's of 1.6 and 1.5 meq/g, respectively. At 10 mA/cm^2, the random copolymer displayed a 14% higher coulombic efficiency, of 89.8%. Despite a trade-off of a marginally lower voltage efficiency, the random copolymer outperformed the homopolymer, with a 7% higher energy efficiency. Cell cycling gave no clear indication of membrane degradation, however slight discoloration of the aminated film was observed. All quaternary ammonium materials displayed degradation in a 0.1 M V^{5+} + 5 M H_2SO_4 solution, with the rate of degradation appearing to increase as a function of IEC. Low to moderate films retained their flexibility, perhaps indicating superior stability over sulfonated materials due to electrostatic repulsion.

8.4 References

[1] Li, X.; Zhang, H.; Mai, Z.; Zhang, H.; Vankelecom, I. *Energy Environ. Sci.* **2011**, *4*, 1147.

[2] Zhao, C.; Lin, H.; Shao, K.; Li, X.; Ni, H.; Wang, Z.; Na, H. *J. Power Sources* **2006**, *162*, 1003–1009.

[3] Chen, D.; Wang, S.; Xiao, M.; Han, D.; Meng, Y. *J. Power Sources* **2010**, *195*, 7701–7708.

[4] Chen, D.; Wang, S.; Xiao, M.; Meng, Y. *Energy Environ. Sci.* **2009**, *3*, 622.

[5] Chen, D.; Wang, S.; Xiao, M.; Meng, Y. *J. Power Sources* **2010**, *195*, 2089–2095.

[6] Chen, D.; Wang, S.; Xiao, M.; Meng, Y. *Energy Convers. Manag.* **2010**, *51*, 2816–2824.

[7] Fang, J.; Xu, H.; Wei, X.; Guo, M.; Lu, X.; Lan, C.; Zhang, Y.; Liu, Y.; Peng, T. *Polym. Adv. Technol.* **2013**, *24*, 168–173.

[8] Zhang, S.; Yin, C.; Xing, D.; Yang, D.; Jian, X. *J. Memb. Sci.* **2010**, *363*, 243–249.

[9] Sun, C. N.; Tang, Z.; Belcher, C.; Zawodzinski, T. a.; Fujimoto, C. *Electrochem. commun.* **2014**, *43*, 63–66.

[10] Xing, D.; Zhang, S.; Yin, C.; Zhang, B.; Jian, X. *J. Memb. Sci.* **2010**, *354*, 68–73.

[11] Chen, D.; Hickner, M. a.; Agar, E.; Kumbur, E. C. *Electrochem. commun.* **2013**, *26*, 37–40.

[12] Zhang, B.; Zhang, S.; Xing, D.; Han, R.; Yin, C.; Jian, X. *J. Power Sources* **2012**, *217*, 296–302.

[13] Hwang, G.; Ohya, H. *J. Memb. Sci.* **1997**, *132*, 55–61.

[14] Yanagia, H.; Fukuta, K. *ECS Trans.* **2008**, *16*, 257–262.

[15] Sukkar, T.; Skyllas-Kazacos, M. *J. Appl. Electrochem.* **2004**, *34*, 137–145.

[16] Mai, Z.; Zhang, H.; Li, X.; Bi, C.; Dai, H. *J. Power Sources* **2011**, *196*, 482–487.

[17] Mohammadi, T.; Kazacos, M. *J. Appl. Electrochem.* **1997**.

[18] Chen, D.; Hickner, M. a. *Phys. Chem. Chem. Phys.* **2013**, *15*, 11299–11305.

Chapter 9 Conclusion and Recommendations

The main objective of this research was to study the interrelationship of physical, electrochemical, and transport properties of a series of anionic and cationic Diels-Alder poly(phenylene)s, and assess energy storage performance in a working vanadium redox flow battery. Material preparation required the synthesis of parent polymers, including poly(phenylene) (PP) and methylated poly(phenylene) (mPP) homopolymers, a random copolymer, and block copolymers. The materials displayed good solubility in various organic solvents, and high glass transition temperatures (365-390 °C). The homopolymers PP and mPP displayed the highest and lowest densities of 1.178 and 1.107 g/cm^3, respectively. An x-ray structural analysis (WAXS) displayed an amorphous peak describing inter-chain spacing, with d-spacing values correlating to 14.1 Å and 9.6 Å for mPP and PP, respectively. Correlations were found between *–mer* length and inter-chain spacing, glass transition temperature, and occupied volume. Through a physical, rheological and structural characterization, it was concluded that the addition of the methyl moiety had a significant effect on the packing of polymer chains, reducing chain entanglements and increasing free volume.

The sulfonation of the poly(phenylene) homopolymer produced cation exchange membranes of various ion exchange capacities (IEC's). WAXS revealed an "ionic peak" corresponding to 24 Å that increased in intensity with increasing IEC, as well as a large decrease in intensity of the feature correlating to side-chain interactions. AFM surface images revealed a highly homogeneous morphology. The materials displayed good mechanical strength, and thermal stabilities of over 345 °C. An IEC of 2.4 meq/g possessed a proton conductivity of 122 mS/cm and a water content of 105%. sPP2.0 required twice the ion exchange capacity and total water content

of Nafion 117 to achieve competitive electrochemical properties. A state of water analysis concluded that sPP2.0 and Nafion 117 displayed comparable free water content, and emphasized the importance of free water for ion exchange. Permeability studies revealed that sPP2.0 possessed superior ion selectivity versus various alcohol species, suggesting smaller and less interconnected hydrophilic domains.

Quaternary amination of a methylated homopolymer, random copolymer, and block copolymers was performed to obtain anion exchange membranes. Two amination methods were employed, a "*heterogeneous*" method involving amination of a preformed film, and a solution cast "*homogeneous*" amination method. The heterogeneous aminated homopolymers and random copolymers displayed moderate mechanical strength, and thermal stabilities up to 190 °C. An AmPP membrane was synthesized with an IEC of 2.2 meq/g, displaying a conductivity of 26.9 mS/cm, and a water content of 73.1%. The aminated random copolymers displayed lower water content for a given IEC, accompanied by superior mechanical properties and alcohol rejection, suggesting larger, well-defined, hydrophobic regions. A state of water analysis revealed decreased available free water, correlating to lowered ion conductivities. Homogeneous amination of the random and block copolymers resulted in adverse effects on mechanical, electrochemical, and transport properties. The increase in free water content did not improve electrochemical properties, indicating a dilution effect. The utilization of two amination techniques suggests that poor electrochemical properties commonly observed in anion exchange membranes is predominantly due to poor hydroxyl ion mobility and quaternary ammonium basicity, rather than morphology.[1,2]

The ion exchange membranes displaying the most competitive electrochemical and transport properties were analyzed in a working vanadium redox flow battery. Sulfonated materials displayed voltage efficiencies (VE) proportional to ion conductivity. An sPP material displayed

comparable VE to Nafion 117, however superior ion rejection. By modification of the film thickness and IEC, sPP was optimized to outperform Nafion 117 at all current densities. It is concluded that the sulfonated materials, due to excellent ion conductivities and proton selectivity, are highly competitive candidates for use in vanadium redox flow batteries. The aminated materials displayed good vanadium ion rejection, however, due to electrochemical limitations, low voltage efficiencies. The quaternary ammonium random copolymerization improved the coulombic efficiency at the cost of increased resistance, corresponding to observations made during the electrochemical and transport property analysis. It is concluded that, in their current state, quaternary ammonium Diels-Alder poly(phenylene)s are poor candidates for use in vanadium redox flow batteries.

In order to observe membrane stability, charge-discharge cycling was performed. After 40 cycles, only minor changes in efficiency were observed. A post analysis of the ionomer films revealed that the sulfonated poly(phenylene)s darkened substantially more than the quaternary ammonium poly(phenylene)s. Rigorous *ex-situ* stability testing in a pure V^{5+} solution revealed degradation of all functionalized poly(phenylene) materials. Degradation was not evident in the parent polymers, and degradation rate appeared to increase with increasing IEC. All sulfonated materials quickly became discolored and brittle. Low and moderate IEC quaternary ammonium poly(phenylene)s darkened, but retained some flexibility. It is concluded that functionalized poly(phenylene)s were susceptible to phenyl ring degradation, as documented elsewhere,[3–8] however results suggest improved stability in the anion exchange membranes likely due to electrostatic effects.

In future work, it is recommended that attention be given to hybrid anionic and cationic Diels-Alder poly(phenylene)s. Although this study strongly suggests that anion exchange

membranes are largely non-competitive due to electrochemical limitations, good coulombic efficiency and increased vanadium chemical stability gives some optimism for their use in tandem with cation exchange membranes. Many forms of hybrid anionic/cationic materials have been developed, including zwitterionomers,[9,10] sandwich membranes,[11] and core-shell nanomaterials.[12,13] In such work, the anion and cation exchange membrane would participate in ionic crosslinking, binding the materials together. The anion exchange membrane may be able to improve vanadium ion rejection through electrostatic repulsion. This could increase coulombic efficiencies in high ion content cation exchange membranes, and reduce vanadium ion induced backbone degradation.

9.2 References

[1] Kreuer, K. D. *J. Memb. Sci.* **2001**, *185*, 29–39.

[2] Vanysek, P. *CRC Handb. Chem. Phys.* **2000**, *83*.

[3] Kim, S.; Tighe, T. B.; Schwenzer, B. **2011**, 1201–1213.

[4] Kim, S.; Tighe, T. B.; Schwenzer, B.; Yan, J.; Zhang, J.; Liu, J.; Yang, Z.; Hickner, M. a. *J. Appl. Electrochem.* **2011**, *41*, 1201–1213.

[5] Sukkar, T.; Skyllas-Kazacos, M. *J. Appl. Electrochem.* **2004**, *34*, 137–145.

[6] Chen, D.; Hickner, M. a. *Phys. Chem. Chem. Phys.* **2013**, *15*, 11299–11305.

[7] Sun, C. N.; Tang, Z.; Belcher, C.; Zawodzinski, T. a.; Fujimoto, C. *Electrochem. commun.* **2014**, *43*, 63–66.

[8] Fujimoto, C.; Kim, S.; Stains, R.; Wei, X. *Electrochem. …* **2012**, *20*, 48–51.

[9] Yang, C.-Z.; Hwang, K. K. S.; Cooper, S. L. *Die Makromol. Chemie* **1983**, *184*, 651–668.

[10] Hwang, K. K. S.; Yang, C.-Z.; Cooper, S. L. *Polym. Eng. Sci.* **1981**, *21*, 1027–1036.

[11] Bakangura, E.; Ge, L.; Muhammad, M.; Pan, J.; Wu, L.; Xu, T. *J. Memb. Sci.* **2015**, *475*, 30–38.

[12] Sanwaria, S.; Singh, S.; Horechyy, A.; Formanek, P.; Stamm, M.; Srivastava, R.; Nandan, B. *RSC Adv.* **2015**, *5*, 89861–89868.

[13] Harada, A.; Kataoka, K. *Sci. (Washington, D. C.)* **1999**, *283*, 65–67.